UNIVERSITY OF SIENA

Department of Biotechnology, Chemistry, and Pharmacy

Doctorate in Chemical and Pharmaceutical Sciences

Coordinator: Prof. Stefano Mangani

XXXII Cycle

MARIE SKŁODOWSKA-CURIE ACTIONS

TRAining in Cancer mechanisms & Therapeutics (TRACT)

Innovative Training Networks (ITN): H2020-MSCA-ITN-2016

Project Coordinator: Prof. Daniela Zisterer, Trinity College Dublin, Ireland

Early Stage researcher (ESR) 6

Development of New Drugs for the Treatment of Oral Cancers

Doctorate Supervisors:

Prof. Giuseppe Campiani

Prof. Stefania Butini

Doctorate Fellow:

Akella Prasanth Saraswati

Academic Year: 2019/2020

Contents

Preface

Chapter 1

Introduction

Chapter 2

Rational design of novel HDAC6 inhibitors

Preface:

Le terapie epigenetiche rappresentano una delle aree più promettenti e innovative della scienza moderna. In particolare, l'uso di inibitori delgli enzimi della famiglia histone deacetylases (HDAC) 'HDAC ha acquisito un notevole interesse come strumenti terapeutici grazie al successo dell'approvazione della FDA di quattro farmaci. Tuttavia, a causa della natura pan-inibitoria di questi composti e dei loro effetti collaterali, vi è un urgente bisogno di identificare inibitori selettivi delle differenti isoforme. A questo proposito, l'unicità dell'isoforma HDAC6 ha attirato l'attenzione diffusa su vari programmi di scoperta di farmaci. A differenza di altre isoforme HDAC, HDAC6 contiene due domini catalitici e quindi agisce sia su substrati istonici che non-istonici. La sovraespressione di HDAC6 è stata collegata a molte condizioni patologiche come cancro, neurodegenerazione, autoimmunità, malattie infettive e disturbi rari. Inoltre, recenti studi che evidenziano la bassa incidenza di letalità nei modelli di topi knockout per HDAC6 sottolinea i benefici dell'uso di inibitori selettivi di HDAC6 rispetto agli inibitori pan o parzialmente selettivi. Sulla base di questi fatti, molti gruppi di ricerca hanno sviluppato attivamente numerosi inibitori selettivi dell'HDAC6 per varie terapie.

Questo lavoro di tesi si concentra sulla porgettazione razionale, fatta presso il notro laboratirrio di chimica computazionale, sullo studio delle ralazioni struttura-affinità (SAR) sulla sintesi e lo svuluppo di nuovi inibitori potenti e selettivi per HDAC6 come agenti antitumorali. Saranno anche discussi i risultatii ottenuti relativamente agli studi a raggi X e alla valutazione biologica dei composti sviluppati e oggetto del presente lavoro di tesi. In particolare, sulla base della struttura modulare deio composti sviluppati, sono stati sintetizzati due nuovi "cap-groups" che hanno consentito l'inserimento di diverse decorazioni per ottenere elevata potenza e selettività nei confronti di HDAC6. I composti con le migliori prestazioni sono stati sottoposti a screening in varie linee cellulari tumorali per valutarne la loro citotossicità, i loro effetti sul ciclo cellulare e il potenziale pro-apoptotico. Inoltre, sulla base dei rapporti che indicano l'uso di inibitori di

HDAC6 su STAT3, alcuni dei composti sono stati valutati per la loro attività inibitoria su STAT3. Inoltre, è stato valuatato il potenziale di mutagenicità e citotossicità per i composti per determinare il loro profilo di sicurezza e tossicità. In conclusione, questo lavoro ha consentito lo sviluppo di una nuova serie di inibitori potenti e selettivi per HDAC6 come agenti antitumorali dotati di promettenti profili terapeutici.

Chapter 1

Introduction

1.1. Epigenetics

The groundbreaking discovery of the double-stranded structure of the DNA by James Watson and Francis Crick represents one of the most pivotal milestones in modern science.[1] Following this discovery, several remarkable developments have been made to elucidate the "central dogma" involving the transcription of genetic information contained in DNA into RNA, and its subsequent translation into proteins.[2] Half a century later, this central dogma remains a guiding principle to study environment-genome interaction that is necessary to understand the effect of stimuli on cellular functions and gene expression. These events paved the way for the development of "epigenetics" (the term coined by Waddington is 1942), which represents one of the most innovative areas of research in modern biology and medicine. Epigenetics involves elucidating the modifications to DNA and/or its associated proteins in response to external stimuli. Such modifications often lead to inheritable or non-inheritable phenotypic changes and can occur anywhere in the human genome. Since these are phenotypical changes, they do not alter the underlying sequence of the DNA. However, they can have profound effects on gene transcription, especially on cell lineage, fate and function. In most cases "epigenetic memory" is conferred in response to external stimuli that allow the genetic information and the associated phenotype to pass through the cells. In addition to the DNA template, epigenetic mechanisms work by stabilizing gene expression programs thereby canalizing cell-type identities. The widespread success of the Human Genome Project coupled with various technological advancements such as chromatin immunoprecipitation and next-generation sequencing (ChIP-seq) have facilitated scientists to perform "epigenomic profiling" of both normal and abnormal cells. Epigenomic profiling has also allowed defining the critical DNA control elements

namely, gene enhancers or promoters. Furthermore, in combination with DNA sequence analyses, deeper insights into the disease processes have been gained. Considering the reversibility of the chromatin epigenetic modifications, several promising therapies have evolved based on the adaptive nature of epigenetic control.

Epigenetics comprises of a series of mechanisms that can alter the DNA and its associated, or other crucial protein substrates chemically or structurally. Chemical alterations involve modification to histones and DNA, whereas structural alterations happen *via* chromatin remodelling and inter/intra-chromosomal DNA interactions. In general, three main epigenetic modifications include DNA methylation, histone modifications and gene silencing associated with non-coding RNA (ncRNA).

1.1.1. DNA methylation: DNA methylation involves the enzymatic addition of a methyl (CH_3) group onto the cytosine rings of DNA with both spatial and temporal precision. In the human genome, 60-80% DNA methylation occurs in the 28 million CpG dinucleotides, to form 5-methylcytosine (5-mC).[3] In contrast to the previously established concept of DNA methylation being a stable heritable genetic trait, recent reports indicate that methyl groups can be erased or added dynamically.[4] DNA methylation in the promoter genes, particularly in the transcription suppression sites (TSSs), suppresses the downstream genes expression *via* the recruitment of DNA binding proteins and histone modifiers that ultimately suppress transcription.[5-8] Interestingly, the DNA methylation process can also take place in gene bodies, however, unlike methylation of promoters, it is involved in active transcription.[9] Imprinting of the insulin-growth factor 2 gene (*IgF2*) in humans is an excellent example of methylation influencing gene expression. The dynamic DNA methylation process is characterized by the generation of methylation marks which can be synthesized *de novo*, maintained, or removed. An intricate balance between DNA methyltransferases (DNMTs) and DNA methylases is crucial for the mediation of such processes.

The human genome encodes three DNMTs (1, 3A, and 3B) to catalyse the DNA methylation process. DNMT1 demonstrates greater activity on the hemimethylated DNA to exert control over the maintenance of the methylation process after DNA replication and DNA damage repair.[10, 11] Whereas, DNMT3A and DNMT3B play vital roles in the *de novo* methylation, without the ability to distinguish unmethylated and hemimethylated DNA substrates.[12] 5-Aza-2'-deoxycytidine (5-Aza, **1**, **Figure 1**), a cytosine nucleoside analogue that inhibits DNMTs, has been extensively used for the investigation of DNA methylation in many cellular functions necessary for mechanistic and translational studies.[13] Specifically, due to its ability to activate tumor suppressor genes in leukemic cells, 5-Aza (**1**) has been employed clinically as a first-line antileukemic agent and is considered as the first "epigenetic drug".[14, 15]
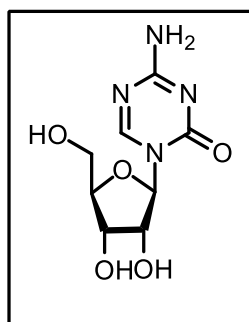
5-aza-2'-dioxycytidine, 1

Figure 1. 5Aza, a DNMT inhibitor used as a first-line antileukemic agent.

Ten-eleven translocation methylcytosine dioxygenase (TET) family proteins, catalyze the major pathway mediating DNA demethylation, wherein the methyl group of the 5-methyl cytosine (5-mC) gets oxidized to yield 5-hydroxymethyl cytosine (5-hmC).[16] This on further oxidation affords 5-formylcytosine and 5-carboxylcytosine. These derivatives of 5-mC represent novel epigenetic markers with potentially new biological roles.

1.1.2. Histone modifications: histones, the core components of the nucleosome, undergo more than 130 post-translational modifications (PTM), including methylation, acetylation, phosphorylation, sumoylation, and ubiquitination.[17] Histone PTMs are extensively distributed

8

all over the human genome forming the histone code, that can control the accessibility of DNA.[18] Also, it recruits transcription factors (TFs) and coactivators/suppressors to result in active, poised or silenced transcriptional states. Distinct histone modifications can result in activation or inactivation of the adjacent genes by recruitment of regulatory mechanisms such as chromatin remodeling complexes, TFs, and transcriptional coactivators/suppressors.[19] Transcriptional activities are affected by histone modifications by two main mechanisms. Firstly, histone PTMs can modify the structure and conformation of chromatin. For example, H3K27 acetylation can decrease the positive charge on the histones, thereby reducing DNA binding and in turn increasing their accessibility. Secondly, histone PTMs can deliver signals to the 'reader' enzymes to recruit transcriptional activators/repressors. For instance, H3K27 trimethylation gets recognized by the polycomb repressive complex 1 (PRC1), that mediates ubiquitination of histone H2A, a key process required for transcriptional repression.[20]

For each histone PTM, three specific enzymes catalyze the "writing", "reading" and "erasing" of the modifications. "Writers" include histone acetyltransferases (HATs), histone methyltransferases (HMTs), and protein arginine methyltransferases (PRMTs). Whereas "erasers" are histone deacetylases (HDAC) and lysine demethylase (KDM). The "reader" proteins that contain distinct domains (bromodomains, chromodomains) recognize the differentially modified histones.

1.1.3. Non-coding RNA (ncRNA): even though three-quarters of the human genome can be transcribed, only a limited portion of the genes can be translated into proteins.[21] Non-coding RNAs (ncRNAs) are the RNAs that cannot be translated into proteins. ncRNAs can be clustered based on their size, namely small ncRNA (that includes small interfering RNA (siRNA), microRNA (mRNA), piwi-interacting RNA (piRNA), transfer RNA (tRNA), and small nucleolar RNA (snRNA)), and long ncRNA (lncRNA). lncRNAs are the most crucial in the epigenetic regulations and are the least understood. They are more than 200 bases in length and

can be classified based on their genomic loci or associated DNA strands/regions into sense, antisense, enhancer, intergenic, intronic or circular RNAs.[22] Functionally they can be grouped into signals, decoys, guides, and scaffolds.[23] lncRNA associated with signals or decoys are involved in gene activation or suppression, respectively. lncRNA as guides, recruit chromatin-modifiers to regulate gene expression in the form of *cis* or *trans*. lncRNA as scaffolds perform recruitment of proteins involved in the assembly of ribonucleoprotein complexes, that modulate histone markers by acting on chromatin.

1.2. Histone deacetylases (HDACs)

1.2.1. HDAC family

Protein acetylation balance maintained by histone acetyltransferases (HAT) and deacetylases (HDACs) play a crucial role in post-translational modifications.[24] HDACs are enzymes responsible for deacetylating lysine residues from histones and other large sets of proteins involved in various functions, from gene expression to protein activity. Some of these proteins include transcription factors, HATs, metabolic enzymes and proteins involved in cell signaling, apoptosis, DNA recombination, repair, and replication.[25] HDACs perform their functions by forming large multiprotein complexes and act as a scaffold for different temporal and spatially regulated interactions.[26] Deacetylation by HDACs confers a tag for epigenetic repression and plays a crucial role in cell cycle progression, transcriptional regulation and developmental events. Their involvement has also been implicated in infection and inflammation. Moreover, deregulation of HDAC has been observed in disease conditions such as cancer, autoimmunity, and neurodegeneration.[27-29]

In mammals, a total of 18 HDACs have been identified to date. Basing on their homology to yeast HDACs, cellular localization and enzymatic actions, HDACs are clustered into four classes. While classes I, II and IV are Zn^{2+} dependent, class III (also called sirtuins, SIRT1-7)

are NAD$^+$ dependent. Class I contains nuclear enzymes HDAC1, 2, 3 and 8, whereas class II is further subdivided into two classes of enzymes with nucleocytoplasmic shuttling capability, namely class IIa (HDAC4, 5, 7 and 9) and class IIb (HDAC6, 10). class IV includes only one member, HDAC11.[30] (**Figure 2**)
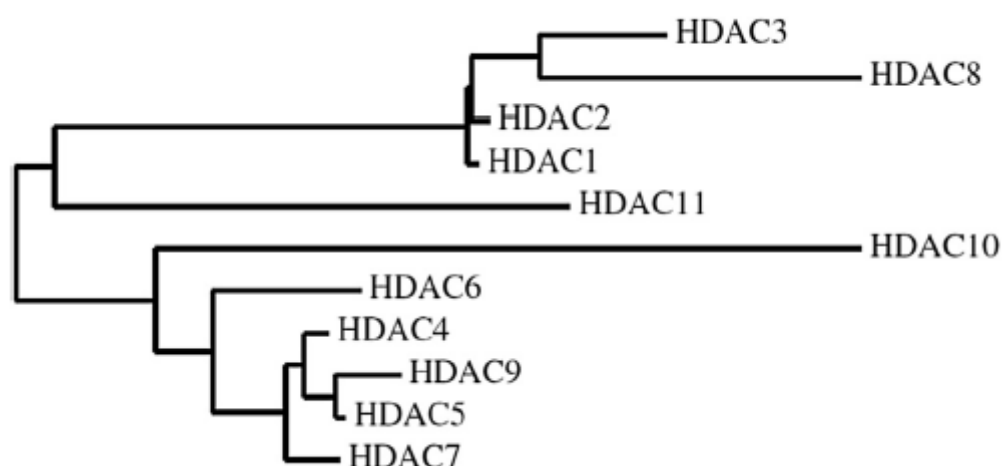
Figure 2. Phylogenic tree of human HDACs established with tools available at http://www.phylogeny.fr/. Wherein, the branch length is proportional to the number of substitutions per site, that is the number of changes or 'substitutions' divided by the length of the sequence.

Structurally, HDACs are heterogeneous in length ranging from 347 amino acid residues (shortest, HDAC11) to 1215 residues (longest, HDAC6) and contain a conserved deacetylase domain.[31, 32] Their deacetylase activity on the lysine residues on histones and other proteins is due to the binding of the Zn^{2+} present in the active site with the *N*-ɛ acetylated lysine. On activation, the *N*-acetyl group gets attacked by a water molecule, resulting in an *N*-ɛ free lysine and acetic acid. HDACs differ based on the different residues present at the entry of the active site. Specifically, class I HDACs have an additional internal cavity for water entry and acetic acid removal. However, class II HDACs are devoid of this secondary pocket, wherein the water

and acetic acid might utilize an alternate entry/exit. In the case of class III SIRTs, the acetyl group and ADP-ribose are associated at the end of the catalytic reaction.[25]

1.2.2. Mechanistic aspects: mechanism of lysine deacetylation

The catalytic activity of HDACs was first reported by Finnin (**Figure 3**), followed by the studies on coordination in the catalytic site and the mechanism of zinc protease chelation.[33-35] The most intriguing feature in the structure of HDAC8 is the encircling of the Zn^{2+} by two dipeptides (His131-Asp166 and His132-Asp173). It is linked to a tyrosine (Tyr297) and coordinated with Asp258, Asp168, and His170 for proton assistance.

In Class I enzymes, a Tyr-His pair is accessible for proton assistance, whereas in Class II enzymes histidine is present in place of tyrosine for proton assistance.[36] Although the bacterial HDAC (HDAH) is classified as Class II HDACs, they share structural similarity with Class I HDACs with two potassium ions bound as in the case of HDAC8. However, HDAH has more similarities with HDAC6 and therefore thought to be a tubulin deacetylase.[37] The first step of the proposed mechanism is the intermediate chelation of the assisted water molecule and the carbonyl group of the acetyl moiety to the zinc atom. Once the Zn^{2+} is chelated, the protonation of His 132 occurs. His 132 deprotonates water to produce the oxide ion that attacks the carbonyl of the acetyl group. The anion formed leads to the formation of an acetate ion and a terminal ammonium ion on the side chain of lysine. At the final stage of protection and deprotection, His131 gets protonated while His132 does not.

There exists a coplanar arrangement between the His131-Asp166 pair (HDLP) with the Asp carboxylate group at 2.5 Å from the basic imidazole ring.[34] Inversely, the His132-Asp173 pair (HDLP) does not have a similar coplanar arrangement with the Asp carboxylate group at 2.8 Å from the basic imidazole ring, with a deviation of 90º being acidic. The binding of SAHA (**2**) to HDLP, HDAH, and HDAC8 generates the same geometry. His843 is 10 Å far from the

metal ion and in case of Class II HDACs the tyrosine residue for proton transfer is replaced.[36, 38] The second dyad is formed by Asn712 similar to HADH (Asn185). In the case of TSA (Trichostatin A, **3**) bound to HDAC7, the two dyads display a planar relation. HDAC4 contains an Asn845 in one of the dyads.[39] In the case of HDAC6 modeled with tubacin, the catalytic site represents the dyad pair (His112-Asp149 and His113-Asn156), both being distorted. All the histidine residues surrounding the central metal ion are not found, one being pushed away.
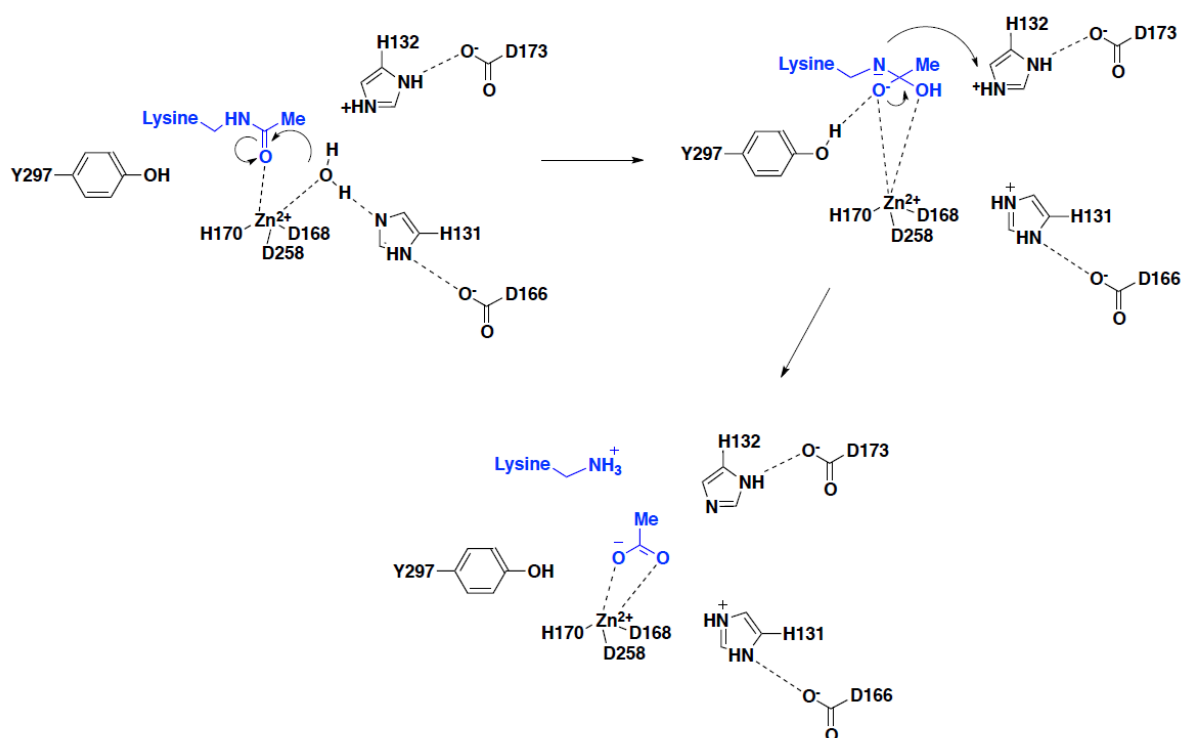

Figure 3. Mechanism of lysine deacetylation proposed by Finnin.

1.2.3. HDAC6, a unique deacetylase

Originally discovered in 1999, HDAC6 represents the only member of the HDAC family possessing a complete duplication of the class I/II HDAC-homology domain.[40] Human HDAC6 (*h*HDAC6) comprises of the two deacetylase catalytic domains DD1 and DD2, a Ser-Glu-containing tetradecapeptide (SE14) repeat domain, a ubiquitin C-terminus hydrolase-like zinc finger (ZnF-UBP) domain at the end of the C-terminal, and a nuclear export signal (NES) at the N-terminal tail (**Figure 4**).[41, 42] These features allow clear identification of its orthologs in other species namely, *Caenorhabditis elegans*, *Drosophila melanogaster,* and others.[43]

HDAC6 in class IIb distinguishes itself from the class IIa HDACs owing to the presence of the two domains DD1 and DD2. However, the exact role of the dual catalytic domain organization concerning the deacetylase activity of the enzyme is not yet established. Some studies indicate the indispensability of both the domains for tubulin deacetylase activity, whereas other investigations have ascribed all the activity to DD2 alone, which is inhibited by tubacin, a selective HDAC6 inhibitor.[44, 45] To support this, experiments conducted with purified HDAC6 suggested that DD2 was solely essential for its catalytic activity for histone and α-tubulin substrates.[46] Further studies led to the conclusion that the spacer region linking both domains of the protein is crucial for the complete activity of HDAC6. Also, amino acid insertion or deletion in the spacer region significantly affected tubulin deacetylase activity.[41]

HDAC6, in addition to the two catalytic domains, also contains peptide regions necessary for its intracellular localization. Human HDAC6 is characterized by the unique SE14-repeat domain-containing eight consecutive tetradecapeptide repeats contributing to its stable cytoplasmic retention.[47, 48] Also, the accumulation of HDAC6 in the nucleus is prevented by an NES located on the N-terminus side of DD1.[42] HDAC6 undergoes nucleocytoplasmic shuttling in response to certain cellular signals, and NES and SE14 are key factors in its active and stable maintenance in the cytoplasm.

Another unique feature of HDAC6 is the presence of a zinc finger motif, with conserved regions rich in cysteine- and histidine at the C-terminus end.[40] The central part of this motif resembles the regions found in several ubiquitin-specific proteases (UBPs), therefore referred as ZnF-UBP.[49] ZnF-UBP can bind specifically to mono- and poly-ubiquitin chains.[49-51] This ubiquitin-binding activity of HDAC6 is critical for the transport of ubiquitinated proteins along the microtubule tracks to pericentriolar structures, known as aggresomes, that enables cells to deal with aberrant accumulations of misfolded proteins.[52]
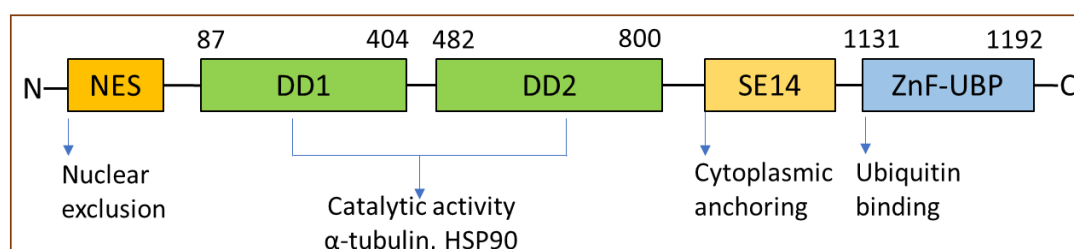
Figure 4. HDAC6 structure: domain organization and functions.

1.2.4. Functions of HDAC6

1.2.4.1. Deacetylase-dependent functions of HDAC6

HDAC6 regulates diverse functions by deacetylating multiple targets, such as histone, tubulin, cortactin, and HSP90 (**Figure 5**).[53, 54] By far its most studied interaction with a substrate is with α-tubulin subunit of microtubules.[44, 55] α-Tubulin acetylation at lysine 40 is common in microtubules, but it is uncertain how the acetylating enzyme gains access to this site.[56, 57] Recent reports have indicated that acetylated α-tubulin plays a crucial role in motor-based trafficking in mammalian cells.[58, 59] Reed *et al.* demonstrated that the tubulin-binding and motility of motor protein, kinesin-1, are controlled by acetylation of α-tubulin and HDAC6 inhibition induces the kinesin-1 cargo protein transport, JNK-interacting protein 1 (JIP1) transport to neurites and the aggregation of JIP1 in neuritis.[59] This process highlights the fact that the selective binding of kinesin-1 to acetylated α-tubulin can mediate the effect of HDAC6

inhibition of JIP1 transport. Moreover, amplified tubulin acetylation in response to HDAC6 inhibition with TSA increases dynein and kinesin-1 bindings to microtubules *in vivo*, which also enhances the intracellular protein transport of brain-derived neurotrophic factor (BDNF), a kinesin-1 cargo protein. On the contrary, impairment in α-tubulin lysine acetylation leads to a decrease in both recruitment of motor complexes and transport of BDNF.[60] Together, these studies shed light on the tubulin deacetylase activity of HDAC6 as an important factor of microtubule-dependent intracellular trafficking.

Recently, a cytoplasmic protein involved in the structural dynamics of the actin cytoskeleton, referred to as cortactin has been identified as another non-histone HDAC6 substrate regulating the control of intracellular trafficking.[61] Cortactin acts on the filamentous F-actin to increase its polymerization and branching, however, acetylation of cortactin precludes its attachment. This activity indicates the role of cortactin as a modulator of filament-based trafficking of actin, which consequently may affect autophagy.[62] Intriguingly, a novel study showed that HDAC6 can also link actin filaments with microtubule dynamics by interacting with formin homology protein mDia2, thereby controlling actin polymerization.[63]

HSP90 was recognized as the second substrate of HDAC6 which suggested that HDAC6 could also act on cellular circuits. HDAC6-dependent HSP90 acetylation influences the binding of an essential HSP90 cochaperone, p23 and subsequently the maturation of the glucocorticoid receptor.[64] HSP90 consists of multiple acetylation sites, and its acetylation activity is a key factor in the binding of cochaperones and client proteins. HDAC6 is sensitive to ubiquitinated cellular aggregates and thereby induces the expression of major cellular chaperones. This is achieved by promoting the dissociation of a repressive HDAC6-heat shock transcription factor 1 (HSF1)–HSP90 complex and consequently inducing HSF1 activation.[65]
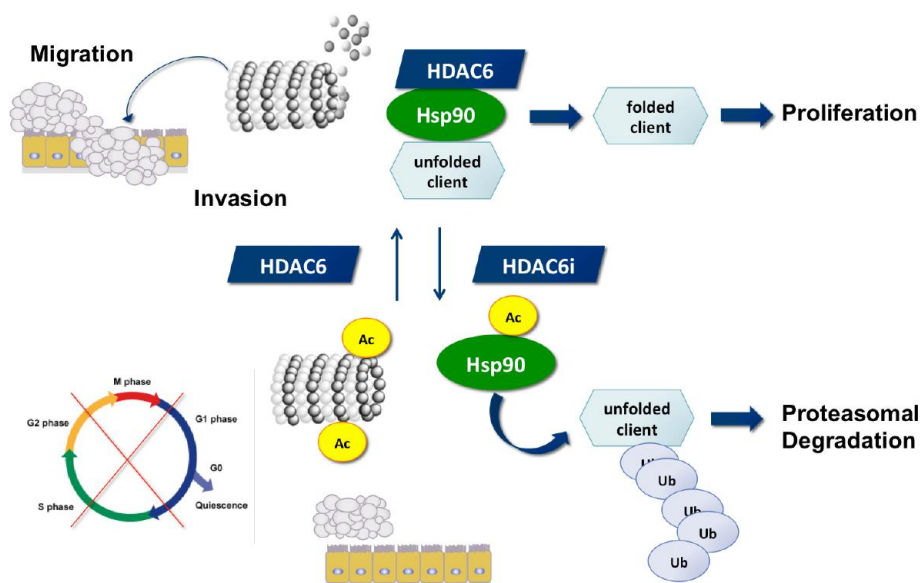
Figure 5. HDAC6 and its role in the acetylation status of HSP90 and α-tubulin

1.2.4.2. Ubiquitin-dependent functions of HDAC6

The first indications of the ubiquitin-dependent functions of HDAC6 were observed after the study of its ubiquitin-binding activity and its localization in ubiquitinated aggresomes.[52] Aggresomes are inclusion bodies juxtaposed to the nucleus in the vicinity of the microtubule-organizing center and represent the termination point of microtubule-dependent transport of misfolded polyubiquitinated protein aggregates.[66] Aggresomes also employ motor proteins that transport misfolded or aggregated proteins to chaperones and proteasomes for consequent destruction.[67] HDAC6 plays a crucial role in aggresomes degradation. The ubiquitin-binding activity of HDAC6 mediates the transport of ubiquitinated proteins along microtubule tracks to aggresomes. HDAC6 binds to polyubiquitinated proteins and dynein proteins, thereby recruiting protein cargo to dynein motors that transport misfolded proteins to aggresomes. This microtubule-dependent intracellular trafficking potential of HDAC6 is associated with its tubulin deacetylase activity. HDAC6 binds ubiquitin with an equilibrium constant (Kd) of 60 nM, which is much higher in comparison to other ubiquitin-binding proteins (range: 5 to 500 μM).[49-51, 68] Such high binding affinity enhances polyubiquitin chain stability and the inhibition

of proteasomal degradation of ubiquitinated substrates through the disruption of their recognition and accumulation into aggresomes. HDAC6 interacts with two proteins, phospholipase A2 inactivating protein (PLAP) and p97/valosin containing protein (p97/VCP), involved in managing ubiquitinated proteins.[49, 50] Interestingly, p97/VCP causes dissociation of the HDAC6–ubiquitin complexes and offers resistance to HDAC6 to promote the accumulation of polyubiquitinated proteins. Therefore, a precise equilibrium of cellular concentrations of HDAC6 and p97/VCP seems to be a critical factor that determines whether polyubiquitinated proteins are subjected to proteasomal degradation by p97/VCP or for sequestration into the aggresome by HDAC6 (**Figure 6**).
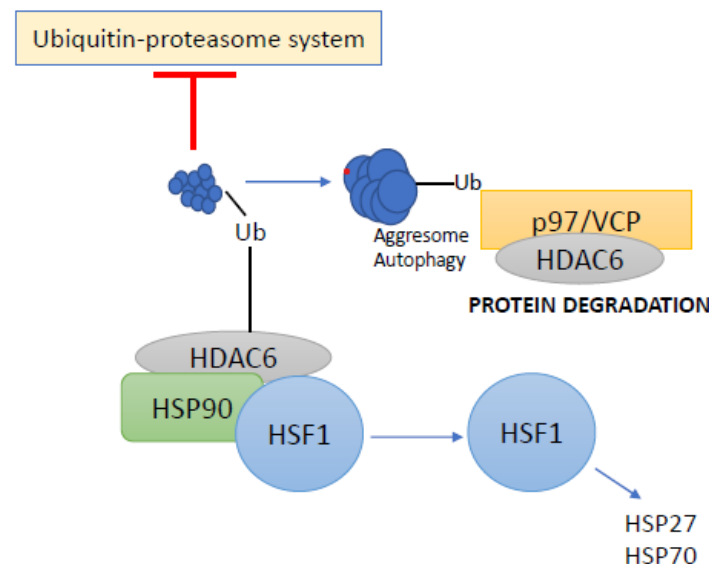

Figure 6. HDAC6-Ubiquitin interplay.

1.3. HDAC6 and cancer

1.3.1. HDAC6 is required for oncogenic cell transformation

Anchorage-independent proliferation enables cells to survive by escaping anoikis, a special kind of programmed cell death, resulting from disengaging of the cell from the extracellular matrix and the surrounding basement membrane.[69] Lee *et al.* in their studies suggested that HDAC6 promotes tumorigenesis and oncogenic transformation by expediting anchorage-independent proliferation in transduced cells. Furthermore, HDAC6 knockdown in MCF7 breast cancer, SKOV3 ovarian cancer, and SKBR3 breast carcinoma cell lines decreased anchorage-independent growth to 3–20%.[69] Further *in vivo* studies were performed using steadily expressed HDAC6-scrambled control and specific shRNA cells that were injected separately into immunocompromised and severe combined immunodeficient-Beige mice, respectively. After two weeks, the mice injected with HDAC6-shRNA showed fewer tumors than control mice.

Another interesting aspect regarding HDAC6 was observed in the inflammatory breast cancer (IBC) cells. Even though HDAC6 is not overexpressed in the IBC cells, its activity is considerably higher in IBC cells in comparison to the non-IBC cells.[70] The HDAC6 inhibitor ACY1215 (ricolinostat, **4**) was observed to significantly inhibit IBC cell proliferation, both *in vitro* and *in vivo*, but was less sensitive in the case of non-IBC cells.[70] This shows that in cancer cells, HDAC6 functions involve alterations in its expression and activities by controlling its cellular deacetylation.

1.3.2. HDAC6 modulates tumor development through non-histone substrates

HDAC6 participates in cell movement by acting on the non-histone substrates. Increased cell mobility results in a) microtubule depolymerization during cellular movement and b) remodeling of new adhesions at the constantly forming front of the spreading cells. This leads to an enhancement in tumor cell movement, metastasis, and invasion.[45, 71] Being an estrogen-

regulated gene, HDAC6 expression in estrogen receptor-positive breast cancer MCF-7 cells was increased, thereby increasing cell motility by promoting HDAC6 binding to α-tubulin and enhancing MT activity.[72, 73] Accordingly, cell motility studies in neuroblastoma demonstrated that HDAC6 inhibitors reduce MT dynamics, resulting in focal adhesion accumulation and decreased fibroblast motility.[74] In addition to cell motility, HDAC6 also regulates the cell cycle through α-tubulin deacetylation and promoting CYLD and BCL3 interaction.[75, 76]

HDAC6 is highly expressed in malignant melanoma. In cases where HDAC6 is silenced or knocked down, acetylated α-tubulin increases, accumulation of acetylated MTs take place, and CYLD is translocated to the perinuclear region, resulting in a reduced interaction between CYLD and BCL3.[77, 78] BCL3 is therefore increased in the cytoplasm, and its transfer into the nucleus is reduced. Low levels of BCL3 in the nucleus prevents the transcriptional activity of NF-κB, resulting in decreased expression of cyclin D1 and a significant interruption of the cell cycle in the G1/S phase.[75] Thus, the HDAC6 mediated regulation of α-tubulin leads to enhanced cell motility and mitosis, which consequently affects proliferation, metastasis, and invasion.[79, 80]

In lung cancers, epidermal growth factor receptor (EGFR) and activation of its downstream pathways lead to cell proliferation.[81, 82] Therefore, altering the synthesis and degradation of EGFR may affect the role of EGFR in tumors. Gao *et al.* demonstrated that HDAC6 expression is tightly involved in cell endocytosis and regulates EGFR trafficking and degradation *via* α-tubulin deacetylation.[83] Loss of HDAC6 results in accumulation of acetylated α-tubulin, resulting in the dysregulation of microtubule-dependent endocytic vesicle trafficking, and hastening EGFR degradation.[84-86]

Mounting evidence suggests that HSP90 is essential for the stability and function of proteins involved in tumor metastasis, and HSP90 affects the growth of tumor cells by stabilization of

key chaperone protein levels, in particular, AKT.[87] HSP90, when bound to AKT, shields AKT from phosphates thereby maintaining AKT phosphorylation and activity. Accordingly, AKT binding of HSP90 safeguards HSP90 from proteasomal degradation.[88] Also, as HSP90 influences the functional stability of AKT, it affects the PI3K/AKT signaling pathway, thereby playing a role in cell survival, migration, differentiation, and angiogenesis.[88, 89] Selective inhibition of HDAC6 has been linked to elevated HSP90 acetylation, leading to a decrease HSP90 and ATP binding, thereby decreasing the combination of chaperone and oncogene, which could be beneficial for cancer treatment.[90]

1.3.3 HDAC6 and apoptosis

The role of HDAC6 in the regulation of apoptosis has been widely reported. The acetylation status of cytoplasmic Ku70 and its interaction with the proapoptotic Bax (Bcl-2-associated X protein) protein is regulated by HDAC6. In the acetylated state, Ku70 no longer interacts with BAX, which leads to the activation of apoptosis. In contrast, HDAC6 mediated deacetylation of the Ku70 results in BAX sequestration and consequently the inhibition of apoptosis.[91] Moreover, dissociation of acetylated Ku70 from the antiapoptotic protein FLIP (FLICE [FADD-like IL-1 β-converting enzyme] inhibitory protein) results in proteasomal degradation and induction of apoptosis.[92] HDAC6 involvement with PI3K (phosphoinositide 3-kinase)/AKT and mitogen-activated protein kinase (MAPK)/ERK signaling pathways have also been reported.[69] HDAC6 knockdown or its catalytic inhibition promotes dephosphorylation of AKT and ERK with reduced cell proliferation and induction of cancer cell death. HDAC6 inhibition also disrupts its interaction with protein phosphatase 1 that may lead to dephosphorylation of its targets, phospho-AKT and phospho-ERK. Also, HDAC6 inhibition promotes HSP90 hyperacetylation resulting in decreased levels of phosphorylated AKT and ERK.[93-95]

1.3.4. The essential role of HDAC6 in the regulation of immunity in cancer

Immunotherapeutic strategies hold great promise for cancer patients, especially for the tumors that lack molecular targets.[96, 97] Therefore, deeper insights into the mechanisms for immune tolerance can significantly lead to an improvement in the prognosis of patients. HDAC6 has been reported to regulate the expression of specific tumor-associated antigens, MHC class I proteins, co-stimulatory molecules, and cytokine production.[98, 99] In the case of human melanoma cell lines, melanoma antigens TYRP1, TYRP2, gp100, and MART1 are elevated at the mRNA level on treatment with HDAC6 inhibitors. Genetic disruption of HDAC6 also leads to an increase in protein expression of gp100 and MART1.[99]

Interestingly, HDAC6 has been reported as an important regulator of the STAT3 pathway.[100] Being a key transcriptional promoter, STAT3 is involved in various processes such as pathogenesis and sustainable development of many malignancies, induction and maintenance of tumor immune tolerance.[101] Recent reports have elucidated that STAT3 modulates PD-L1 expression in antigen-presenting cells (APCs) and also in several tumor cells, including melanoma and lung cancer, to inhibit the tumor immune response.[102] Woan *et al.* have reported that HDAC6 participates in antitumor immunity through STAT3-PD-L1 pathway.[103] Increased HDAC6 expression results in STAT3 phosphorylation and nuclear ectopia at an invariant acetylation level, without an acetylation change in PP2A, Shp-2, and JAK2 proteins, which are key factors in phospho-STAT3 homeostasis.[104] On entering the nucleus, pSTAT3 and HDAC6 are recruited to PD-L1 promoter leading to the activation of PD-L1 gene transcription. However, in the case of HDAC6 knockdown, STAT3 remains undetected at the PD-L1 promoter, implying HDAC6's requirement for STAT3-mediated PD-L1 expression.[103]

In the case of antigen-presenting cells (APCs), HDAC6 binds to STAT3 *via* the 503–840 amino acid region in HDAC6, and this complex binds to a specific sequence in the promoter region

of the immunosuppressive and anti-inflammatory cytokine IL-10, to enhance its gene expression.[105] Reduced HDAC6 expression leads to decreased IL-10 by lowering STAT3 phosphorylation and by inducing inflammatory APCs, that efficiently activating antigen-specific naive T cells and improve the reactive ability of CD4+ T cells.[100, 105]

Recent preclinical trials have also shown that HDAC6 inhibitor ACY-241 (citarinostat, **5**) in combination with PD-L1 antibody augments pDC-induced T- and NK cell-mediated cytolytic activities in the cells of multiple myeloma patient.[106]

1.4. HDAC inhibitors

The active site of zinc-dependent HDACs consists of four distinct binding domains: a) surface binding domain, b) hydrophobic channel, c) the catalytic zinc-binding domain, and d) the adjacent internal cavity. The general pharmacophoric model of HDAC inhibitors (HDACi) (**Figure 7a**) encompasses three structural domains: a zinc-binding group (ZBG) interacting with the zinc ion at the catalytic pocket, a linker occupying the hydrophobic channel and a cap group. In some HDACi, an internal cavity motif is also present.[107, 108] The cap group generally consists of an aromatic or heteroaromatic hydrophobic moiety which mediates the interaction with the amino acids at the surface of the enzyme, responsible for the HDAC isoforms selectivity.[109, 110] On the other hand, modification of the ZBG can lead to a change in the potency of the inhibitors.[111]

Based on the chemical structures of the ZBGs, HDACi can be clustered into five main classes: hydroxamates, cyclic peptides, benzamides, short-chain fatty acids, ketones, and others.[112, 113]

a)

b)

2, SAHA (Vorinostat)

3, Trichostatin A (TSA)

4, Ricolinostat, ACY1215

5, Citarinostat, ACY-241

6, FK-228

7, Belinostat

8, Panobinostat
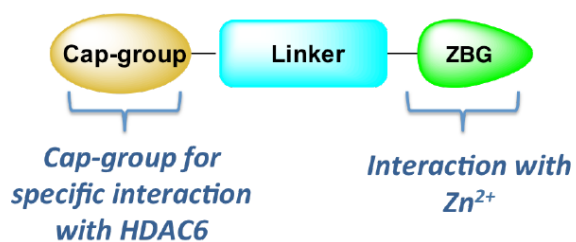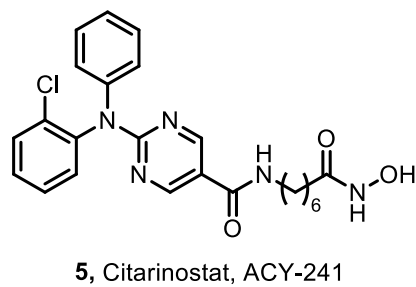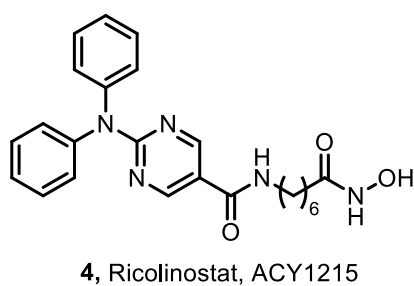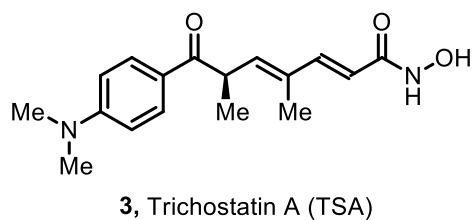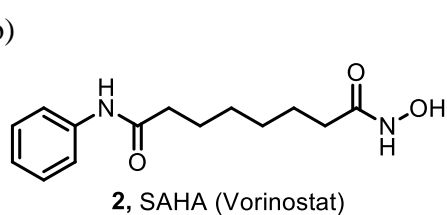
Figure 7. a) General structure of HDACi b) Representative structures of HDACi.

24

Among these, hydroxamate containing HDACi are the most potent and are extensively investigated.[114] However, most hydroxamates possess pan-inhibitory activities, whereas the benzamides clas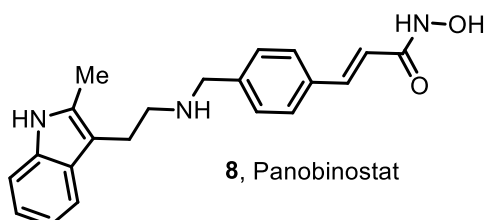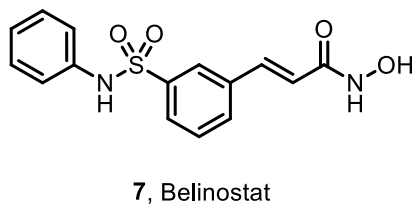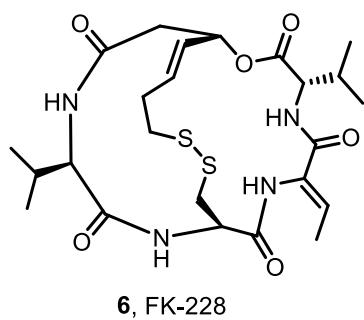s of inhibitors are more selective towards class I enzymes. To date, four HDACi, vorinostat (SAHA, **2**), romidepsin (FK-228, **6**), belinostat (PXD-101, **7**) and panobinostat (LBH-589, **8**), (**Figure 7b**) have received FDA approval for the treatment of cutaneous T-cell lymphoma, T-cell lymphoma, and multiple myeloma.[115] However, the use of such nonselective or partially selective HDACi result in undesirable side effects such as fatigue, nausea/vomiting, and cardiotoxicity.[116, 117] Therefore, an increasing number of research efforts are being focused on the development of isotype-selective HDAC inhibitors to study the complex interactions of these proteins involved in the transcriptional regulation.[25, 118, 119]

1.5. Selective inhibitors of HDAC6

Recent reports have shown that when compared to the lethal effect of HDAC1-3 genetic ablation, HDAC6-knocked out mice are not affected by severe symptoms, suggesting that HDAC6 selective inhibitors may have lesser side effects than HDAC1-3 isoform-selective inhibitors or pan-HDACi.[120] Selective HDAC6i have been widely investigated for a range of therapeutic purposes, such as cancer, autoimmunity, neurodegenerative diseases, infectious diseases, and rare diseases.[90, 121-123] Design of selective HDAC6i has been primarily dependent on the homology model of HDAC6, until the report of the crystal structures of HDAC6 in the previous years.[124, 125] Zinc-dependent HDACi have been discovered from many different structural classes, such as hydroxamic acids, electrophilic ketones, cyclic peptides, short-chain fatty acids, and benzamides. However, they inhibit all or many subtypes of classes I, II or IV. In particular, hydroxamic acid derivatives, such as TSA and suberoylanilide hydroxamic acid (SAHA, **2**) inhibit HDAC isoforms. Only a limited number of HDAC6 selective inhibitors have

been reported so far. In particular, three types of HDAC6 selective inhibitors have been discovered, namely tubacin (**9**), mercaptoacetamides, and thiolate analogs.

1.5.1. Tubacin

Tubacin (**9**, **Figure 8**) was discovered in Stuart Schreiber's laboratory by a multidimensional chemical genetic screen of 7392 small molecules.[45, 126] Tubacin induces α-tubulin acetylation ($EC_{50} = 2.9$ μM) without producing a significant increase in acetylation of histones ($EC_{50}=217$ μM).[126] Moreover, tubacin does not cause HSP90 acetylation.[127] Besides this, it does not affect gene expression profiling, global histone deacetylation, or cell cycle progression. In terms of selectivity, tubacin exhibits 4-fold selectivity for α-tubulin over HDAC1 and HDAC4.[128] Tubacin has been employed in many experiments to elucidate several functions of HDAC6, that have shed light on the many effects of tubacin on apoptosis, cancer-cell motility, and axonal vesicular transport.[60, 72, 129] These findings indicate that HDAC6i could be effective as novel antitumor and neuroprotective agents. Also, synergistic cytotoxicity of the proteasome inhibitor bortezomib with tubacin was demonstrated in multiple myeloma cell lines.[129]
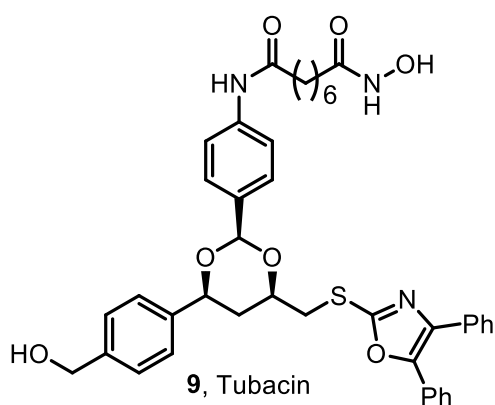
Figure 8. Chemical structure of tubacin.

1.5.2. Mercaptoacetamides

Itoh *et al.* and other groups have demonstrated that potent HDAC inhibition can be achieved with compounds bearing a mercaptoacetamide moiety that chelates the zinc ion in the active

site of HDACs.[130-133] Recent functional analytical studies have confirmed that mercaptoacetamide compounds show potent HDAC6 selectivity (EC_{50} = 0.2–2 μM). Intriguingly, mercaptoacetamides also protected the cortical neurons from oxidative stress-triggered death in culture.[134] These results imply that HDAC6-selective inhibition by mercaptoacetamides is neuroprotective in nature.

1.5.3. Thiolates

Itoh, Suzuki, and their co-workers generated a set of different thiol-containing derivatives based on small-molecule HDAC6-selective substrates: NCT-10a, NCT-14a, and S-isobutyryl prodrugs NCT-10b and NCT-14b.[133, 135-137] NCT-10a (EC_{50} = 29 nM) and NCT-14a (EC_{50} = 82 μM) show high selectivity for HDAC6 over HDAC1 and HDAC4 in enzymatic assays.[133, 135] NCT-10b and NCT-14b induced a dose-dependent increase in acetylation of α-tubulin without causing a major increase in histone H4 acetylation, indicating that these compounds selectively inhibit HDAC6. Also, biological experiments indicate that thiolate-analogue based HDAC6-selective inhibitors are potential anticancer agents.[133, 135]

Chapter 2

Rational design of novel HDAC6 inhibitors

2.1. Background

2.1.1. Tubastatin A

The potential toxicity associated with the inhibition of some HDAC isoforms discourages the use of pan-HDAC inhibitors. With regard to HDAC6 enzyme, its specific involvement in many diseases (in the areas of both oncology and neurological disorders) underscores the importance of selectively targeting this isoform with *ad-hoc* developed inhibitors (**Figure 9**).

In this scenario, tubastatin A (TubA, **10**) represents an ideal reference molecule owing to its potency and selectivity (HDAC6 IC_{50} =15 nM, HDAC1 IC_{50} = 16 μM), and to its chemical tractability and derivatization potential.

The selectivity of **10** was studied by comparison of α-tubulin acetylation (cytosolic localization) and histone acetylation (nuclear localization). At 2.5 μM, **10** preferentially induced tubulin acetylation with a strong *in vitro* preference for HDAC6 rather than HDAC1. Moreover, **10** was examined on an oxidative stress model induced by homocysteic acid (HCA) demonstrating dose-dependent protection against HCA-induced stress. Kozikowski *et al.* commenced their rational design of selective HDAC6 inhibitors by comparing the structures of HDAC6 and HDAC1 since these two enzymes display diverse phylogeny and belong to two distinct classes (I for HDAC1, IIb for HDAC6). The bioinformatic analysis of the two catalytic pockets showed that the catalytic channel rim dimension is different in the two enzymes. In the case of HDAC6, the channel appears wider and shallower, therefore a larger cap-group can fit better into the rim region.

Structurally, **10** contains a) tricyclic ring system bearing a tertiary amine, that further enlarges the dimensions of the cap group favoring the interactions with HDAC6, b) tolyl linker and hydroxamate as ZBG. Notably, the replacement of the traditional alkyl chain in the linker (as in tubacin and SAHA) with bulkier and shorter aromatic moieties led to a clear improvement of selectivity.

HDAC6 channel is mainly lined by apolar residues that explain its ability to accommodate the tolyl linker. The carbazole moiety establishes a π-π stacking with the aromatic residues surrounding the rim cavity (His500, His611, Phe620, and Phe680). Similarly, the indole moiety retains the aromatic contacts with His611 and Phe680 and elicits additional polar interactions between the ammonium head, and Asp567 and Ser568.[125]
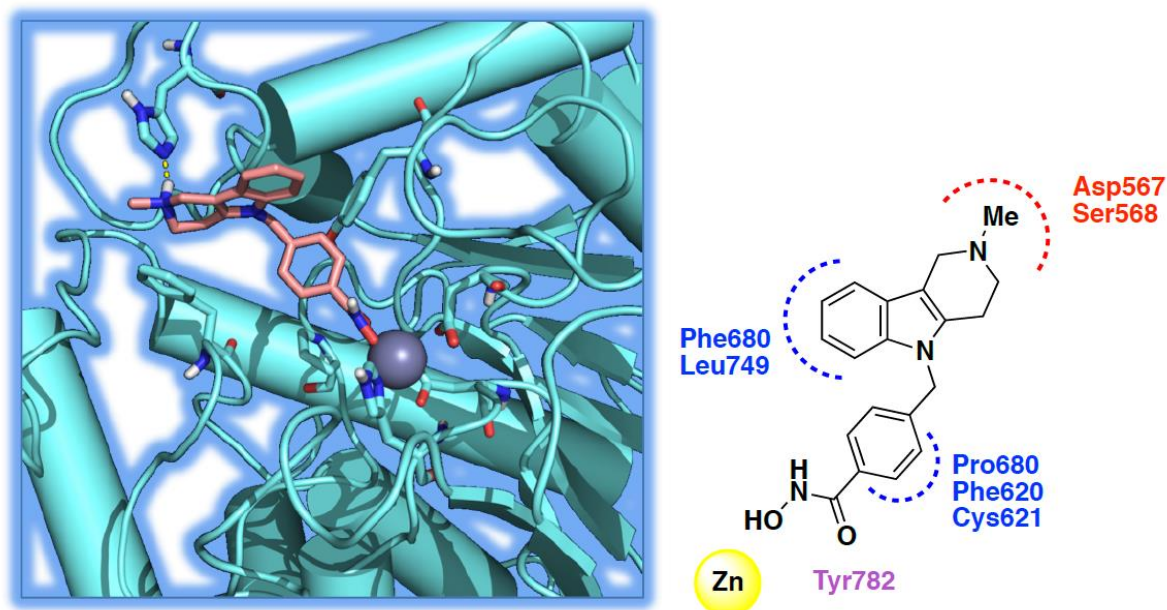
Figure 9. The docked pose of tubastatin A, **10** into HDAC6 and its interactions with the residues in the active site (polar interaction are represented in red, aromatic interaction in blue and hydrogen-bond in violet).

2.1.2 The hydroxamate group

Hydroxamates are the most widely explored ZBGs for HDAC inhibition. Zinc is a very commonly found cofactor in different classes of enzymes such as endopeptidases, matrix metalloproteases (MMPs) and HDACs. The challenges encountered with the use of hydroxamate is the possibility of indiscrimination among the different classes of metalloenzymes and vulnerability to cross-reactions. However, a recent study conducted by Day and Cohen demonstrated that metal-binding groups for Zn^{2+} ions such as hydroxamic acids and thiols will not indiscriminately inhibit Zn^{2+} metalloenzymes in the absence of favorable inhibitor backbone-protein interactions.[138]

Other issues often related to the use of hydroxamates are toxicity and pharmacokinetic liabilities. In this regard, a recent perspective by Shen and Kozikowski has shed light on the potential mutagenicity of the hydroxamate group. The mutagenic properties of hydroxamates are associated with their ability to undergo the Lossen rearrangement, a reaction which converts an activated hydroxamate into the corresponding isocyanate (**Figure 10**). Isocyanates can readily react with the nucleophilic groups of the DNA and cause subsequent DNA damage.[139] The rate-limiting step of the Lossen rearrangement is the formation of an activated hydroxamate since the rate of reaction is directly proportional to the acidity of the conjugate acid of the leaving group.[140] Under physiological conditions, the activation of the hydroxamic group is a key step for the rearrangement that takes place by *O*-acetylation due to the presence of acetyl-CoA present in bacteria. Most rearrangements take place in a basic medium; however, the low acidity of hydroxamates ($pKa \approx 8.5$) does not allow deprotonation at the physiological pH.[141]
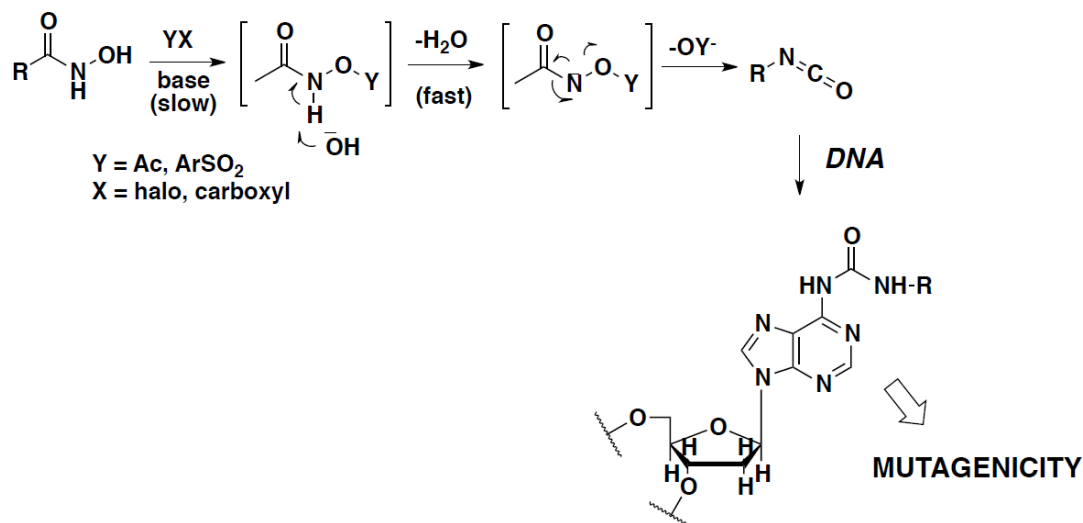
Figure 10. Mechanism of mutagenicity by HDACi

Soon, a metal-assisted mechanism was then proposed, described in **Figure 11** wherein a zinc-triggered rearrangement takes place involving two hydroxamic groups that bind zinc as neutral or anionic ligands. Thereafter, hydrogen migration from nitrogen to oxygen leads to the formation of an unsaturated complex followed by its rearrangement to form the more stable isocyanate.[142]
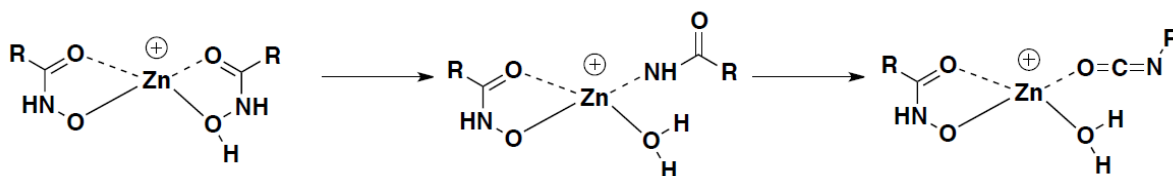
Figure 11. Lossen rearrangement: metal-assisted mechanism.

However, driven by this evidence and the importance of hydroxamate for its ability to chelate zinc as well as its isoform selectivity, the rational design of less activated hydroxamates can be beneficial to synthesize compounds that do not display mutagenicity potential. This is supported by many reported HDAC inhibitors bearing hydroxamate that do not exert mutagenic

effects in normal human lymphocytes. Among these inhibitors are givinostat (**11**) and abexinostat (**12**), bearing a diethylamino group and a dimethylamino group respectively (**Figure 12**). These compounds are being studied for the treatment of chronic myeloproliferative neoplasms and hepatocellular carcinoma and are under phase II clinical trials.[143, 144]

11, Givinostat   **12**, Abexinostat
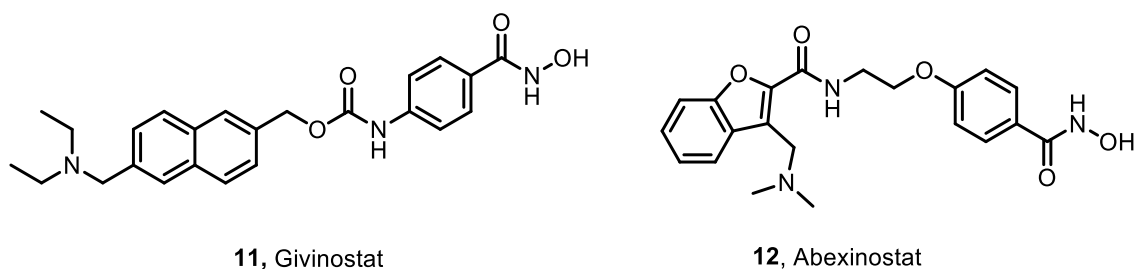
Figure 12. Chemical structures of Givinostat and Abexinostat.

2.2. Aim of the thesis

Aim of the thesis can be divided into four main objectives:

a) Rational design, synthesis, structure-activity relationships (SAR) of novel HDAC6 inhibitors as anticancer agents by introducing new cap groups with structural modifications aimed at increasing the potency and selectivity towards HDAC6 isoform. This would be achieved by linking the cap group with suitable aromatic linkers followed by the attachment of hydroxamate ZBG.

b) Characterization of the newly synthesized compounds utilizing ^{1}H and ^{13}C NMR spectroscopy, LC-MS, and also X-ray crystallography (performed by Prof. David Christianson at the University of Pennsylvania).

c) Biological evaluation of the newly developed HDAC6 inhibitors using binding affinity studies on HDAC1, HDAC6, HDAC8 enzymes and cell-based assays on different cancer cell lines (performed in collaboration with Prof. Vincent Kelly, Dr. Jeff O'sullivan and Prof. Daniela Zisterer at Trinity College Dublin, Dr. Richard Turkington

at Queens University Belfast, Prof. Manfred Jung at University of Freiburg and Dr. Giovina Ruberti at the Institute of Biochemistry and Cell Biology, IBBC).

d) Assessment of toxicity by determining cytotoxicity and mutagenicity (performed by Dr. Stefania Lamponi at the University of Siena).

2.2.1. Spiroindoline-based HDAC6 inhibitors

To develop novel HDAC6i, our group recently identified a highly potent and selective spiroindoline-capped HDACi (**13**, **Table 1**) with promising anticancer activity against several cancer cell lines.[145] This previous work permitted us to narrow down the spiroindoline scaffold as an optimal cap group for developing selective HDAC6 inhibitors. In this work, we examined the effect of a strategical overturning of the linker and the ZBG moieties from the indoline nitrogen (as in compound **13**) to the piperidine nitrogen (compounds **14-23**). The prototype of this novel series of compounds (**14**, **Table 1**) exhibited a promising HDAC6 inhibition potency with an IC$_{50}$ value of 264.4 nM and a selectivity index of 85 over HDAC1 and 7 over hHDAC8. To get a deeper insight into the binding mode of this compound, a 2.09 Å-resolution X-ray crystal structure was determined of the complex between **14** and the catalytic domain of HDAC6 from *Danio rerio* (zebrafish). The active site features of zebrafish HDAC6 is identical to that of the *human* HDAC6 isoform, and zebrafish HDAC6 yields crystals of higher quality compared to the *human* HDAC6 crystals.[146] Subsequently, molecular modeling approaches were utilized to analyze the binding mode and the structural requirements to design novel "reversed" spiroindolines with an increased HDAC6 inhibitory profile and greater selectivity index. This was realized following two key approaches: i) synthesizing derivatives with bulkier cap-groups, and ii) controlling the outdistancing between the cap-group and the ZBG by inserting amide, urea and carbamate functionalities to the linker portion. The resulting compounds (**15-23**) were then tested for their ability to inhibit the HDAC1, 6 and 8 isoforms.

Thereafter, the most potent and selective compounds were further evaluated for their effects on cell cycle progression and apoptosis in various cancer cell lines.

Table 1: List of newly developed spiroindoline based HDAC6 inhibitors.
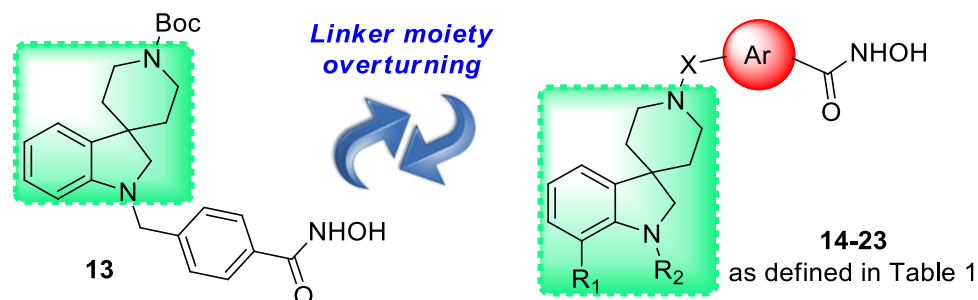
Cmpd	R₁	R₂	X	Ar
14	H	$-CH_3$	$-CH_2-$	
15	H	$-CH_2C_6H_5$	$-CH_2-$	
16	H	$-COC_6H_5$	$-CH_2-$	
17	C_6H_5	$-CH_3$	$-CH_2-$	
18	C_6H_5	$-CH_2C_6H_5$	$-CH_2-$	
19	C_6H_5	$-COC_6H_5$	$-CH_2-$	
20	H	$-CH_3$	$-CH_2-$	
21	H	$-CH_2C_6H_5$	$-COCH_2-$	
22	H	$-CH_2C_6H_5$	$-CONHCH_2-$	
23	H	$-CH_2C_6H_5$	$-COOCH_2-$	

2.2.2. Quinolone based HDAC6 inhibitors

Numerous natural products have been identified as potent anticancer agents, that have inspired chemists to utilize them as building blocks in the synthesis of novel chemotherapeutics.[147] In this context, functionalized 4-arylquinolin-2(1*H*)-ones represent a versatile scaffold for developing biologically active molecules, that includes an orally active anticancer agent

currently under clinical investigation.[148] Based on a comprehensive literature search, we identified the quinolone moiety as a potential cap group due to lipophilic nature *in vitro*. This system fits perfectly in the cap region of the HDACi pharmacophore.[149]

Several quinolone containing compounds are well known as antibiotics (e.g. ciprofloxacin, norfloxacin) and anticancer agents (voreloxin).[150] Quinolone-based anticancer agents exhibit their activity influencing the DNA intercalation process, inhibiting topoisomerase II activity and tubulin polymerization.[151] In our quest to identify novel cap groups to design new potent and selective HDAC6i, we exploited the potential of a naturally occurring compound namely, viridicatin (3-hydroxy-4-phenylquinolin-2(1H)-one), containing the quinolone skeleton as an effective and versatile cap-group suitable for a wide variety of scaffold decorations.[152, 153] Inspired from a multi-component protocol to construct the 3-hydroxy-4-arylquinolin-2(1*H*)-ones, we exploited this method to synthesize a varied set of cap groups.[154] With this methodology, we were able to develop novel HDAC6i bearing *N-* or *O*-appended linker moieties (**Table 2**) and an array of focused modifications at both their heterocyclic core and the aromatic portions. Consequently, we aimed to obtain compounds with high selectivity index over HDAC6 and effectively screen them over different cancer cell lines.

Table 2. List of newly developed quinolone based HDAC6 inhibitors.
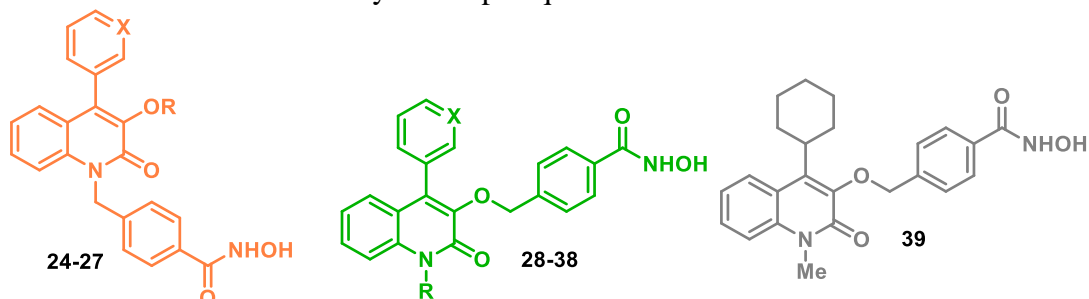
Cmpd	R	X
24	H	CH
25	Me	CH
26	⟨benzyl⟩	CH
27	H	N
28	H	CH
29	Me	CH
30	⟨propargyl⟩	CH
31	⟨benzyl⟩	CH
32	⟨pyridylmethyl⟩	CH
33	⟨benzylpiperidinyl⟩	CH
34	⟨diethylaminomethylbenzyl⟩	CH
35	Me	N
36	⟨benzyl⟩	N
37	⟨pyridylmethyl⟩	N
38	⟨diethylaminomethylbenzyl⟩	N
39	-	-

Chapter 3

Chemistry

3.1. Spiroindoline based HDAC6 inhibitors

For the synthesis of compounds **14-23**, four key-steps were employed to obtain the desired products which include: i) a Fischer indole synthesis, starting from suitable arylhydrazines and *N*-Boc-piperidine-4-carboxaldehyde providing 3,3-disubstituted indolenines, ii) reduction of the imine bond of the indolenines to get the respective indolines, iii) appropriate substitution at the *N*-1 position of the indoline, and, iv) insertion at the piperidine nitrogen with suitable linkers.

3.1.1. Synthesis of compounds 14-19

Synthesis of compounds **14-19** is described in **Scheme 1.** Commercially available 1-Boc-4-piperidone (**40**) was converted to its homologated enol ether derivative by Wittig reaction using (methoxymethyl)triphenylphosphonium chloride in the presence of NaHMDS as the base.[21] The corresponding enol ether was hydrolyzed with cerium(III)chloride in MeCN to obtain **41** in high yield. Compound **41** and the suitable phenyl hydrazine were heated in AcOH at 80 ºC to obtain the corresponding spiroindolenines, by applying a Fischer indole synthetic protocol.[155, 156] These intermediates were then reduced by catalytic hydrogenation to provide thet spiroindolines **42a** and **42b**. A reductive amination of these latter with the suitable aldehydes in the presence of NaBH$_3$CN or treatment with benzoyl chloride in the presence of TEA afforded the *N*-substituted derivatives, which, upon Boc-deprotection, provided amines **43a-f**. A second reductive amination protocol, performed on the piperidine using methyl 4-formyl benzoate followed by treatment of the resulting ester derivatives with NH$_2$OH and aqueous KOH, afforded the desired compounds **14** and **15-19**.

Scheme 1

42a, R_1 = H
42b, R_1 = -C_6H_5

43a, R_1 = H, R_2 = -Me
43b, R_1 = H, R_2 = -$CH_2C_6H_5$
43c. R_1 = H, R_2 = -COC_6H_5
43d, R_1 = C_6H_5 , R_2 = -Me
43e, R_1 = C_6H_5 , R_2 = -$CH_2C_6H_5$
43f, R_1 = C_6H_5 , R_2 = -COC_6H_5

14-19
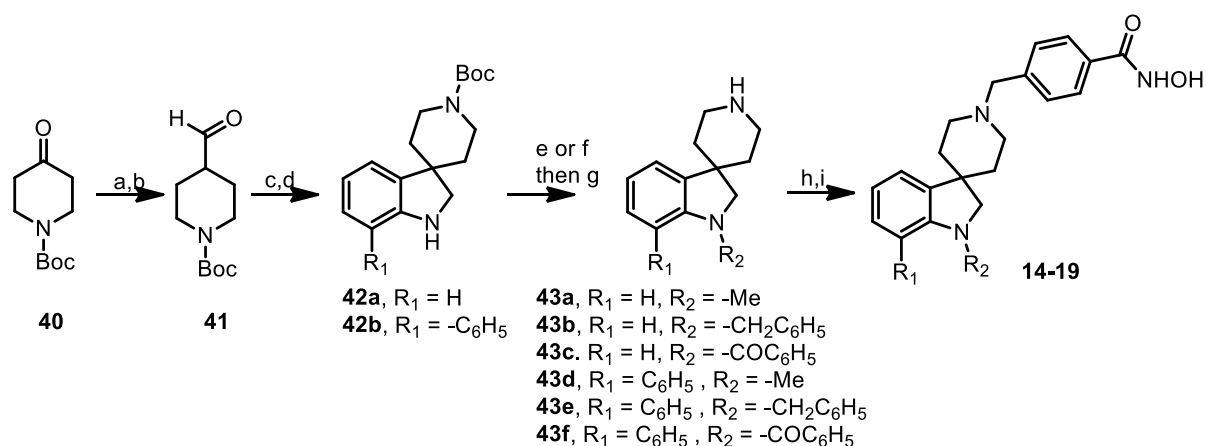
Reagents and conditions: a) $Ph_3P(Cl)CH_2OMe$, NaHMDS, THF, 0 to 25 ℃, 30 min; b) $CeCl_3 \cdot 7H_2O$, NaI, 40 ℃, MeCN, 16 h; c) phenylhydrazine or (1,1-biphenyl)-2-ylhydrazine·HCl , AcOH, 80 ℃, 2 h; d) H_2, Pd/C, MeOH, 25 ℃, 3 h; e) paraformaldehyde or benzaldehyde, $NaBH_3CN$, MeOH, 25 ℃, 8 h; f) benzoyl chloride, TEA, DCM, 25 ℃, 1 h; g) 1 N HCl in MeOH, 25 ℃, 15 min; h) methyl 4-formyl benzoate, $NaBH_3CN$, MeOH, 25 ℃, 8 h; i) NH_2OH (50% wt in H_2O), 4 M KOH in MeOH, DCM/MeOH, 25 ℃, 2 h

3.1.2. Synthesis of compound 20

Synthesis of compound **20** is described in **Scheme 2**. Aldehyde **45** was obtained from the bromo derivative **44** upon reaction with 4-methylmorpholine *N*-oxide (NMO) in MeCN. The successive reductive amination reaction involving **43a** and **45** afforded the methyl ester intermediate, which was converted to the hydroxamate **20**.

Scheme 2
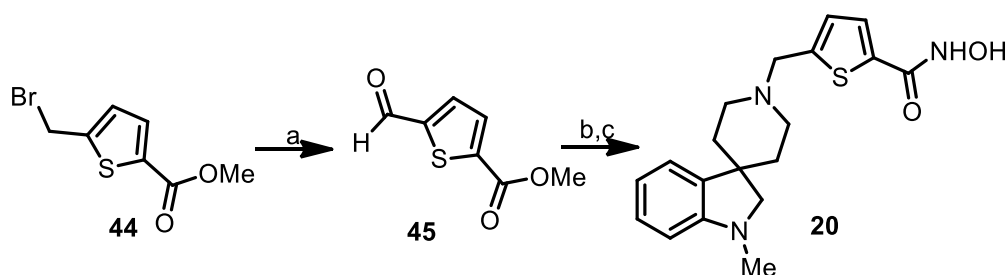
Reagents and conditions: a) NMO, MeCN, 25 ºC, 12 h; b) **43a**, NaBH$_3$CN, MeOH, 25 ºC, 8 h; c) NH$_2$OH (50% in H$_2$O), KOH, DCM, MeOH, 25 ºC, 2 h.

3.1.3. Synthesis of the compounds 21-23

Synthesis of the compounds **21-23** is described in **Scheme 3**. 2-(4-(methoxycarbonyl)phenyl)acetic acid was coupled with amine **43b** and the resulting methyl ester intermediate was converted to the corresponding hydroxamic acid **21**. To synthesize the urea **22**, the key intermediate was methyl 4-(isocyanatomethyl)benzoate which was reacted with **43b** to obtain the methyl ester intermediate subsequently converted to the hydroxamic acid **22**. Finally, the carbamate **23** was prepared by reacting amine **43b** with the commercially available methyl 4-(hydroxymethyl)benzoate in the presence of CDI in DCM to afford the methyl ester intermediate needed for subsequent conversion into the corresponding hydroxamic acid **23**.

Scheme 3

22, X = NH
23, X = O,

43b

21
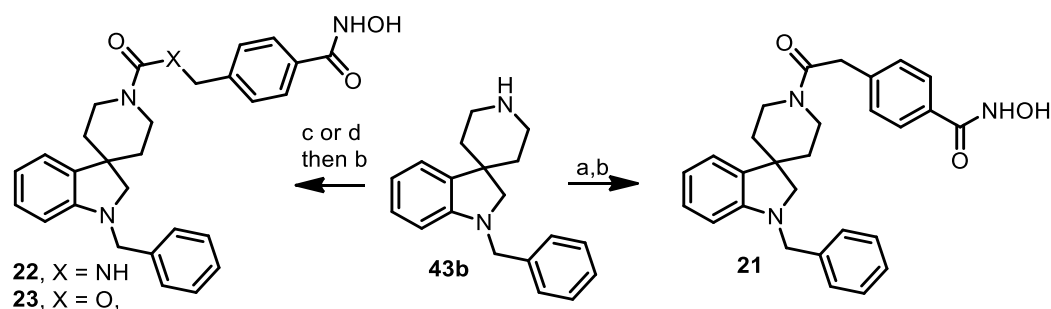
Reagents and conditions: (a) 2-(4-(methoxycarbonyl)phenyl)acetic acid, EDCI, HOBt, DIPEA, DCM, 0° to 25 °C, 24 h; b) NH_2OH (50% in H_2O), KOH, DCM, MeOH, 25 °C, 2 h; c) methyl 4-(isocyanatomethyl)benzoate, TEA, dry THF, 45 °C, 2 h; d) methyl 4-(hydroxymethyl)benzoate, CDI, DCM, 0° to 25 °C, 6 h.

3.2. Quinolone based HDAC6 inhibitors

In order to achieve the synthesis of the quinolone core of the compounds **24-39**, the ring expansion procedure described by Tangella *et al* was applied.[154] It is a multicomponent reaction involving: an aldehyde, activated with *p*-toluenesulfonyl hydrazide (PTSH), and a *N*-substituted isatin in the presence of K_2CO_3 as base.

3.2.1. Synthesis of compounds 24-27

In **Scheme 4** the synthesis of the compounds **24-27** is described. Isatin (**46**) was alkylated with methyl 4-(bromomethyl)benzoate and the resulting product **47** was subjected to the ring expansion procedure with benzaldehyde or 3-pyridinecarboxaldehyde obtaining compounds **48a,b**, respectively. As expected, a transesterification with EtOH occurred in this step. Intermediates **48a** and **48b** were converted to their corresponding hydroxamic acid derivatives **24, 27** after treatment with a strong excess of NH_2OH in the presence of KOH. Intermediate **48a** was also submitted to *O*-alkylation with MeI or benzyl bromide providing derivatives **49a,b**, respectively. These latter were converted into final compounds **25, 26** upon reaction with hydroxylamine and potassium hydroxide.

Scheme 4

46 47 48a X = CH
48b X = N

24 X = CH
27 X = N

49a R = Me
49b R = Bn

25 R = Me
26 R = Bn
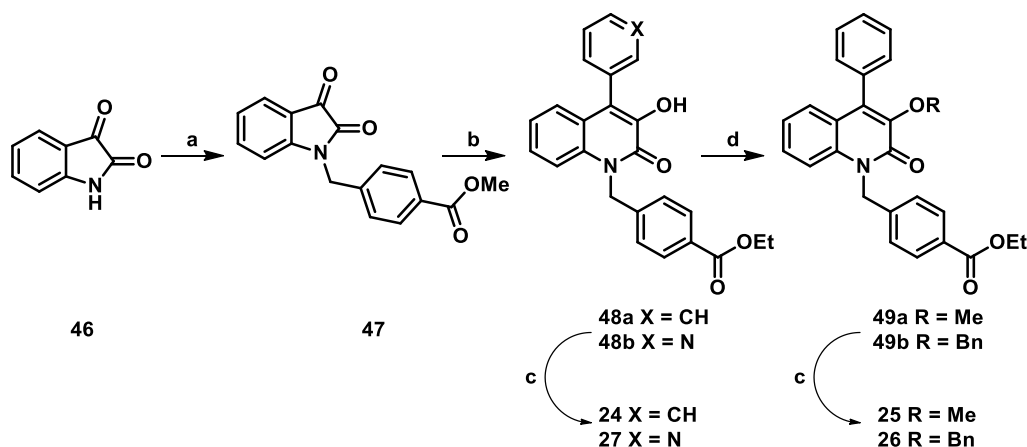
Reagents and conditions: (a) methyl 4-(bromomethyl)benzoate, NaH, DMF, 0 to 25 °C, 12 h; (b) PTSH, benzaldehyde or 3-pyridinecarboxaldehyde, K_2CO_3, EtOH, 80 °C, 12 h; (c) NH_2OH, KOH, DCM, MeOH, H_2O, 25 °C, 3 h; (d) MeI, NaH, THF, 0 to 25 °C, 12 h; or BnBr, KI, K_2CO_3, DMF, 80 °C, 12 h.

3.2.2. Synthesis of compounds 28-30, 35 and 39

In **Scheme 5** is reported the synthesis of compounds **28-30, 35** and **39**. The ring expansion performed on isatin (**46**) in the presence of benzaldehyde or 3-pyridinecarboxaldehyde provided quinolone derivatives **50a,b**, respectively. These latter were subjected to alkylation reaction with methyl 4-(bromomethyl)benzoate in the presence of K_2CO_3 as the base to furnish the *O*-alkylated intermediates **51a,b**. Treatment of **51a** with NH_2OH in the presence of KOH led to compound **28**. Alternatively, alkylation of the lactam nitrogen of **51a,b** with MeI or propargyl bromide followed by reaction with NH_2OH, led to the *N*-alkyl derivatives **29, 30,** and **35**. For the synthesis of compound **39**, isatin was alkylated with MeI and successively subjected to the ring expansion reaction with cyclohexanecarboxaldehyde obtaining compound **53**. From this intermediate, compound **39** was obtained as previously described.

Scheme 5
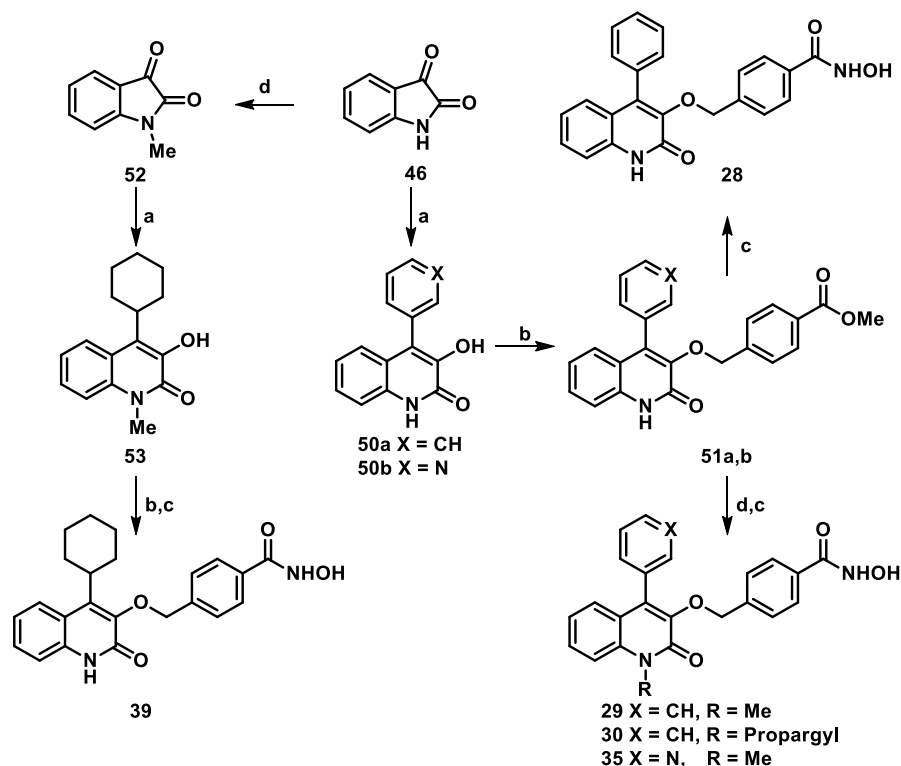
Reagents and conditions: (a) PTSH, benzaldehyde or 3-pyridinecarboxaldehyde, K_2CO_3, EtOH, 80 °C, 12 h; (b) Methyl 4-(bromomethyl)benzoate, K_2CO_3, KI, DMF, 80 °C, 12 h; (c) NH_2OH, KOH, DCM, MeOH, H_2O, 25 °C, 3 h; (d) MeI/ propargyl bromide, NaH, THF, 0 to 25 °C, 12 h.

3.2.3. Synthesis of bromo-derivatives 56 and 59.

In **Scheme 6** is reported the synthesis of bromides **56** and **59** used as alkylating agents for the synthesis of final compounds **32**, **34** and **38**. 4-Pyridinecarboxaldehyde (**54**) was reduced to alcohol **55** with $NaBH_4$ and then converted to the corresponding bromide **56** after treatment with PBr_3. Instead, for the synthesis of the intermediate **59**, 4-(bromomethyl)benzonitrile (**57**) was reduced with DIBAL to the corresponding benzaldehyde **58**, that was successively protected to its dioxolane derivative **59** with ethylene glycol in the presence of PTSA.

Scheme 6

Reagents and conditions: (a) NaBH$_4$, MeOH, 0 to 25 to 25 °C, 2 h; (b) 48% HBr, 100 °C, 4 h then PBr$_3$, DCM, 45 °C, 4 h; (c) DIBAL, DCM, -78 to 0 °C, 1 h; (d) ethylene glycol, PTSA, toluene, 110 °C, 12 h.

3.2.4. Synthesis of compounds 31, 32, 36, and 37

In **Scheme 7** the synthesis of final compounds **31, 32, 36,** and **37** is described. Isatin (**46**) was alkylated with benzyl bromide or bromide **56** using NaH as the base to generate intermediates **60a,b**. These compounds were subjected to the previously described ring expansion procedure with benzaldehyde or 3-pyridinecarboxaldehyde to provide the desired quinolones **61a-d** that were converted to the final compounds **31, 32, 36,** and **37** in the presence of NH$_2$OH as previously described.

Scheme 7
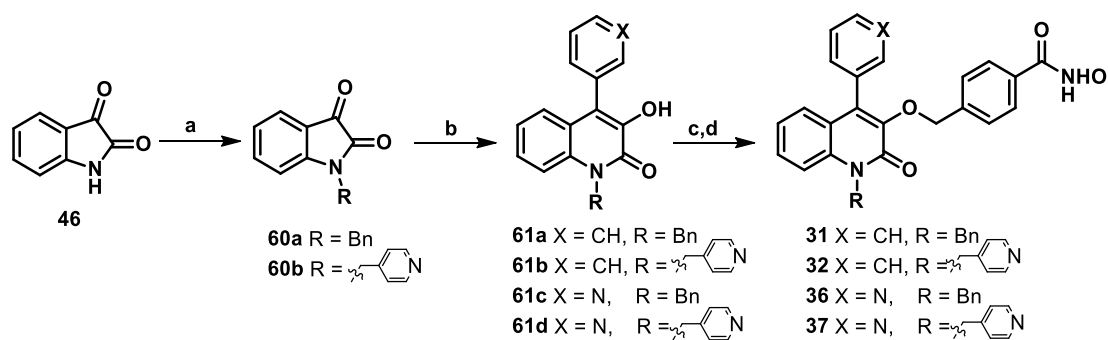
Reagents and conditions: (a) BnBr or **56**, NaH, DMF, 0 to 25 °C, 12 h; (b) PTSH, benzaldehyde or 3-pyridinecarboxaldehyde, K_2CO_3, EtOH, 80 °C, 12 h; (c) methyl 4-(bromomethyl)benzoate, K_2CO_3, KI, DMF, 80 °C, 12 h; (d) NH_2OH, KOH, DCM, MeOH, H_2O, 25 °C, 3 h.

3.2.5. Synthesis of compound 33

The synthesis of compound **33** is described in **Scheme 8**. Since alkylation of the isatin with 1-benzyl-4-bromo or iodopiperidine failed in all the attempted conditions, *N*-alkylated isatin **65** was prepared starting from piperidone (**62**) which was first *N*-benzylated and then subjected to a reductive amination protocol with aniline in presence of $NaBH(OAc)_3$ providing intermediate **64**. This compound was treated with oxalyl chloride, obtaining an unstable intermediate that was immediately treated with $AlCl_3$ in DCM to afford isatin derivative **65** under Friedel-Craft conditions. Ring expansion, alkylation and final reaction with NH_2OH were then performed as previously described, leading to the formation of compound **33**.

44

Scheme 8
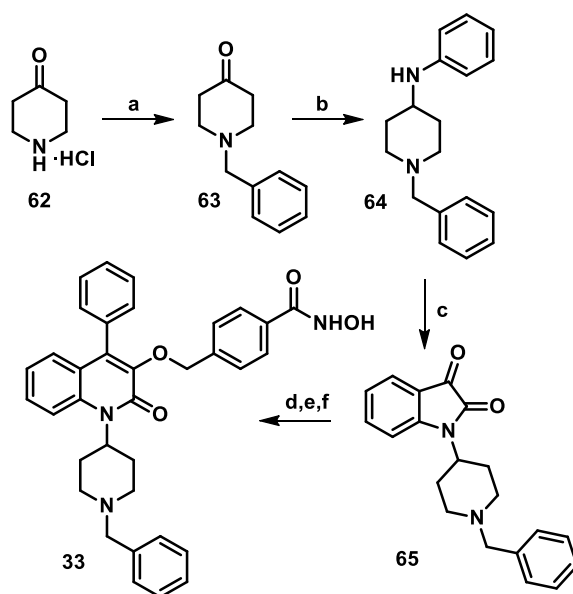
Reagents and conditions: (a) benzyl bromide, K_2CO_3, DMF, 80 °C, 12 h; (b) aniline, $NaBH(OAc)_3$, DCM, AcOH, 0 to 25 °C, 12 h; (c) oxalylchloride, DCM, 25 °C, 2 h; then $AlCl_3$, DCM, 40 °C, 2 h; (d) PTSH, benzaldehyde, K_2CO_3, EtOH, 80 °C, 12 h; (e) methyl 4-(bromomethyl)benzoate, K_2CO_3, KI, DMF, 80 °C, 12 h; (f) NH_2OH, KOH, DCM, MeOH, H_2O, 25 °C, 3 h.

3.2.6. Synthesis of compounds 34 and 38

In **Scheme 9** the synthesis of the compounds **34, 38** is described. Isatin was alkylated with bromide **59** affording intermediate **66**. This compound was subjected to the previously described ring expansion procedure to get the desired quinolones **67a,b**. These intermediates were alkylated with methyl 4-(bromomethyl)benzoate obtaining **68a,b** which were subsequently deprotected in acidic medium, and the corresponding free aldehydes were subjected to a reductive amination protocol with diethylamine in the presence $NaBH(OAc)_3$, affording the corresponding diethylamino derivatives, that were converted to the final compounds **34, 38** as previously described.

45

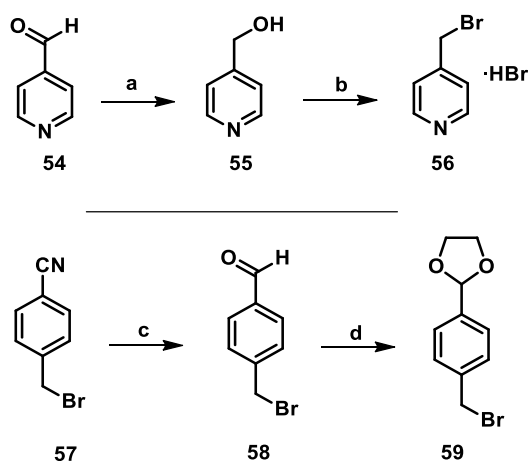**Scheme 9**
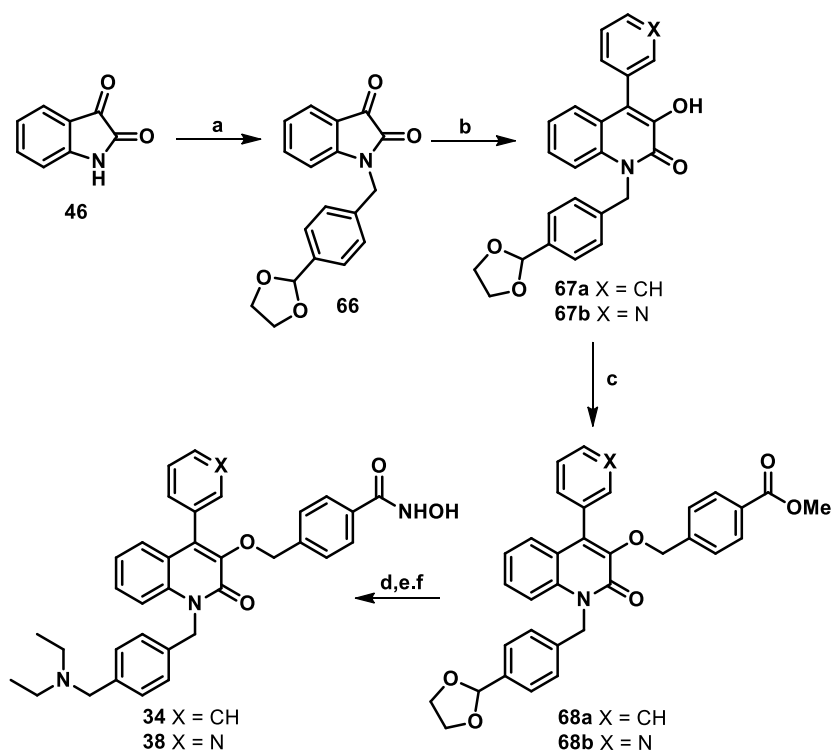
Reagents and conditions: (a) **59**, NaH, DMF, 0 to 25 °C, 12 h; (b) PTSH, benzaldehyde or 3-pyridinecarboxaldehyde, K_2CO_3, EtOH, 80 °C, 12 h; (c) methyl 4-(bromomethyl)benzoate, K_2CO_3, KI, DMF, 80 °C, 12 h; (d) 6 N HCl, THF, 25 °C, 1 h; (e) diethylamine, $NaBH(OAC)_3$, DCM, AcOH, 0 to 25 °C, 12 h; (f) NH_2OH, KOH, DCM, MeOH, H_2O, 25 °C, 3 h.

46

Chapter 4

Results and discussion

4.1. Spiroindoline series (compounds 14-23)
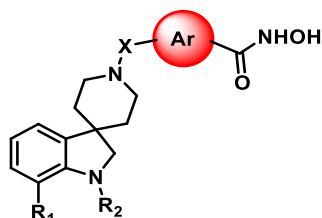
Table 3. Inhibitory activity of compounds **14-23** and reference compounds (tubastatin A) against hHDAC1, as IC$_{50}$ (μM), and hHDAC6, as IC$_{50}$ (nM)**.**

Cpd	R$_1$	R$_2$	X	Ar	HDAC1 IC$_{50}$ (μM)[a] or % of inhibition at 1 μM	HDAC6 IC$_{50}$ (nM)[a] or % of inhibition at 1 μM	HDAC1/HDAC6
14	H	-CH$_3$	-CH$_2$-		22.4 ± 6	264.4 ± 45	85
15	H	-CH$_2$C$_6$H$_5$	-CH$_2$-		6.5 ± 0.8	561.0 ± 203	12
16	H	-COC$_6$H$_5$	-CH$_2$-		10.1 ± 2.1	155.0 ± 26	65
17	C$_6$H$_5$	-CH$_3$	-CH$_2$-		8.5%	50.0%	n.d.
18	C$_6$H$_5$	-CH$_2$C$_6$H$_5$	-CH$_2$-		2.9%	29.7%	n.d.
19	C$_6$H$_5$	-COC$_6$H$_5$	-CH$_2$-		4.7 ± 0.5	465.0 ± 122	10
20	H	-CH$_3$	-CH$_2$-		6.6 %	51.3%	n.d.
21	H	-CH$_2$C$_6$H$_5$	-COCH$_2$-		10.2 ± 1	227.0 ± 97	45
22	H	-CH$_2$C$_6$H$_5$	-CONHCH$_2$-		3.6 ± 0.3	110.0 ± 19	33
23	H	-CH$_2$C$_6$H$_5$	-COOCH$_2$-		6.8 ± 0.3	48.5 ± 23	140
Tubastatin A	-	-	-	-	1.91 ± 0.42	30.4 ± 2.1	63

[a]All compounds were assayed at least two times, and the results are expressed with standard deviations.

The 2.09 Å-resolution crystal structure of the HDAC6 CD2-**14** complex reveals that the inhibitor hydroxamate group coordinates to the catalytic Zn^{2+} ion with a bidentate geometry (**Figure 13**). The Zn^{2+}-bound hydroxamate C=O group accepts a hydrogen bond from Y745, the Zn^{2+}-bound hydroxamate N-O⁻ group accepts a hydrogen bond from H573, and the hydroxamate NH group donates a hydrogen bond to H574. This constellation of intermolecular interactions with catalytically important residues accounts for the generally high affinity of hydroxamate-based inhibitors in the HDAC6 active site.

The *para*-substituted phenyl linker makes favorable offset π-π interactions in the aromatic crevice defined by F583 and F643. The piperidine ring adopts a chair conformation and the piperidine nitrogen forms a hydrogen bond with a water molecule that in turn hydrogen bonds with the backbone carbonyl of R798. The spiroindoline capping group is oriented toward the L2 pocket at the mouth of the active site. There, the indoline nitrogen hydrogen bonds with a water molecule that in turn hydrogen bonds with N645 and a second water molecule; a third water molecule completes a hydrogen bond network between the indoline nitrogen and Zn^{2+} ligand H614. Although the inhibitor makes no direct enzyme-inhibitor hydrogen bonds apart from those made with the hydroxamate moiety, it is interesting that three water molecules comprise a "wet" hydrogen bonded interface in such a high-affinity enzyme-inhibitor pair.

It is relatively rare to see inhibitor capping groups bind in the L2 pocket, since most tend to bind in the L1 pocket on the opposite side of the active site. [124, 157-160] It appears that the chair conformation of the piperidine ring combined with the molecular structure of the novel spiro-fused indoline moiety yields a structure and a conformation that is ideal for binding within the L2 pocket.
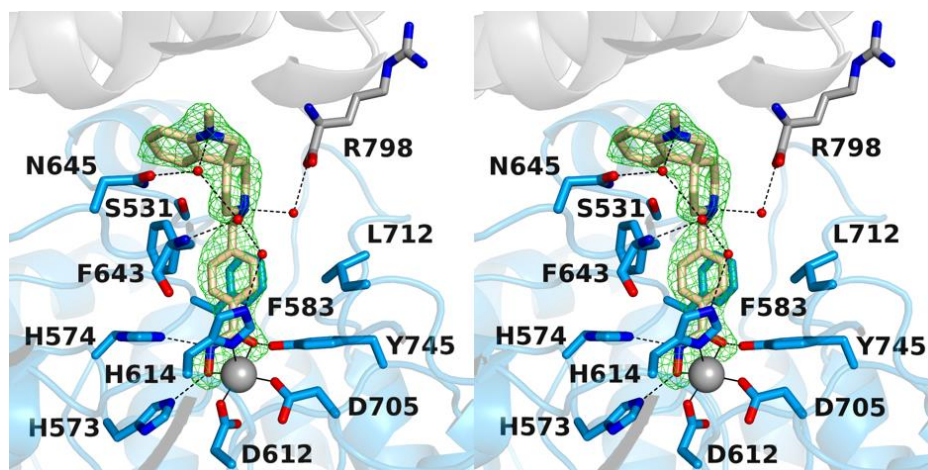
Figure 13. Stereoview of a Polder omit map of the HDAC6-**14** complex for which the atomic coordinates of **14** were omitted from the structure factor calculation (PDB 6V7A; contoured at 5.0 σ). Atoms are color-coded as follows: C = light blue (HDAC6 catalytic domain 2), light gray (symmetry mate), or wheat (inhibitor), N = blue, O = red, Zn^{2+} = gray sphere, and solvent = small red spheres. Metal coordination and hydrogen bond interactions are indicated by solid and dashed black lines, respectively.

The *in vitro* inhibitory profile of the newly developed compounds **14-23** (**Table 4**) was evaluated against both *h*HDAC1 and 6 isoforms. SAR studies were performed by taking into consideration the data obtained from *in vitro*, X-ray and computational studies. These calculations outlined the preferential binding of the "reversed" spiroindoline compounds towards HDAC6. To get a better understanding of the behavior of the compounds in the binding sites of *h*HDAC1 and 6 we performed docking studies based on a previously reported protocol.[152, 153] It was observed that the hindrance imposed by a bulkier cap group allowed the compound to be better accommodated into the HDAC6 enzyme with respect to the HDAC1 isoform. Accordingly, we herein report the docking outputs of **14** (**Figure 14**) and **23** (**Figure 15**), two of the most selective derivatives of the series with respective selectivities for HDAC 1 of 85- and 140-fold.

Figure 14. Docked poses of **14** into HDAC1 (panel A) and HDAC6 (panel B). Compound **14** is represented by purple sticks while the residues in the active sites are represented by lines and the protein is represented in cartoon form. Zn^{2+} is represented by a gray sphere. H-bonds are shown as by black dotted lines, while the red solid lines represent the metal coordination bonds.

Based on these studies, limited contacts were established by **14** within the HDAC1 binding site (**Figure 14A**) compared to the contacts established within the HDAC6 binding site (**Figure 14B**). In fact, **14** was able to coordinate with the metal ion in HDAC1 by its hydroxamic moiety through polar contacts with the backbone of G149 and the sidechain of Y303. In addition, we observed only a π-π stacking with H141 and some hydrophobic interactions with Y204, F205 and L271. On the contrary, the docking output of **14** into HDAC6 showed an improvement of the number of the contacts. In this accommodation, the hydroxamic acid moiety in addition to the metal coordination bond with the Zn^{2+} ion, established a series of supplementary H-bonds

50

with the sidechain of Y782 and H610 and with the backbone of G619. Moreover, the benzyl linker was able to establish a double π-π stacking with F620 and H651. We also noted relevant hydrophobic interactions with F679, F680, M682 and L749. This pattern of interaction perfectly supported the selectivity of **14** towards HDAC6 over HDAC1 (IC$_{50}$ HDAC1 = 22.4 µM; IC$_{50}$ HDAC6 = 264.4 nM).

Compounds **15-20** were mainly synthesized in order to investigate the role of the cap-group and its bulkiness on HDAC potency and selectivity, while maintaining unvaried the benzyl moiety of the linker.

Compound **15**, bearing a pendant benzyl group on the indoline nitrogen of the cap portion, was found to be largely solvent exposed owing to its bulkiness thereby reducing the ligand efficiency. In particular, it showed a π-π stacking with F150 through its benzyl moiety. **15** showed a decreased number of the contacts with HDAC6 with the loss of the key π-π stacking with F680 (IC$_{50}$ HDAC1 = 6.5 µM; IC$_{50}$ HDAC6 = 561 nM). The *N*-benzoyl functionality led to a similar pattern of interaction as for **15** with the exclusion of a π-π stacking with F150. As regards HDAC6, **16** was able to restore the π-π stacking with F680. Moreover, the carbonyl group belonging to the benzoyl functionality established an H-bond with the sidechain of F680 (IC$_{50}$ HDAC1 = 10.1 µM; IC$_{50}$ HDAC6 = 155 nM). In compound **17**, the bulk was increased by introducing a phenyl ring on the indoline aromatic moiety, while inserting a methyl group on the indoline nitrogen. In this case, we observed a reduction in hydrophobic contacts as well as a loss of key H-bond interaction, namely with the sidechain of Y303 in HDAC1 and the sidechain of H610 in HDAC6. This pattern accounted for a weak inhibition towards both enzymes with respect to compound **14** with a percentage of inhibition of 8.5% for HDAC1 and of 50% for HDAC6 when tested at 1 µM. The introduction of a *N*-benzyl moiety as in compound **18** resulted in the least potent compound of the series. In full agreement with *in vitro* data, the cap group was found completely solvent exposed for both enzymes. Notably, **19**,

bearing a benzoyl group in place of the benzyl of **18**, was able to establish a H-bond with the backbone of F205 by its carbonyl group. In addition, a strong network of hydrophobic interactions with Y204 and L271 in HDAC1, while an additional π-π stacking with F679 was detected in HDAC6. This accounted for the three-digit nM potency of inhibition of HDAC6 and a µM inhibitory activity for HDAC1 (IC_{50} HDAC6 = 465 nM: IC_{50} HDAC1 = 4.7 µM). In compound **20** the bioisosteric replacement of the phenyl ring of **14** with a thiophene led to a decrease in affinity towards both enzymes as already observed by us in the previously reported series of spiroindoline-based HDAC inhibitors.[152]

Based on the computational insights and X-ray co-crystal structure, we synthesized compound **21** in which we moderately extended the region between the linker and the cap group by replacing the benzyl -CH_2- with a -$COCH_2$- moiety. Moreover, we increased the bulkiness of the cap-group by introducing a pendant benzyl group on the indoline nitrogen. As expected, we observed a slight improvement in the inhibitory potency against both isoforms. In fact, in addition to the contacts found for **14, 21** was able to produce an additional π-π stacking with F205 of HDAC1 through the benzyl functionality. With respect to HDAC6, we observed for the same pattern of interaction for **21** as already described for **14** with an additional π-π stacking with F680. This incremental increase in the number of contacts is reflected by an improved inhibitory potency towards both enzymes, although the stronger affinity for HDAC6 was preserved (IC_{50} HDAC1 = 10.2 µM; IC_{50} HDAC6 = 227 nM). Compound **22** demonstrated that the urea functionality was very well tolerated by both enzymes, as we registered a strong improvement in inhibitory potencies against HDAC1 as well as HDAC6. In the case of HDAC1 enzyme, **22** established two further interactions besides those described for **21**, namely i) an H-bond with the sidechain of H178, and ii) a cation-π stacking with K200. With respect to the HDAC6 enzyme, **22** interacts with the same residues described for **21**, displaying an additional

H-bond between the sidechain of S568 and the urea NH. This accounts for an increase in inhibitory potency against both enzymes (IC$_{50}$ HDAC1 = 3.6 µM; IC$_{50}$ HDAC6 = 110 nM).
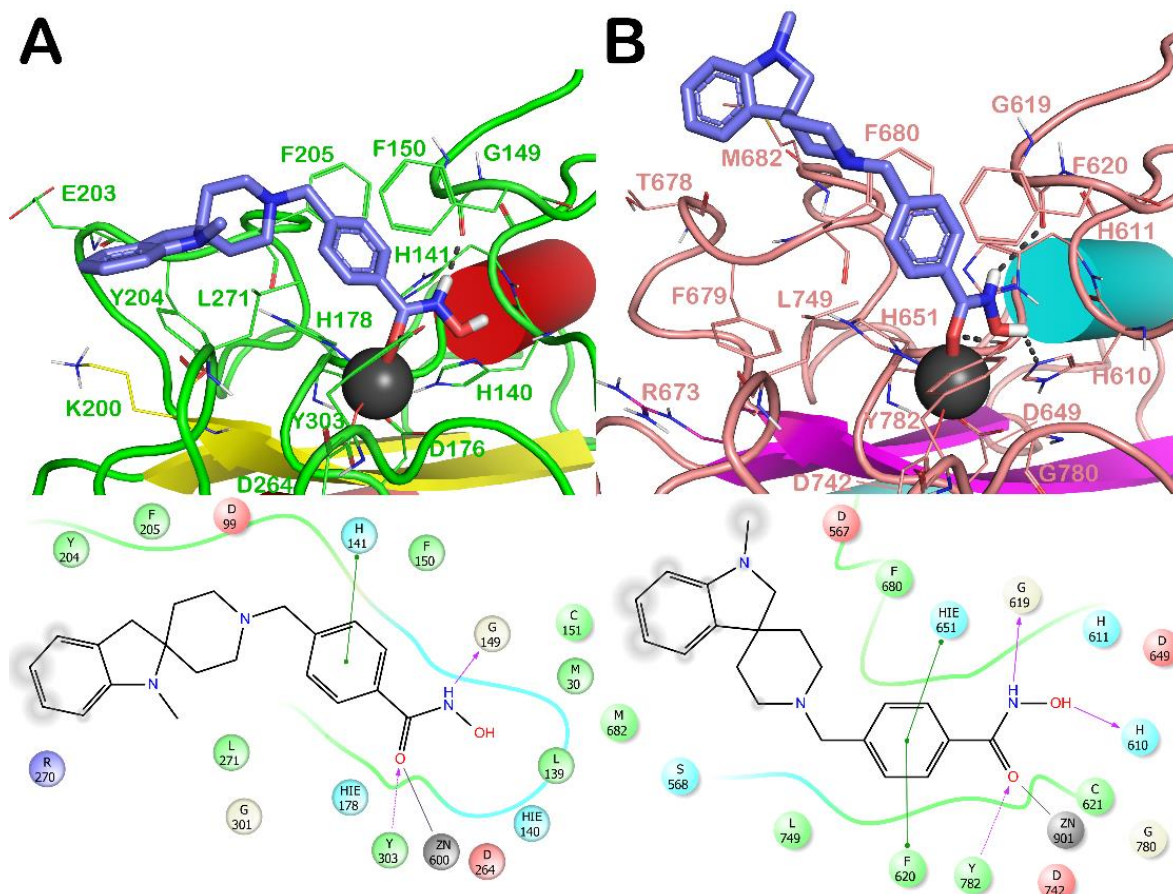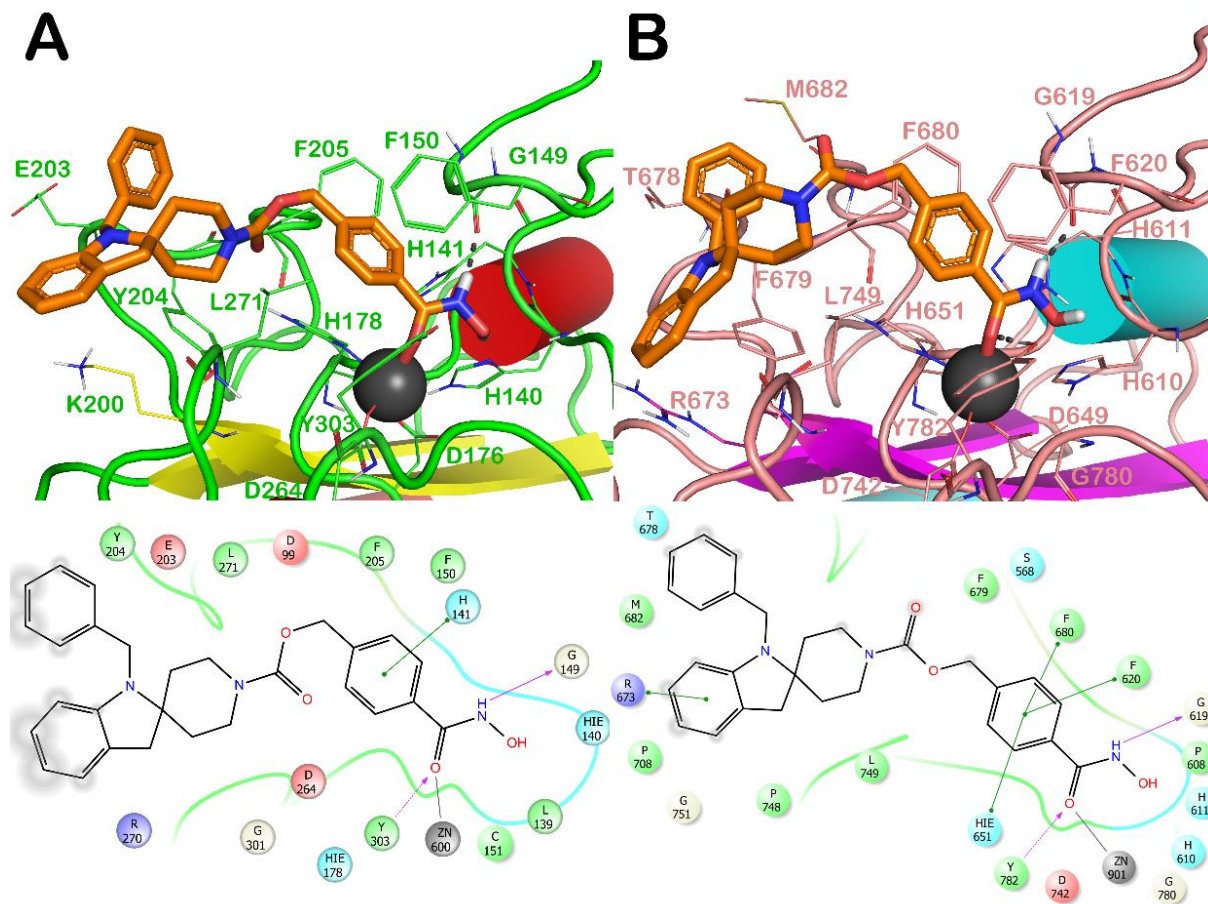

Figure 15. Docked poses of **23** into HDAC1 (panel A) and HDAC6 (panel B). Compound **23** is represented by orange sticks while the residues in the active sites are represented by lines and the protein is represented by cartoon. Zn^{2+} is represented by a gray sphere. H-bonds are represented by black dotted lines, while the red lines represent the metal coordination bonds.

Gratifyingly, the introduction of a carbamic functionality to replace the urea moiety led to **23** that showed a relevant improvement in terms of both potency and selectivity towards HDAC6 over HDAC1. The limited contacts established by **23** within the HDAC1 binding site (**Figure 15A**) relative to HDAC6 (**Figure 15B**) explain the improved potency and selectivity profiles

of **23** over **14**. Indeed, **23** was only able to form with HDAC1 the same contacts already described for **14** without any additional interaction. In addition, the bulkier cap group was found to be largely solvent exposed reducing the ligand efficiency. On the other hand, the docking output of **23** into HDAC6 showed a huge improvement of the number of the contacts. Its hydroxamic acid moiety in addition to the metal coordination bond with the Zn^{2+} ion, established a series of H-bonds with the sidechain of Y782 and with the backbone of G619. Moreover, for this compound the benzyl linker was able to establish a triple π-π stacking with F620, F680 and H651. Also, relevant hydrophobic interactions with T678, F679, M682 and L749 were observed. Notably, the pendant benzyl group of the cap portion established a cation-π stacking with R673. This pattern of interaction is in strong agreement with the potency and selectivity profile observed for **23** (IC$_{50}$ *h*HDAC1 = 6.8 µM; IC$_{50}$ *h*HDAC6 = 48 nM; IC$_{50}$ *h*HDAC8 = 3.9 µM). A further computational investigation on **14** was performed using the crystal structure of *zf*HDAC6 (zebrafish HDAC6) in complex with **14** in comparison with docking 3D models of **14** with *h*HDAC6 and *zf*HDAC6. **14** accommodated in a similar fashion in both *zf*HDAC6 and *h*HDAC6 enzymes, with only slight differences caused by the different residues within the binding sites. In fact, we noted three main differences in the studied binding sites, the residues D567, T678 and M682 in *h*HDAC6 are replaced by N530, A641 and N645 in *zf*HDAC6. In particular, the presence of M682 in *h*HDAC6 contributed to a slightly different orientation of the cap group that is more solvent exposed with respect to the crystal structure and the docked pose of *zf*HDAC6. However, this study confirms that the *zf*HDAC6 could represent a valuable model for translating the results of potential inhibitors to the *h*HDAC6.

In addition to HDAC1 and 6, the potency of three representative inhibitors (**14, 22, 23 Table 5**) was assessed on HDAC8 isoform, which represents a unique member of the class I HDAC family. HDAC8 is endowed with the ability to recognize both histone and non-histone substrates and is ubiquitously expressed and it can localize either in the nucleus or in the

cytoplasm.[28] To our delight, the three compounds demonstrated low activity on HDAC8 (from 1.91-3.19 µM, **Table 4**), thus confirming their significant selective profile towards HDAC6 enzyme.
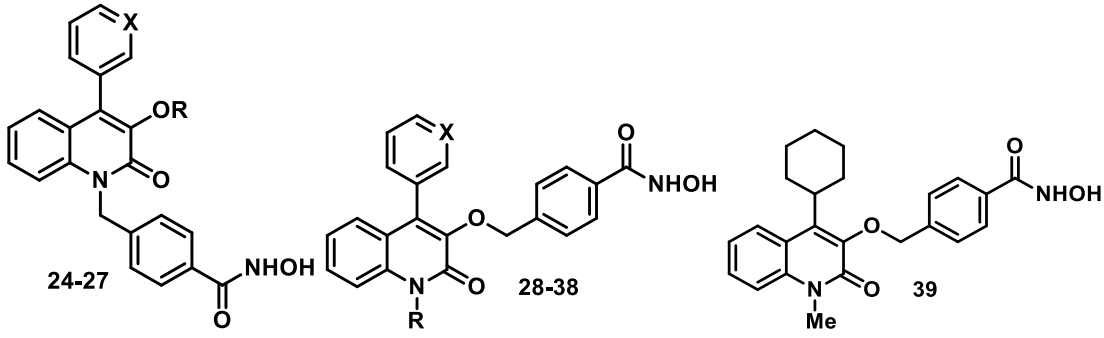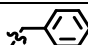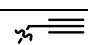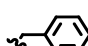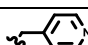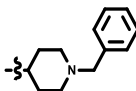
Table 4. Inhibitory activity of compounds **14, 22, 24** as IC_{50} (µM), against the *h*HDAC8 enzyme
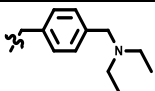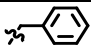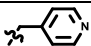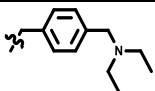
Cpd	**14**	**22**	**23**	**TubA**
IC_{50} (µM)[a]	1.91 ± 0.33	2.48 ± 0.67	3.19 ± 1.51	0.695

[a]All compounds were assayed at least two times, and the results are expressed with standard deviations.

4.2. Quinolone series (compounds 24-39)

Table 5. Novel HDAC6 inhibitors **24-39**.

Cpd	R	X	HDAC1 IC50 (μM) or inhibitory%	HDAC6 (nM)	HDAC6/HDAC1
24	H	CH	10.9 ± 1.3 μM	307.7 ± 50.7	3.6
25	Me	CH	4.5 ± 0.31 μM	61.6 ± 7.5	73
26	(benzyl)	CH	5.5 ± 0.3 μM	84.5 ± 7.9	65
27	H	N	50 μM 96,4% 25 μM 82,1% 10 μM 36,4% 1 μM - 4,2%	295.6 ± 24.4	n.d.
28	H	CH	6.6 ± 0,38 μM	146.9 ± 14.2	45
29	Me	CH	50 μM 79,9% 25 μM 45,9% 10 μM 26,2% 1 μM 0,0%	518.9 ± 17.1	n.d.
30	(propargyl)	CH	6.1 ± 0.93 μM	82.3 ± 11.4	74
31	(benzyl)	CH	50 μM 96,8% 25 μM 92,5% 10 μM 76,2% 1 μM 17,1%	176.0 ± 14.7	n.d.
32	(pyridylmethyl)	CH	1.2 ± 0.20	84.1 ± 9.9	14
33	(benzylpiperidinyl)	CH	50 μM 79,1% 25 μM 66,7% 10 μM 46,1%	870.4 ± 87.8	n.d.

			1 µM 0,01%		
34		CH	0.322 ± 0.073	6.9 ± 0.9	46
35	Me	N	5.01 ± 0.44	45.6 ± 4.8	109
36		N	2.5 ± 0.41	25.6 ± 3.1	96
37		N	1.7 ± 0.31	45.3 ± 5.6	38
38		N	0.319 ± 0.08	11.5 ± 1.5	29
39	-	-	3.0 ± 0.18	33.0 ± 2.6	91

By coupling the *in vitro* data with computational studies, we performed a SAR analysis for our compounds. Starting from the molecular docking calculations using Glide employing Standard Precision (SP) as scoring function and visual inspection we were able to understand the general trend of the preferred binding modes of quinolone derivatives on HDAC1 and HDAC6 isoforms. Keeping on with the already described inhibitors, for our newly developed derivatives we retained the *para*-hydroxamic functionality, anchored to the benzyl linker, as the ZBG. Among the derivatives the polar contacts established by the hydroxamic acid of the ZBG were similar and represented by three H-bonds established between the carbonyl and Y782, the NH and G619, the OH and H610. Considering the specific contacts, we primarily focused our attention to the best positioning of the ZBG on the quinolone scaffold (heterocyclic nitrogen *vs* exocyclic hydroxy group). The binding mode of compounds **25**, **28**, **30**, **35**, **37**, **38** and **39** is depicted in **Figure 16A**. The whole orientation of the scaffold of compound **25**, the best performing derivative among the ZBG *N*-substituted series, presented a binding mode different from the other analogues. The pendant phenyl ring and the benzo-fused system of **25** were projected towards the hydrophobic residues of the pocket L749, F679 and F680 while the methoxy substituent at C3 was not able to target any residue within the binding site. The optimal accommodation within the catalytic site was achieved by the introduction of the ZBG

on the oxygen atom at C3. In the ZBG *N*-substituted analogues the whole molecule was oriented to the opposite side. This effect was amplified when *N*1 bulky substituents were introduced on the nitrogen. Accordingly, compound **28**, with no substituents on *N*1, was able to establish three π-π stackings with F620, H651 and F680 through the phenyl ring of the ZBG, and an additional H-bond between H651 and the carbonyl of the quinolone core. The introduction of a hydrophobic substituent on the nitrogen determined a different rotation of the cap group compared to **28**, as observed for compounds **29-31** (methyl, propargyl and benzyl moieties respectively). These two structural arrangements led to a comparable inhibitory activity for the two series of analogues (ZBG *N*-substituted **24-27** and ZBG *O*-substituted **28-31**) and no gain in selectivity for the two investigated HDAC isoforms. The docking output showed a different putative binding mode for both the series (a representative pose of compound **30** is reported in **Figure 16C**). Compound **30**, besides the already described polar contacts established by the hydroxamic acid, stacks with F620, placing the propargyl substituent towards the loops surrounding the binding site. This event was also observed for compounds **29** and **31**, which prompted us to explore and add some moieties able to establish more polar contacts within the region between the loop comprising D567 and S568 and the opposite one that comprises of residue D497 of the HDAC6 binding site. In contrast, these two loops present in the HDAC1 isoform are different in terms of arrangement and length (**Figure 17**). With the aim to improve the solubility of these molecules we introduced some basic functionalities on the quinolone scaffold. These considerations led to the development of compounds **27**, **32-38** bearing a pyridine at C4, benzylpiperidine and diethylaminomethylbenzyl groups at *N*1 (**Figure 16**). The introduction of a pyridin-3-yl instead of the phenyl ring in 4-position (compound **27**), gave better results in terms of selectivity between the two investigated isoforms, compared to its parent compound **24**. These findings prompted us to evaluate the introduction of the 4-methylenepyridine system at *N*1 on the O-

substituted series. With compound **32** although establishing a polar contact through the nitrogen of the pyridine with the backbone of S568, the selectivity profile towards the HDAC6 was not satisfactory, since a similar set of contacts were established also with the HDAC1 isoform. The insertion of the different basic functionalities like the benzylpiperidine, as for compound **33**, resulted in an increase in the size of the molecule that precluded the formation of any relevant H-bond, decreasing the HDAC6 inhibitory potency. On the contrary, with the development of compound **34** bearing a diethylaminomethylbenzyl portion at *N*1 we obtained the best performing compound on HDAC6, with a potency in the low nanomolar range. Moreover, compound **34** showed a different bidentate chelation pattern of interaction, since the ZBG was able to bind deeper in the catalytic site. As expected, the more flexible and protonatable diethylaminomethylbenzyl substituent allowed to form not only a new and not previously observed H-bonding with the D497 residue, but also a strong salt bridge with the same residue. A remarkable fact is that in the HDAC1 isoform, the D497$_{HDAC6}$ residue is replaced by a glutamine (Q26), and the compound was not able to target it precluding the formation of an H-bond (at a higher distance from Q26) and/or a salt bridge. Moreover, in all the potential binding modes found in the docking output of HDAC1, **34** was found in a turned pose, compared to that observed for HDAC6, targeting the residues in the opposite loop of the Q26, because the cavity of HDAC1 binding site in proximity to the zinc binding region is restricted compared to the one of HDAC6. In summary, the introduction of a flexible and protonable moiety, able to establish a salt bridge and a polar contact with D497 in HDAC6, is a preferred choice to improve the potency of enzyme inhibition. On the other hand, selectivity towards isoforms was improved by introducing at C4, the pyridin-3-yl substituent, retaining a significant potency (**35, 36**) and with over 100-fold selectivity ratio towards HDAC6 over HDAC1. Binding modes of compounds **35, 36** are shown in **Figure 16D-E**. In these analogues, the small methyl group and the benzyl moiety resulted to be largely solvent exposed with a

limited contribution to the enzyme/inhibitor complex. In compounds **35, 36** the contacts that highly contributed to the stabilization of the complex are, H-bonding between the pyridin-3-yl and H651 and a π-π stacking with F679. The accommodation of the mentioned molecules into HDAC1 isoform were quite different and consequently the stacking and the H-bond were not formed. Accordingly, we developed compound **37**, bearing a pyridine-3-yl at C4 and a 4-methylenepyridine at *N*1. As depicted in **Figure 16F**, in contrast with the binding mode of **35, 36**, the scaffold of **37** was differently oriented by targeting the pyridine-4-yl substituent at *N*1 position the backbone of S568 and not that of H651. As for **34**, targeting D497, compound **38** showed a different binding mode compared to the other compounds of the series. With the introduction of the pyridine-4-yl, the bond with H651 was also established (**Figure 16G**), maintaining the same inhibitory profile. Furthermore, taking into consideration the hydrophobic residues present in the interaction site of HDAC6, we introduced a cyclohexyl ring at C4 in place of the aromatic system, obtaining **39**, the binding mode of which is shown in **Figure 16H**. Owing to ring flexibility and lower steric hindrance of the methyl at *N*1 of **29**, different residues were engaged through hydrophobic interactions, namely F679, F680 and L749.
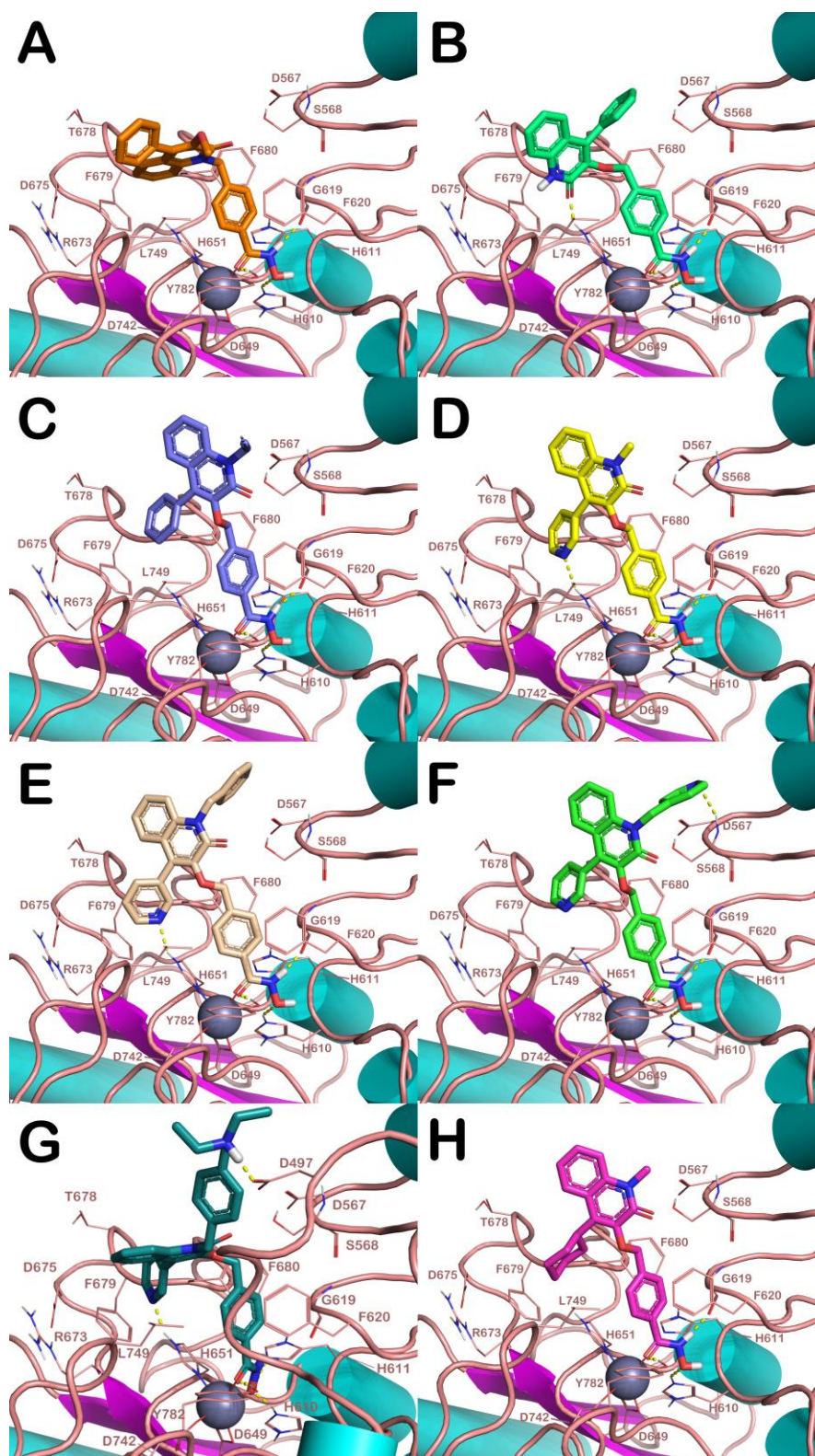
Figure 16. Docked poses into HDAC6 (PDB ID: 5EDU) of compounds **25** (orange sticks) panel A; **28** (lime green sticks) panel B; **30** (slate gray sticks) panel C; **35** (yellow sticks) panel D; **36** (light orange sticks) panel E; **37** (green sticks) panel F; **38** (deep teal sticks) panel G; **39**

(magenta sticks) panel H. The residues of the active sites are represented as lines and the whole protein is represented as cartoon. The Zn^{2+} ion is represented as a gray sphere. The polar contacts are depicted as dotted yellow lines while the coordination bond as plain lines. For the clarity of the pictures, starting from panel A to F and panel H, the initial residues of the protein from AA 479 to 511 were hidden, while for panel G the visualization was restored considering the contacts established between **38** and D497. The pictures were generated by means of PyMOL.
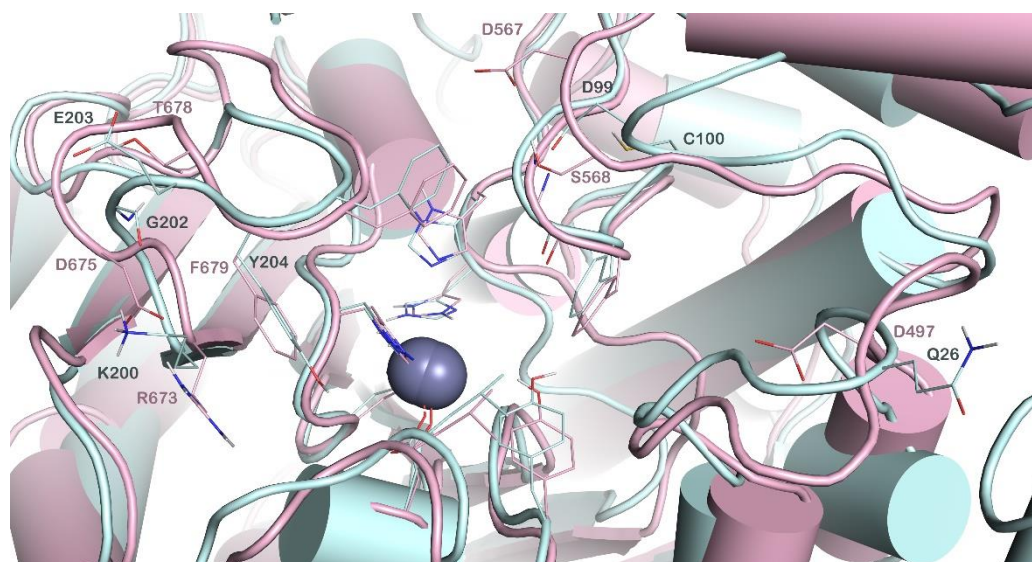
Figure 17. Superposition of the two isoforms of HDAC1 (pale cyan cartoon) and HDAC6 (light pink cartoon). The picture highlights the binding sites of the two proteins and the different residues between are labeled in different colors according to the protein color. The picture was generated by means of PyMOL.

Binding affinity studies towards *h*HDAC8 isoform were conducted on the best performing compounds (**34, 38** and **39**) to have an indication of the potency and selectivity of these new quinolone-based derivatives also against this isoform. Based on the data obtained, compound **34** demonstrated the highest selectivity of the three compounds with an index of 80

(HDAC8/HDAC6) with an IC_{50} value of 0.554 µM (**Table 5**), while compound **39** was the least potent with an IC_{50} value of 1.64 µM and a selectivity index of 50. These results highlighted a high selectivity profile of this new series of compounds towards HDAC6.

Table 6. Inhibitory activity of compounds **34, 38** and **39** as IC_{50} (µM), and apparent inhibitor constant (K^{app}) against the *h*HDAC8 enzyme

Cmpd	**34**	**38**	**39**	**TubA**
IC_{50} (µM)[a]	0.554 ± 0.146	0.485 ± 0.202	1.64 ± 0.3	0.695
K^{app} (µM)[a]	0.364 ± 0.06	0.395 ± 0.06	1.93 ± 0.22	n.d.
HDAC6/HDAC8	80	42	50	23

[a]All compounds were assayed at least two times, and the results are expressed with standard deviations.

We predicted the ADME properties of the newly developed compounds calculated by means of QikProp, a software implemented in Maestro suite (QikProp, version 4.3, Schrödinger, LLC, New York, NY, 2015). The output of the calculation is reported in **Table 7**. The predicted values for every molecule can be considered acceptable since they were within the recommended range of the software.

Table 7. Predicted drug-like features for compounds **24-39**

Cpd	SASA[a]	QPlogP[b]	QPlogS[c]	QPPCaco[d]	QPPMDCK[e]	QPlogHERG[f]	%HOA[g]
24	666.98	2.22	-4.58	111.54	46.21	-6.67	76.60
25	676.19	2.88	-4.75	272.79	121.49	-6.45	87.39
26	798.16	4.58	-6.48	334.04	151.23	-7.98	100
27	658.93	1.35	-4.06	61.33	24.21	-6.45	66.85
28	608.461	2.15	-3.78	136.87	57.65	-5.59	77.80
29	636.46	2.64	-4.10	273.90	122.03	-5.68	86.02
30	675.68	3.10	-4.41	304.62	136.88	-6.14	89.54
31	754.11	4.29	-5.73	339.34	153.82	-7.19	100
32	748.16	3.38	-5.12	182.59	78.72	-7.00	87.24
33	877.83	4.67	-5.92	104.66	47.72	-8.42	77.46
34	858.76	4.16	-5.27	85.16	38.19	-8.03	72.90
35	675.15	2.12	-4.26	187.75	81.22	-6.40	80.07
36	791.56	3.66	-5.85	184.40	79.56	-7.79	88.94
37	785.58	2.75	-5.23	99.22	40.72	-7.59	78.78
38	849.77	3.29	-4.58	56.07	24.31	-7.83	64.57
39	684.14	3.01	-5.04	264.54	117.53	-5.45	87.94

[a]SASA predicted the total solvent accessible surface (range or recommended value for 95% of known drugs 300 - 1000); [b]QPlogP predicted octanol/water partition coefficient (range or recommended value for 95% of known drugs -2 - 6.5); [c]QPlogS predicted aqueous solubility in mol/dm^3(range or recommended value for 95% of known drugs -6.5-0.5); [d]QPPCaco predicted apparent Caco-2 cell permeability in nm/sec (range or recommended value for 95% of known drugs >500 great); [e]QPPMDCK predicted apparent MDCK cell permeability in nm/sec (range or recommended value for 95% of known drugs >500 great); [f]QPlogHERG predicted IC_{50} values for blockage of HERG K^+ channels (range or recommended value for 95% of known drugs below -5); [g]h%HOA predicted human oral absorption on 0 to 100% scale (range or recommended value for 95% of known drugs >80% high). Range or recommended values are reported in QikProp user manual.

We further assessed the *in vitro* solubility and chemical stability of selected compounds **25**, **32**, **38**. The solubility (at pH = 3 and 7.4, Table **8**) and the chemical stability (at pH = 3, Table **8**) of these compounds were measured by means of HPLC methods. As expected, the presence of

basic groups on compounds **32** and **38**, improved the solubility profile at pH = 3 with respect to compound **25**. Gratifyingly, our analysis also revealed that both **32** and **38** exhibited a favorable chemical stability profile at acidic pH. In particular, the chemical stability was almost quantitative for the selected compounds with more than 95% of the compound remaining unaltered at pH = 3 after 24 h.

Table 8

Cmpd	Solubility (µM) after 24 h		Chemical Stability (%) after 24 h
	pH = 3	pH = 7.4	pH = 3
25	51	35	n.d.
32	281	17	99.0
38	265	90	99.0

Chapter 5

Cellular Assays

5.1. Spiroindoline series

The new molecules were tested in different tumor cell lines which include leukemia, oral and esophageal cancer cells. On the basis of *in vitro* HDAC affinity and HDAC6 isoform selectivity, the best performing compounds were selected to evaluate their antiproliferative activities. Also, in order to verify their mechanism of action, the target compounds were subjected to cell viability, apoptotic assay (AnnexinV/PI staining), cell cycle analysis (PI staining), cell cycle distribution studies and analysis of transcription factor activation. Cell cycle distribution and PI analysis studies were performed on U937 and NB4 cell lines, with compounds **15** and **21** showing the most promising results. Specifically, in U937 cells, **21** exhibited cell death and a significant S phase reduction at 10 µM concentration compared to the control (DMSO). Interestingly, in NB4 cell line, both **15** and **21** displayed identical phenotypic effect in terms of cell death at the two-time intervals 24 and 48 h (**Figure 18A,B**). Inspired from these results, western blot analyses on NB4 total cell extracts using compounds **15** and **21** were performed. Induction of acetylated tubulin was observed (**Figure 18C,D**), thus confirming HDAC6 inhibition. Moreover, cleavage of PARP at 24 h by **21** was also detected indicating apoptosis at molecular level at both 24 and 48 h at 10 µM concentration (**Figure 18D**).
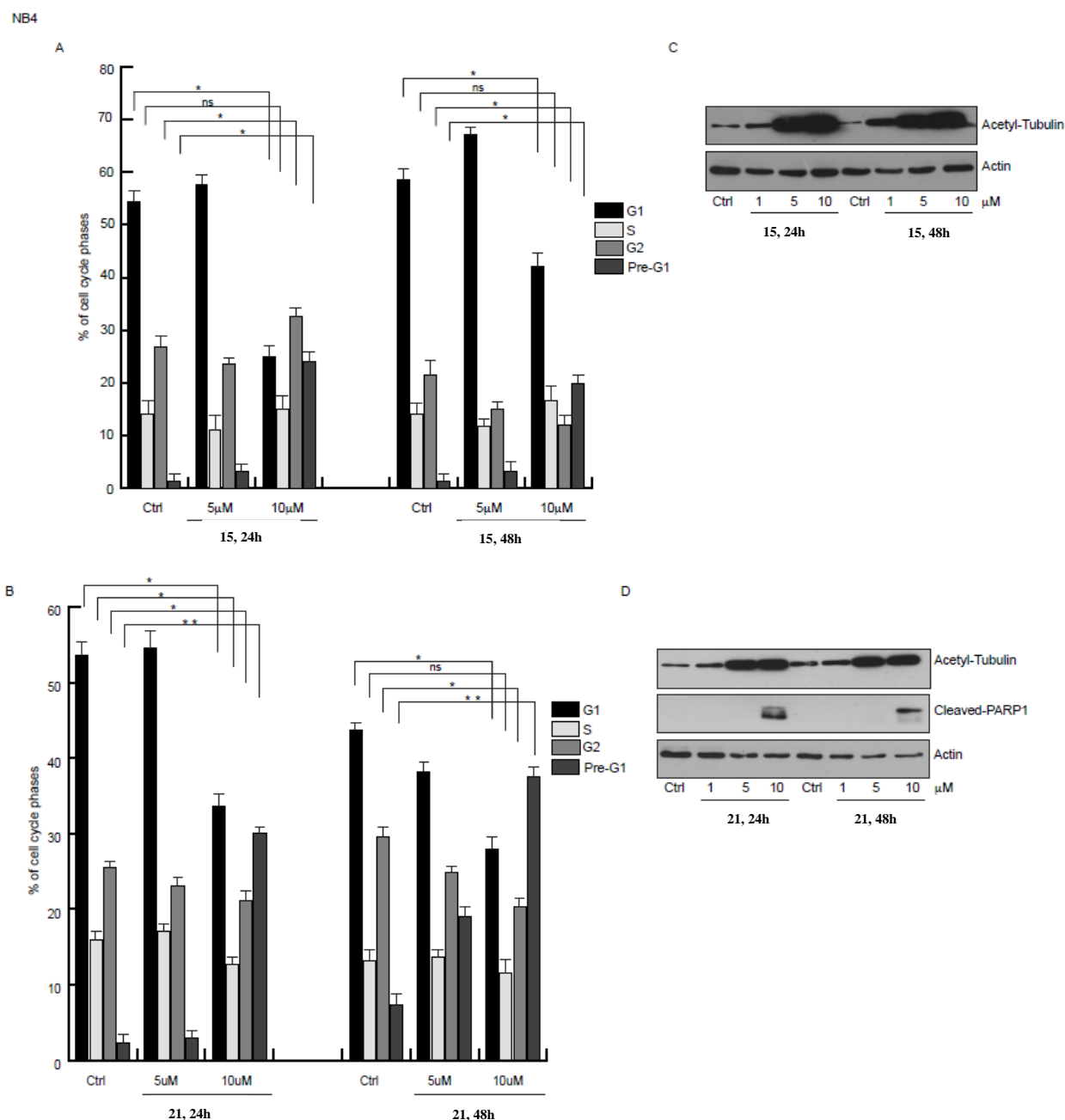
Figure 18. (A, B) FACS analysis of NB4 cells upon **15** (**A**) and **21** (**B**) compounds treatment at three different concentrations (1, 5 and 10 µM) at indicated time points. DMSO-treated cells were used as control. Error bars indicate SD of three biological replicates (*P < 0.05, **P ≤ 0.01). (**C, D**). Western blot analysis of NB4 total cell extracts untreated (DMSO) or treated with 1, 5 and 10 µM of **15** (**C**) or **21** (**D**) compounds at indicated times. Immonoblot were performed against the indicated proteins. Actin was used as loading control.

STAT3 represents an important signal transducer and transcription factor displaying a key role in the tumorigenesis process. This has been confirmed by the fact that 70% of cancers express

activated STAT3.[161] Recent reports highlighting the important crosstalk between HDAC6 and STAT3 has provided deep insights into the mechanistic details regarding cancer therapy. It has been demonstrated that HDAC6 inhibition leads to decrease in phosphorylated levels of STAT3 and inhibits the expression of STAT3-targeted genes.[162] The enhanced survival of leukemic cells in chronic lymphocytic leukemia has been associated with the constitutive activation of the JAK/STAT3 signaling pathway.[163] Therefore, we proceeded to test STAT3 inhibition using the HDAC6 inhibitors **14** (prototypic of the new series) and **23** (most potent HDAC6 inhibitor of the series) at 5 and 10 µM concentration in the human chronic lymphocytic leukemia cell line MEC1.[164] To our delight, both compounds showed a marked decrease in the levels of pSTAT3. Specifically, **23** demonstrated the most potent activity in a dose dependent manner (**Figure 19**).
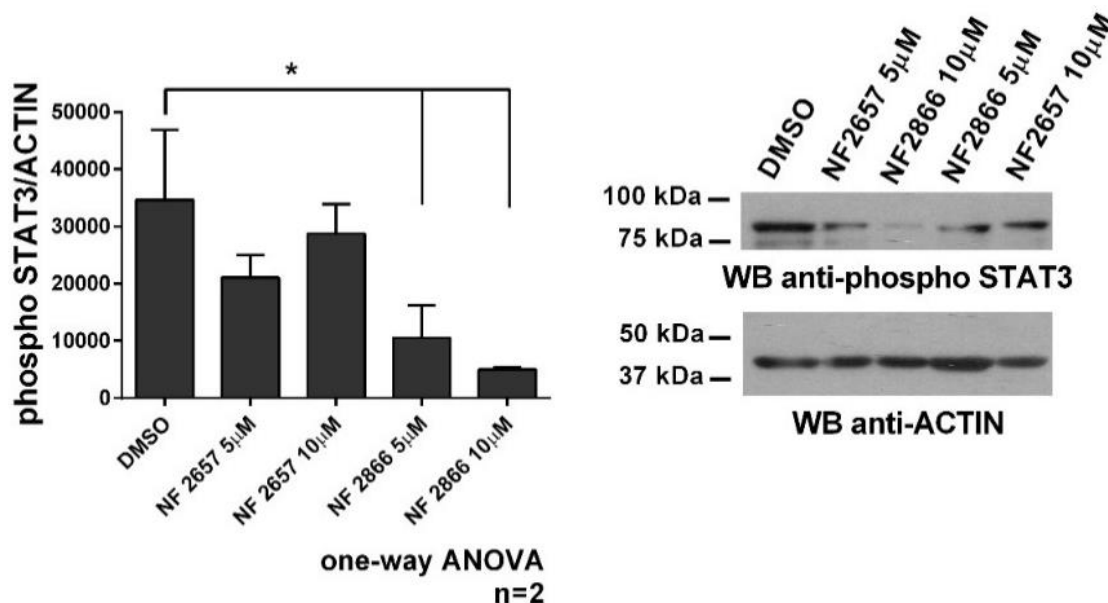
Figure 19. Immunoblot analysis of phosphorylated STAT3 in MEC-1 cells treated with **14** (**NF2657**) or **23** (**NF2866**) (5 µM or 10 µM) for 30 h. Actin was used as loading control. The histogram shows the quantification by densitometric analysis of the levels of phosphorylated STAT3 relative to actin (n = 2). Data are presented as mean value ± SD. One Way ANOVA; *$p < 0.05$

The majority of cases of oral and esophageal cancer (OEC) are detected late and despite recent medical advances, diagnosis is still relatively poor.[165, 166] In a range of malignancies, HDAC6 has been found to be over-expressed and shown to correlate with increased tumor aggressiveness including oral squamous cell carcinoma and esophageal squamous cell carcinoma.[167-172] HDAC6 thus represents a key potential target for therapeutic drug development in OEC. The compounds were also screened against several human cancer cell lines namely, KYSE520 (esophageal squamous cell carcinoma), OE33 (esophageal adenocarcinoma), Ca9-22 (gingival squamous cell carcinoma), TR-146 (buccal mucosa squamous cell carcinoma). The results suggested that the selected compounds exhibit antiproliferative activity. **15** demonstrated the highest activity against KYSE520 (IC_{50} = 12.76 µM), OE33 (IC_{50} = 5.56 µM), Ca9-22 (IC_{50} = 19.00 µM) and TR-146 (IC_{50} = 18.00 µM, Table 3), while **23**, even if it was the best performing analogue in enzymatic assays, was found less potent in these cell-based assays since, being a carbamate it might be vulnerable to hydrolytic processes. Flow cytometric analysis established that **15** was able to trigger apoptosis after 48 h of treatment in KYSE520 cell lines. Furthermore, cytotoxicity assay was performed on the prototype compound **14** and the compound with the best activity against cancer cells **15**, to establish the effect on mouse fibroblasts NIH3T3. The results indicated that compound **15** shows a TC_{50} of 40 µM being slightly less toxic than **14** (TC_{50} of 24 µM).

Potential mutagenicity caused by the use of hydroxamic-based compounds remains a major concern affecting their drug-like profile.[173] To asses this property Ames test towards two strains of *Salmonella typhimurium* (TA98 and TA100), with and without metabolic activation by employing rat liver S9 fraction, was carried out. It was clear from the results that compounds **14** and **15** showed no mutagenic effect on the TA98 strain (with or without S9 activation) but low-to-moderate mutagenicity on TA100 strain. This effect has been reported also for FDA approved HDACi, and it is mostly supposed to be determined by a Lossen rearrangement

involving the hydroxamate group. This process, leads to the generation of the corresponding isocyanate, which can trigger mutagenicity by damaging the DNA due to its susceptibility to undergo nucleophilic attack.[139] Moreover, the capability of HDACi to unwind chromatin may also expose DNA to damage by intracellular factors such as reactive oxygen species (ROS), which can cause further DNA damage leading to genotoxicity.[174, 175]

5.2. Quinolone series

5.2.1. Mutagenicity profile evaluation for 25, 38, and 39.

Potential mutagenicity associated with the use of hydroxamic acid-based compounds poses a significant challenge in terms of their drug-like profile.[173] To date, givinostat is the only compound under clinical trials that has exhibited no mutagenic effect, while the other FDA approved drugs have shown mutagenicity. Therefore, we confirmed for compounds **25**, **38** and **39** the lack of mutagenic effect in the *Salmonella typhimurium* strains TA98 and TA100. The Ames test was employed to detect potential risks of mutagenicity at the early stages of drug development. The assay can be performed with or without the S9 fraction of rat liver. This latter condition allows an in-depth investigation for evaluating the risk of mutagenicity derived from the metabolites of the compounds under study. After applying both the experimental conditions, no mutagenic effect was observed for these compounds at all concentrations tested (5-230 µM).
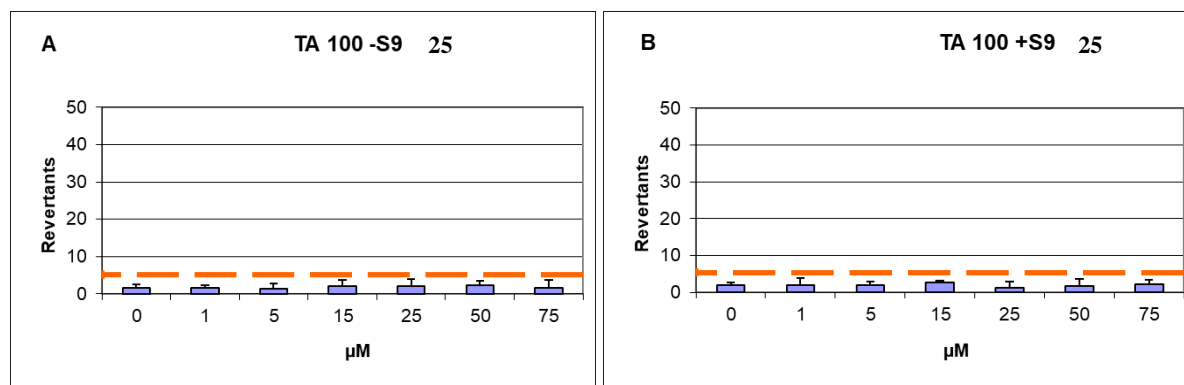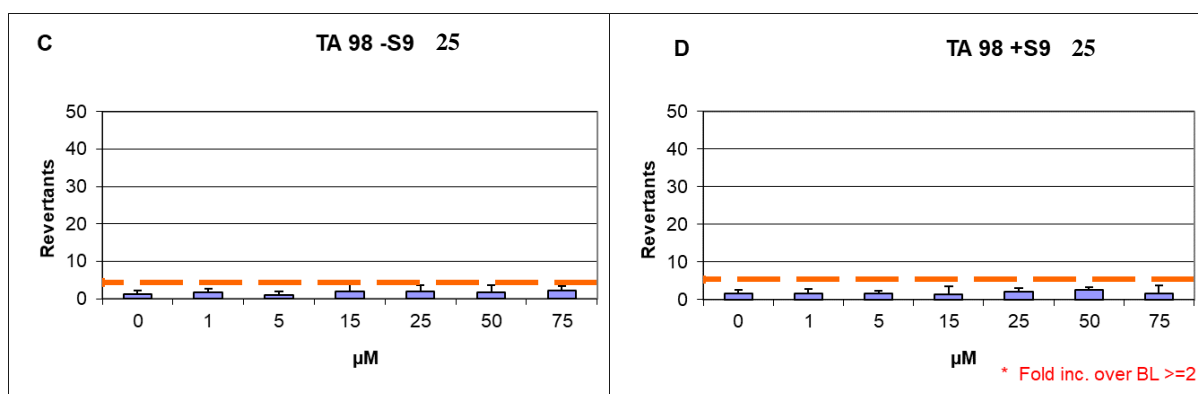
Figure 20. Ames test performed on *S. typhimurium* TA98 and TA100 strains, with and without S9 metabolic activation, for compound **25**.
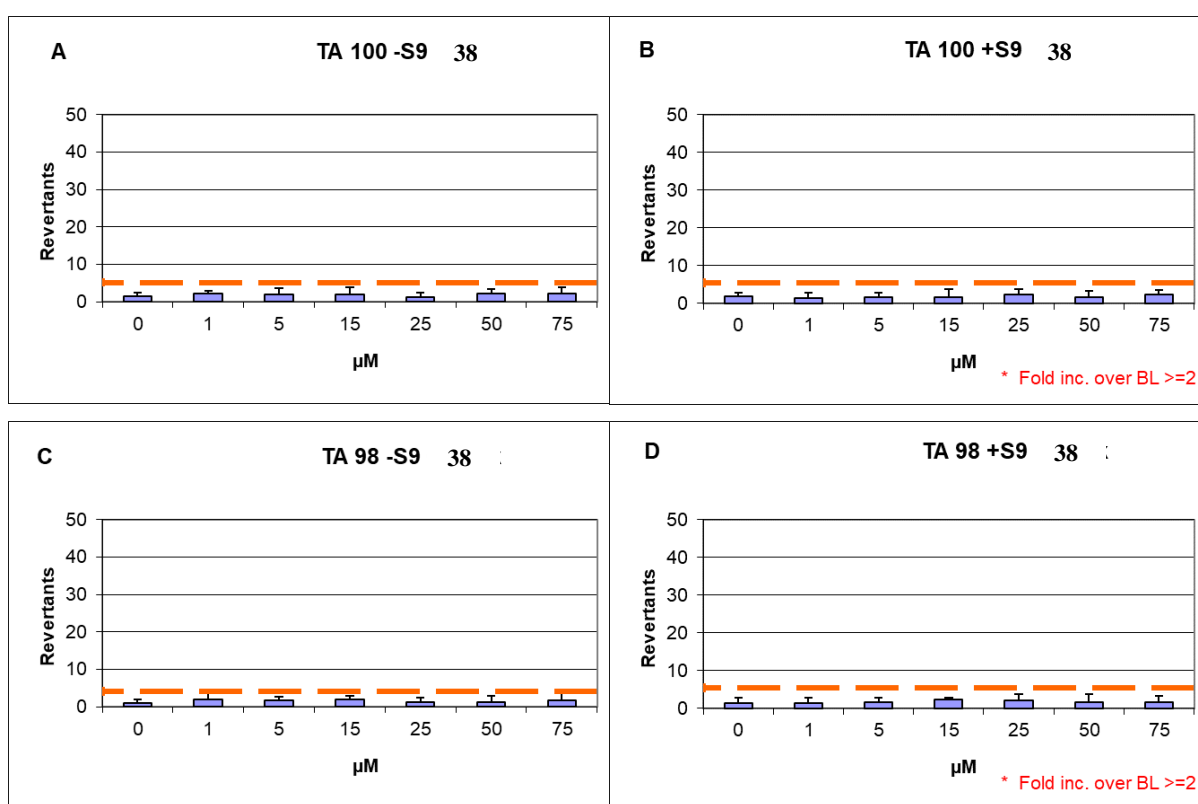
Figure 21. Ames test performed on *S. typhimurium* TA98 and TA100 strains, with and without S9 metabolic activation, for compound **38**.
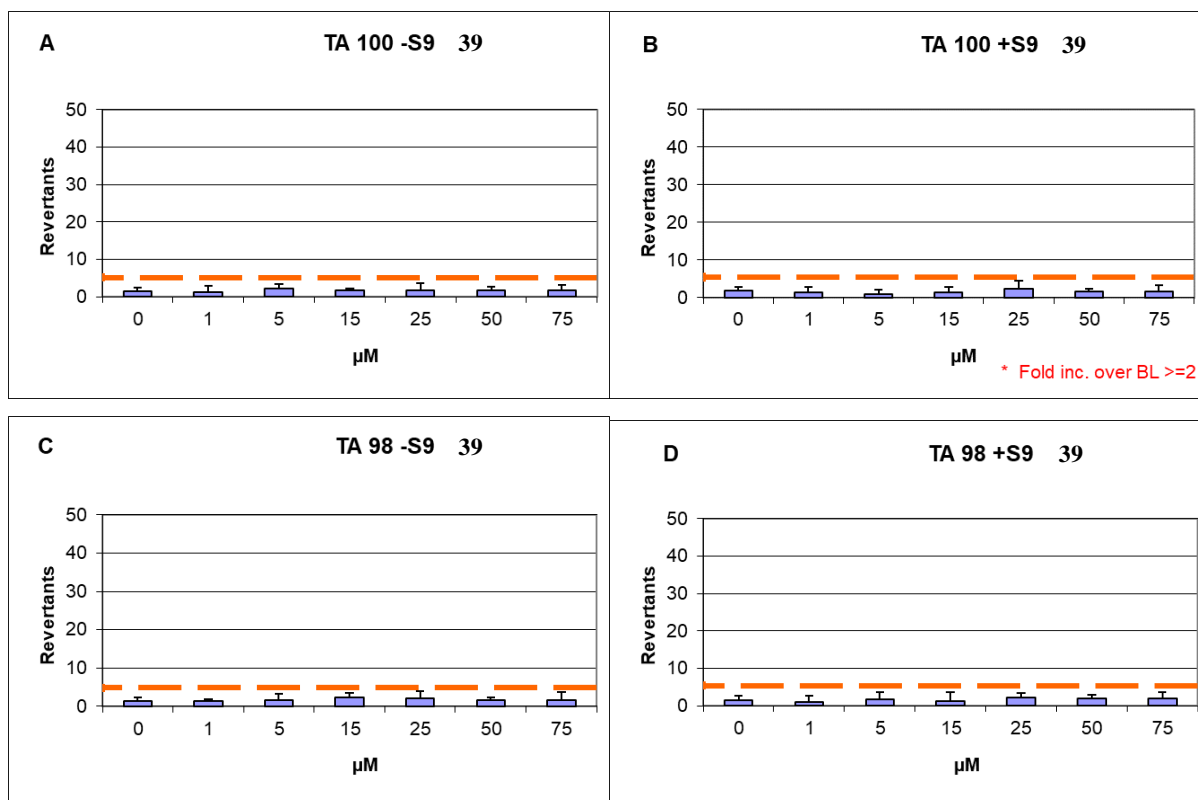
Figure 22. Ames test performed on *S. typhimurium* TA98 and TA100 strains, with and without S9 metabolic activation, for compound **39**.

5.2.2. Lossen rearrangement study on compound 38.

In order to check the susceptibility of our compounds to undergo Lossen rearrangement we decided to investigate **38** for the formation of the corresponding isocyanate (by checking the conversion to aniline) on treatment with one equivalent of K_2CO_3 in DMSO at 40 °C. After 18 h we observed by ESI-MS analysis (**Figure 23**), that the predominant peaks were: the starting material (**38**, $[M+ H]^+ = 563.2$) and the corresponding carboxylic acid ($[M + H]^+ = 548.2$), while only a small peak of the aniline ($[M + H]^+ = 519.2$) deriving from isocyanate was observed. From this study we can assume that the absence of mutagenicity detected from the Ames assay can be explained by a low vulnerability of our compounds to undergo Lossen rearrangement.
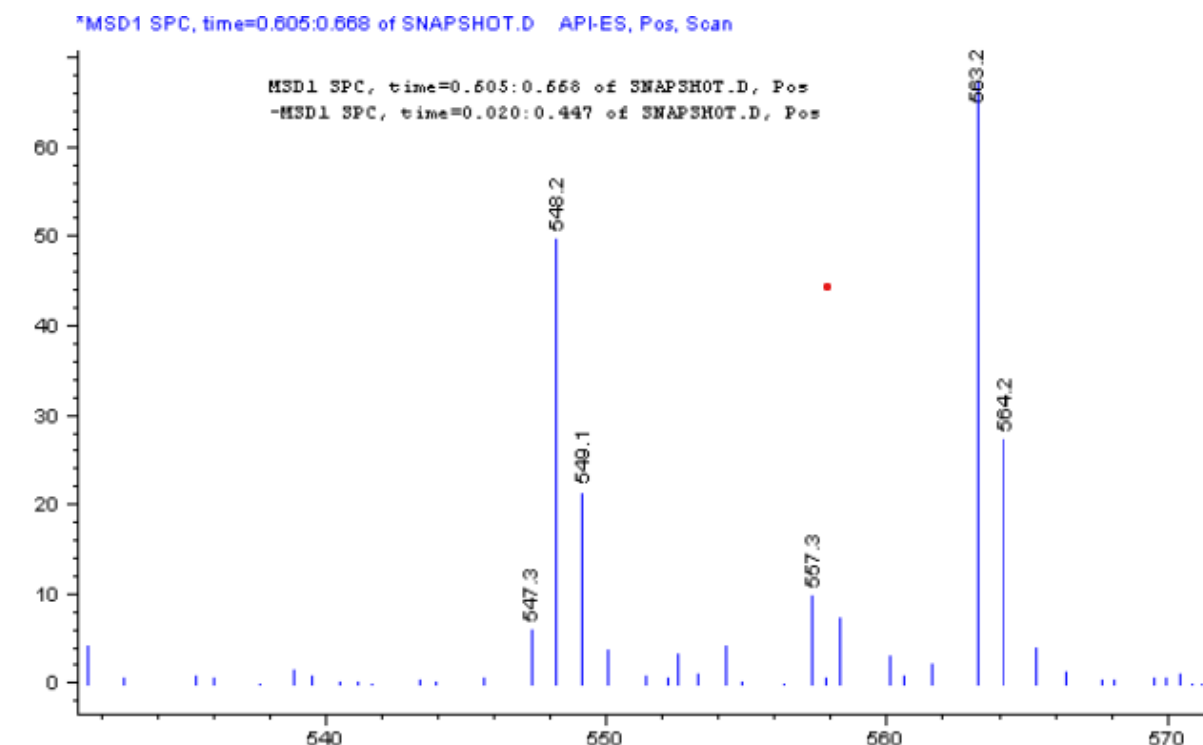
Figure 23. ESI-MS analysis of compound **38** after Lossen Rearrangement.

5.3. Conclusions

This thesis work describes the rational design, synthesis, SAR, and biological evaluation of novel HDAC6 inhibitors as anticancer agents. The pan-selectivity of the majority of known HDAC inhibitors limits their use in exploring the role of HDAC6 in cell growth, migration and death in both cancer and neurodegenerative disorders. Therefore, HDAC6 selective inhibition could be pursued by the design of small molecules bearing a HDAC6 specific interaction moiety (cap-group) and a zinc-binding group (ZBG), opportunely outdistanced with a linker. Driven by computational studies and the structural hints obtained from previously developed selective compounds and pan-inhibitors, the approaches herein described for the design and synthesis of novel HDAC6 selective inhibitors can be summarized as follows:

• the cap-group has been modified by a variety of heterocyclic moieties, designed to improve both selectivity and affinity towards HDAC6.

73

• aryl/heteroaryl moieties were inserted at the linker level in order to improve selectivity.

• the hydroxamate functionality at the ZBG was maintained in most of the newly designed compounds, in order to gain clear-cut insights into the impact of the novel cap-groups and linkers on the affinity and selectivity towards HDAC6.

Overall, the compounds developed can be clustered in two main structural series displaying different activity and selectivity profiles when tested in *in vitro* assays on HDAC1, HDAC6 and HDAC8 isoforms.

The best in *vitro* performing inhibitors have also been evaluated in cellular assays. However, the biological data for the quinolone series of HDAC6 inhibitors is still awaited.

Chapter 6

Experimental section

General. Reactions were carried out under nitrogen atmosphere in oven-dried (120 °C) glassware. All reagents and chemicals were purchased from commercial suppliers and used without further purification. Anhydrous solvents were obtained as follows: dichloromethane from calcium hydride diethyl ether and tetrahydrofuran from sodium benzophenone. All purification procedures were carried out with reagent grade solvents (purchased form Fisher Scientific) in air. TLC analysis was conducted using aluminium foil supported thin-layer silica gel chromatography plates (F254 indicator). Column chromatography was performed using 230–400 mesh, 60 Å pore diameter silica gel. ^{1}H and ^{13}C NMR spectra were recorded at room temperature on a Varian 300 or a Bruker ARX-400. Chemical shifts (d values) are reported in parts per million and are referenced to the deuterated residual solvent peak. NMR data are reported as: d value (chemical shift, J-value (Hz), integration, where s = singlet, d = doublet, t = triplet, q = quartet). Low-resolution mass analyses were performed on an Agilent 1100 spectrometer.

tert-Butyl 4-formylpiperidine-1-carboxylate (41)

Step a: A solution of NaHMDS (1M solution in THF, 13.8 mL, 13.8 mmol) in dry THF (12 mL) was added to a stirred suspension of $(Ph)_3PCH_2OCH_3Cl$ (4.47 g, 13.04 mmol) in dry THF (12 mL) at 0 °C. After 30 min, a solution of 1-boc-4-piperidone (2.0 g, 10.03 mmol) in dry THF (7 mL) was added dropwise at 0 °C and stirred for 1 h. The resulting mixture was diluted with EtOAc and washed with 1N HCl (30 mL), a saturated solution of $NaHCO_3$ (30 mL) and brine. The organic layer was dried over Na_2SO_4 and the solvents removed *in vacuo* to give a residue which was purified by column chromatography on silica gel (EtOAc/Petroleum ether 1:20) obtaining *tert-butyl 4-(methoxymethylene)piperidine-1-carboxylate* (yield: 44%). ^{1}H

NMR (300 MHz, CDCl$_3$) δ 5.81 (s, 1H), 3.51 (s, 3H), 3.46 – 3.23 (m, 4H), 2.20 (t, J = 5.4 Hz, 2H), 2.00 – 1.91 (m, 2H), 1.42 (s, 9H); ESI MS m/z: [M+Na]$^+$ 250. **Step b**: To a solution of this intermediate (1.0 g, 4.40 mmol) in MeCN (30 mL), CeCl$_3$·7H$_2$O (390 g, 1.037 mmol) and NaI (87 mg, 0.583 mmol) were added. The reaction was then heated at 25 °C for 12 h, then MeCN was removed under reduced pressure. The residue was diluted with EtOAc and washed with 1N HCl (30 mL), a saturated solution of NaHCO$_3$ (30 mL) and brine. The organic layer was dried over Na$_2$SO$_4$ and **41** was obtained as a yellow oil without further purification (725 mg, yield: 77%). ^{1}H NMR (300 MHz, CDCl$_3$) δ 9.66 (s, 1H), 3.98 (m, 2H), 2.92 (t, J = 10.7 Hz, 2H), 2.51 – 2.29 (m, 1H), 1.94 – 1.78 (m, 2H), 1.68 – 1.49 (m, 2H), 1.45 (s, 9H). ESI MS m/z [M+H]$^+$ 214.

tert-Butyl spir(indoline-3,4'-piperidine)-1'-carboxylate (42a)

Step c: A stirred solution of **40** (440 mg, 2.06 mmol) and phenylhydrazine (202 µL, 2.06 mmol) in AcOH (10 ml) was heated to 80 °C for 2 h. After completion of the reaction, AcOH was removed *in vacuo* and the residue was diluted with EtOAc (5 mL) and a saturated solution of NaHCO$_3$ was added. The mixture was extracted with EtOAc (3 x 10 mL) and the combined organic layers were dried over Na$_2$SO$_4$, filtered and evaporated *in vacuo*. The crude material was purified by column chromatography on silica gel (EtOAc/Petroleum ether 1:3) obtaining *tert-butyl spiro(indole-3,4'-piperidine)-1'-carboxylate* as a red oil (245 mg, yield: 41%). ^{1}H NMR (300 MHz, CDCl$_3$) δ 8.38 (s, 1H), 7.68 (d, J = 7.6 Hz, 1H), 7.39 (dd, J = 8.3, 7.1 Hz, 2H), 7.33 – 7.24 (m, 1H), 4.01 (d, J = 13.8 Hz, 2H), 3.57 – 3.42 (m, 2H), 1.82 (td, J = 9.6, 4.8 Hz, 2H), 1.68 (s, 2H), 1.51 (s, 9H). ESI MS m/z [M+H]$^+$ 287. **Step d**: To a stirred solution of the previous intermediate (245 mg, 0.85 mmol) in MeOH (10 mL) a catalytic amount of Pd/C was added under N$_2$ atmosphere. After this, N$_2$ atmosphere was replaced with H$_2$ and the reaction was stirred at 25 °C for 3 h. Reaction mixture was filtered through celite and washed

with MeOH. Solvent was evaporated and the crude material was purified by column chromatography on silica gel (EtOAc/petroleum ether 1:4) obtaining **42a** as a transparent oil (110 mg, yield: 45%). ^{1}H NMR (300 MHz, CDCl$_3$) δ 7.05 (d, J = 7.5 Hz, 2H), 6.76 (t, J = 7.4 Hz, 1H), 6.67 (d, J = 7.5 Hz, 1H), 4.04 (s, 2H), 3.48 (s, 2H), 2.92 (t, J = 11.7 Hz, 2H), 1.92 – 1.61 (m, 4H), 1.49 (s, 9H). ESI MS m/z [M+H]$^+$ 289.

tert-Butyl 7-phenylspiro(indoline-3,4'-piperidine)-1'-carboxylate (42b)

To a solution of commercially available 2-amino biphenyl (1.0 g, 5.91 mmol) in conc. HCl (10 mL) cooled at 0 °C, was added NaNO$_2$ (408 mg, 5.91 mmol). The reaction mixture was stirred for 30 min and then a suspension of SnCl$_2$·2H$_2$O in conc. HCl (10 mL) was added dropwise. The reaction mixture was stirred at 25 °C for 2 h. The solid was filtered and dried to obtain pure *(1,1-biphenyl)2-ylhydrazine hydrochloride* (1.01 g, yield: 77%) as a white solid. ^{1}H NMR (300 MHz, DMSO) δ 9.87 (s, 3H), 7.55 – 7.30 (m, 6H), 7.19 (d, J = 7.4 Hz, 1H), 7.07 (t, J = 7.6 Hz, 2H). **Step c:** From this latter intermediate (200 mg, 1.18 mmol) and **7** (252 mg, 1.18 mmol) following the same procedure described for the synthesis of **42a**, *tert-butyl 7-phenylspiro(indole-3,4'-piperidine)-1'-carboxylate* was obtained. The crude material was purified by column chromatography on silica gel (EtOAc/petroleum ether 1:4) as a yellowish solid (153 mg, yield: 36%). ^{1}H NMR (300 MHz, CDCl$_3$) δ 8.46 (s, 1H), 7.80 – 7.68 (m, 2H), 7.56 – 7.43 (m, 3H), 7.43 – 7.31 (m, 3H), 4.18 – 3.98 (m, 2H), 3.56 – 3.34 (m, 2H), 1.99 – 1.79 (m, 2H), 1.77 – 1.60 (m, 2H), 1.51 (s, 9H). ESI MS m/z [M+H]$^+$ 363. **Step d:** Compound **42b** was prepared from *tert-butyl 7-phenylspiro(indole-3,4'-piperidine)-1'-carboxylate* (150 mg, 0.41 mmol) using the same procedure described for the synthesis of **42a** (**Step d**). Crude was purified by column chromatography on silica gel (EtOAc/petroleum ether 1:4) obtaining **42b** as a transparent oil (146 mg, yield: 97%). ^{1}H NMR (300 MHz, CDCl$_3$) δ 7.55 (d, J = 7.4 Hz, 2H), 7.43 (t, J = 7.5 Hz, 2H), 7.32 (t, J = 7.2 Hz, 1H), 7.14 (d, J = 7.5 Hz, 1H), 7.05 (d, J = 7.1

Hz, 1H), 6.86 (t, J = 7.5 Hz, 1H), 4.19 – 3.97 (m, J = 2H), 3.47 (s, 2H), 2.93 (t, J = 10.6 Hz, 2H), 1.95 – 1.72 (m, 4H), 1.48 (s, 9H). ESI MS m/z [M+H]$^+$ 365.

1-Methylspiro(indoline-3,4'-piperidine) (43a)

Step e: To a stirred solution of **42a** (30 mg, 0.10 mmol) in MeOH (2 mL) a catalytic amount of AcOH was added followed by paraformaldehyde (6 mg, 0.20 mmol) at 25 °C. After 1 h, NaBH$_3$CN (10 mg, 0.16 mmol) was added and the reaction was allowed to stir at 25 °C for 8 h. A saturated solution of NaHCO$_3$ (5 mL) and DCM (5 mL) were added to the reaction mixture and extracted with DCM (3 x 5 mL). The combined organic layers were dried over Na$_2$SO$_4$, filtered and evaporated *in vacuo*. The crude material was purified by column chromatography on silica gel (EtOAc/petroleum ether 1:4) obtaining *tert-butyl 1-methylspiro(indoline-3,4'-piperidine)-1'-carboxylate* as a colorless oil (22 mg, yield: 71%). ^{1}H NMR (300 MHz, CDCl$_3$) δ 7.11 (t, J = 7.6 Hz, 1H), 7.01 (d, J = 7.3 Hz, 1H), 6.70 (t, J = 7.4 Hz, 1H), 6.49 (d, J = 7.8 Hz, 1H), 4.05 (d, J = 9.6 Hz, 2H), 3.23 (s, 2H), 2.93 (t, J = 11.9 Hz, 2H), 2.77 (s, 3H), 1.91 – 1.61 (m, 4H), 1.49 (s, 9H). ESI MS m/z [M+H]$^+$ 303. **Step g:** To a stirred solution of *tert-butyl 1-methylspiro(indoline-3,4'-piperidine)-1'-carboxylate* (22 mg, 0.07 mmol) in MeOH (5 mL) was 1N HCl in MeOH (3 mL), stirred for 5 min, and the solvent was evaporated *in vacuo*. This procedure was repeated until complete consumption of the starting material, monitored using TLC. Then a saturated solution of NaHCO$_3$ (5 mL) and DCM (5 mL) were added. The mixture was extracted with DCM (3 x 5 mL) and the combined organic layers were dried over Na$_2$SO$_4$, filtered and evaporated *in vacuo*. **43a** (14 mg, yield: 99%) was used in the next step without further purification. ESI MS m/z [M+H]$^+$ 203.

1-Benzylspiro(indoline-3,4'-piperidine) (43b)

Step e: Compound *tert-butyl 1-benzylspiro(indoline-3,4'-piperidine)-1'-carboxylate* was prepared from **42a** (150 mg, 0.52 mmol) and benzaldehyde (110 mg, 1.04 mmol) following the same procedure employed for the synthesis of **43a** (**Step e**). Crude material was purified by column chromatography on silica gel (EtOAc/petroleum ether 1:4) obtaining *tert-butyl 1-benzylspiro[indoline-3,4'-piperidine]-1'-carboxylate* as a colorless oil (152 mg, yield 77%). ^{1}H NMR (300 MHz, CDCl$_3$) δ 7.34 – 7.26 (m, 5H), 7.12 – 7.02 (m, 2H), 6.73 – 6.68 (m, 1H), 6.51 (d, J = 7.8 Hz, 1H), 4.30 (s, 2H), 4.03 (d, J = 9.9 Hz, 2H), 3.24 (s, 2H), 2.84 (t, J = 11.8 Hz, 2H), 1.81 – 1.68 (m, 4H), 1.47 (s, 9H). ESI MS m/z [M+H]$^+$ 379. **Step g**: Compound **43b** was obtained from *tert-butyl 1-benzylspiro(indoline-3,4'-piperidine)-1'-carboxylate* (152 mg, 0.40 mmol) following the same procedure described to synthesize **43b** (**Step g**). **43b** (102 mg, yield: 92%) was used in the next reaction without further purification. ESI MS m/z [M+H]$^+$ 279.

Phenyl(spiro(indoline-3,4'-piperidin)-1-yl)methanone (43c)

Step f: To a stirred solution of **42a** (20 mg, 0.07 mmol) in dry DCM (2 mL), dry TEA (19 µL, 0.14 mmol), and benzoyl chloride (8 µL, 0.07 mmol) were added at 25 °C. The reaction was stirred for 1 h and water (5 mL) was added. The aqueous layer was extracted with DCM (3 x 5 mL). The combined organic layers were dried over Na$_2$SO$_4$, filtered and evaporated *in vacuo*. The crude material was purified by column chromatography on silica gel (EtOAc/petroleum ether 1:3) obtaining *tert-butyl 1-benzoylspiro(indoline-3,4'-piperidine)-1'-carboxylate* as a yellow oil (24 mg, yield: 89%). ^{1}H NMR (300 MHz, CDCl$_3$) δ 8.09 (d, J = 7.0 Hz, 1H), 7.62 – 7.40 (m, 5H), 7.17-7.05 (m, 3H), 4.04 (d, J = 31.4 Hz, 4H), 2.82 (s, 2H), 1.94 – 1.75 (m, 2H), 1.67 (d, J = 13.2 Hz, 2H), 1.47 (s, 9H). ESI MS m/z [M+Na]$^+$ 415. **Step g:** From this intermediate (24 mg, 0.06 mmol), **43c** was obtained following the same procedure described

to synthesize **43a** (**Step g**). **43c** (18 mg, yield: 99%) was used in the next reaction without further purification. ESI MS m/z [M+H]$^+$ 293.

1-Methyl-7-phenylspiro(indoline-3,4'-piperidine) (43d)

Step e: Compound *(tert-butyl 1-methyl-7-phenylspiro(indoline-3,4'-piperidine)-1'-carboxylate* was prepared from **42b** (38 mg, 0.10 mmol) following the same procedure described for the synthesis of **43a** (**Step e**). Crude material was purified by column chromatography on silica gel (EtOAc/petroleum ether 1:4) obtaining *(tert-butyl 1-methyl-7-phenylspiro(indoline-3,4'-piperidine)-1'-carboxylate* as a colorless oil (29 mg, yield: 77%). ^{1}H NMR (300 MHz, CDCl$_3$) δ 7.48 – 7.23 (m, 5H), 7.03 (d, *J* = 7.4 Hz, 2H), 6.83 (t, *J* = 7.4 Hz, 1H), 4.12 (s, 2H), 3.26 (s, 2H), 2.92 (t, *J* = 12.2 Hz, 2H), 2.37 (s, 3H), 1.94 – 1.65 (m, 4H), 1.51 (s, 9H). ESI MS m/z [M+H]$^+$ 379. From this intermediate (35 mg, 0.09 mmol) **43d** was obtained following the same procedure described to synthesize **43a** (**Step g**). **43d** (25 mg, yield: 99%) was used in the next reaction without further purification. ESI MS m/z [M+H]$^+$ 279.

1-Benzyl-7-phenylspiro(indoline-3,4'-piperidine) (43e)

Step e: Compound *tert-butyl 1-benzyl-7-phenylspiro(indoline-3,4'-piperidine)-1'-carboxylate* was prepared from **42b** (48 mg, 0.13 mmol) following the same procedure described for the synthesis of **43a** (**Step e**). Crude material was purified by column chromatography on silica gel (EtOAc/petroleum ether 1:4) obtaining *tert-butyl 1-benzyl-7-phenylspiro(indoline-3,4'-piperidine)-1'-carboxylate* as a colorless oil (45 mg, yield: 80%). ^{1}H NMR (300 MHz, CDCl$_3$) δ 7.52 (d, *J* = 7.3 Hz, 2H), 7.35 – 7.21 (m, 6H), 7.14 (d, *J* = 6.5 Hz, 2H), 7.06 (t, *J* = 7.1 Hz, 2H), 6.88 (t, *J* = 7.4 Hz, 1H), 4.06 (s, 2H), 3.92 (s, 2H), 3.22 (s, 2H), 2.78 (t, *J* = 12.2 Hz, 2H), 1.84 (td, *J* = 13.0, 4.3 Hz, 2H), 1.66 (d, *J* = 13.1 Hz, 2H), 1.49 (s, 9H). ESI MS m/z [M+H]$^+$ 455. This intermediate (45 mg, 0.08 mmol) was used to obtain **43e** following the same

procedure described to synthesize **43a** (**Step g**). **43e** (35 mg, yield: 99%) was used in the next reaction without further purification. ESI MS m/z [M+H]$^+$ 355.

Phenyl(7-phenylspiro(indoline-3,4'-piperidin)-1-yl)methanone (43f)

Step f: Compound *tert-butyl 1-benzoyl-7-phenylspiro(indoline-3,4'-piperidine)-1'-carboxylate* was prepared from **42b** (30 mg, 0.11 mmol) following the same procedure described for the synthesis of **43c** (**Step f**). Crude material was purified by column chromatography on silica gel (EtOAc/petroleum ether 1:4) obtaining *tert-Butyl 1-benzoyl-7-phenylspiro(indoline-3,4'-piperidine)-1'-carboxylate* as a colorless oil (53 mg, yield: 99%). ^{1}H NMR (300 MHz, CDCl$_3$) δ 8.10 (dd, J = 6.8, 1.5 Hz, 1H), 7.20 – 7.12 (m, 12H), 4.15 – 4.08 (m, 4H), 2.86 (s, 2H), 1.91 (s, 2H), 1.72 (d, J = 13.3 Hz, 2H), 1.47 (s, 9H). ESI MS m/z [M+H]$^+$ 469. **Step g:** This intermediate (53 mg, 0.11 mmol) was used to obtain **10f** following the same procedure described to synthesize **43a** (**Step g**). **43f** (29 mg, yield: 72%) was used in the next reaction without further purification. ESI MS m/z [M+H]$^+$ 369.

N-Hydroxy-4-((1-methylspiro(indoline-3,4'-piperidin)-1'-yl)methyl)benzamide (14)

Step h: Starting from **43a** (70, 0.34 mmol) and methyl 4-formyl benzoate (67 mg, 0.41 mmol), compound m*ethyl 4-((1-methylspiro(indoline-3,4'-piperidin)-1'-yl)methyl)benzoate* (45 mg, yield: 38%) was obtained following the same procedure described for the synthesis of **43a** (**Step e**). ^{1}H NMR (300 MHz, CDCl$_3$) δ 8.06 – 7.98 (m, 2H), 7.45 (d, J = 8.3 Hz, 2H), 7.15 – 7.05 (m, 2H), 6.71 (td, J = 7.4, 0.8 Hz, 1H), 6.48 (d, J = 7.7 Hz, 1H), 3.92 (s, 3H), 3.60 (s, 2H), 3.20 (s, 2H), 2.90 – 2.79 (m, 2H), 2.77 (s, 3H), 2.24 – 2.09 (m, 2H), 1.96 (td, J = 12.8, 3.9 Hz, 2H), 1.72 (d, J = 13.0 Hz, 2H). ESI MS m/z [M+H]$^+$ 351. **Step i**: To a stirred solution of *methyl 4-((1-methylspiro(indoline-3,4'-piperidin)-1'-yl)methyl)benzoate* (45 mg, 0.13 mmol) in DCM (2 mL): MeOH (1 mL) was added a 50% aqueous solution of NH$_2$OH (850 µL, 12.8 mmol)

dropwise followed by the addition of a 4 M solution of KOH in MeOH (1630 µL, 6.5 mmol) and the reaction was allowed to stir at 25 °C for 2 h. The reaction mixture was neutralized with a 6 N solution of HCl and the solvent was evaporated to dryness. Crude material was purified by column chromatography on silica gel (DCM/MeOH/NH$_4$OH 20:1:0.1) obtaining **14** as a white solid (45 mg, yield: 99%). ^{1}H NMR (300 MHz, CD$_3$OD) δ 7.73 (d, J = 7.8 Hz, 2H), 7.47 (d, J = 7.8 Hz, 2H), 7.06 – 6.99 (m, 2H), 6.65 (t, J = 7.3 Hz, 1H), 6.49 (d, J = 7.7 Hz, 1H), 3.63 (s, 2H), 3.16 (s, 2H), 2.85 (d, J = 11.7 Hz, 2H), 2.72 (s, 3H), 2.23 (t, J = 11.1 Hz, 2H), 1.91 (td, J = 13.0, 3.4 Hz, 2H), 1.66 (d, J = 13.1 Hz, 2H). ^{13}C NMR (75 MHz, CD$_3$OD) δ 166.6, 152.2, 141.3, 137.5, 131.2, 129.5, 127.5, 126.7, 121.6, 117.9, 107.4, 64.9, 62.4, 50.4, 42.4, 35.2, 35.0. ESI MS m/z [M+H]$^+$ 352; HRMS (m/z) calcd for C$_{21}$H$_{26}$N$_3$O$_2$ ([M+H]$^+$) 352.2020, found 352.2010.

4-((1-Benzylspiro(indoline-3,4'-piperidin)-1'-yl)methyl)-N-hydroxybenzamide (15)

Step h: Starting from **43b** (23 mg, 0.08 mmol) and methyl 4-formyl benzoate (27 mg, 0.16 mmol), compound *methyl 4-((1-benzylspiro(indoline-3,4'-piperidin)-1'-yl)methyl)benzoate* was obtained following the same procedure described for the synthesis of **43a** (**Step e**). Crude material was purified by column chromatography on silica gel (EtOAc/petroleum ether 1:4) obtaining *methyl 4-((1-benzylspiro(indoline-3,4'-piperidin)-1'-yl)methyl)benzoate* as a colorless oil (18 mg, yield: 51%). ^{1}H NMR (300 MHz, CDCl$_3$) δ 8.00 (d, J = 8.3 Hz, 2H), 7.48 – 7.22 (m, 7H), 7.08 (ddd, J = 8.9, 5.8, 1.9 Hz, 2H), 6.71 (td, J = 7.4, 0.8 Hz, 1H), 6.49 (d, J = 7.7 Hz, 1H), 4.30 (s, 2H), 3.92 (s, 3H), 3.55 (s, 2H), 3.23 (s, 2H), 2.82 (d, J = 11.2 Hz, 2H), 2.17 – 1.88 (m, 4H), 1.73 (d, J = 12.6 Hz, 2H). ESI MS m/z [M+H]$^+$ 427. **Step i:** To a stirred solution of the previous compound (18 mg, 0.04 mmol) in DCM (2 mL): MeOH (1 mL) was added a 50% aqueous solution of NH$_2$OH (281 µL, 4 mmol) dropwise followed by the addition of a 4 M solution of KOH in MeOH (527 µL, 2 mmol) and reaction was allowed to stir at 25

°C for 2 h. The reaction mixture was neutralized with a 6 N solution of HCl and the solvent was evaporated to dryness. Crude was purified by column chromatography on silica gel (DCM/MeOH/NH$_4$OH 20:1:0.1) obtaining **15** as a colorless oil (16 mg, yield: 89%). ^{1}H NMR (300 MHz, CD$_3$OD) δ 7.71 (d, J = 7.7 Hz, 2H), 7.43 (d, J = 7.7 Hz, 2H), 7.36 – 7.18 (m, 5H), 6.99 (m, 2H), 6.63 (t, J = 7.3 Hz, 1H), 6.50 (d, J = 7.8 Hz, 1H), 4.25 (s, 2H), 3.56 (s, 2H), 3.17 (s, 2H), 2.81 (d, J = 11.5 Hz, 2H), 2.11 (t, J = 11.6 Hz, 2H), 1.91 (t, J = 11.3 Hz, 2H), 1.65 (d, J = 13.0 Hz, 2H). ^{13}C NMR (75 MHz, CD$_3$OD) δ 166.6, 151.3, 141.2, 138.4, 137.1, 131.2, 129.5, 128.1, 127.5 (2C), 126.8, 126.7, 121.8, 117.5, 106.9, 62.3, 62.1, 52.4, 50.3, 42.3, 35.4. ESI MS m/z [M+H]$^+$ 428; HRMS (m/z) calcd for C$_{27}$H$_{30}$N$_3$O$_2$ ([M+H]$^+$) 428.2333, found 428.2323.

4-((1-Benzoylspiro(indoline-3,4'-piperidin)-1'-yl)methyl)-N-hydroxybenzamide (16)

Step h: Starting from **43c** (18 mg, 0.06 mmol) and methyl 4-formyl benzoate (20 mg, 0.12 mmol), compound *methyl 4-((1-benzoylspiro(indoline-3,4'-piperidin)-1'-yl)methyl)benzoate* was obtained following the same procedure described for the synthesis of **43a** (**Step e**). Crude material was purified by column chromatography on silica gel (EtOAc/petroleum ether 1:2) obtaining *methyl 4-((1-benzoylspiro(indoline-3,4'-piperidin)-1'-yl)methyl)benzoate* as a colorless oil (16 mg, yield: 59%). ^{1}H NMR (300 MHz, CDCl$_3$) δ 8.12 – 7.91 (m, 4H), 7.60 – 7.33 (m, 7H), 7.29 – 7.19 (m, 1H), 7.04 (s, 1H), 4.68 (s, 2H), 4.03 – 3.82 (m, 5H), 3.58 (s, 2H), 2.87 (s, 2H), 2.03 (s, 2H), 1.69 (d, J = 10.2 Hz, 2H). ESI MS m/z [M+H]$^+$ 441. **Step i:** To a stirred solution of this latter intermediate (16 mg, 0.04 mmol) in DCM (2 mL): MeOH (1 mL) was added a 50% aqueous solution of NH$_2$OH (242 μL, 3.6 mmol) dropwise followed by the addition of a 4 M solution of KOH in MeOH (453 μL, 1.8 mmol) and reaction was allowed to stir at 25 °C for 2 h. The reaction mixture was neutralized with a 6 N solution of HCl and the solvent was evaporated to dryness. Crude was purified by column chromatography on silica

gel (DCM/MeOH/NH$_4$OH 20:1:0.1) obtaining **16** as a colorless oil (10 mg, yield: 63%). ^{1}H NMR (300 MHz, CD$_3$OD) δ 7.71 (d, J = 7.9 Hz, 2H), 7.65 – 7.39 (m, 8H), 7.27 (d, J = 8.4 Hz, 1H), 7.10 (s, 2H), 3.95 (s, 2H), 3.59 (s, 2H), 2.87 (s, 2H), 2.17 – 1.87 (m, 4H), 1.68 (d, J = 11.4 Hz, 2H). ^{13}C NMR (75 MHz, CD$_3$OD) δ 169.8, 168.7, 166.5, 141.3, 141.1, 140.4, 136.5, 131.2, 130.4, 129.4, 129.2, 128.5, 127.4, 126.7, 124.5, 122.5, 62.9, 62.1, 50.2, 35.5, 17.8. ESI MS m/z [M+H]$^+$ 442.

N-Hydroxy-4-((1-methyl-7-phenylspiro(indoline,-3,4'-piperidin)-1'-yl)methyl)benzamide (17)

Step h: Starting from **43d** (50 mg, 0.06 mmol) and methyl 4-formyl benzoate (35 mg, 0.22 mmol), compound *methyl 4-((1-methyl-7-phenylspiro(indoline-3,4'-piperidin)-1'-yl)methyl)benzoate* was obtained following the same procedure described for the synthesis of **10a** (**Step e**). Crude material was purified by column chromatography on silica gel (EtOAc/petroleum ether 1:4) obtaining *methyl 4-((1-methyl-7-phenylspiro(indoline-3,4'-piperidin)-1'-yl)methyl)benzoate* as a white solid (36 mg, yield: 66%). ^{1}H NMR (300 MHz, CDCl$_3$) δ 8.01 (d, J = 8.3 Hz, 2H), 7.49 – 7.28 (m, 7H), 7.09 (dd, J = 7.3, 1.2 Hz, 1H), 7.01 (dd, J = 7.6, 1.2 Hz, 1H), 6.82 (t, J = 7.4 Hz, 1H), 3.92 (s, 3H), 3.60 (s, 2H), 3.21 (s, 2H), 2.86 (d, J = 11.5 Hz, 2H), 2.35 (s, 3H), 2.16 (t, J = 10.9 Hz, 2H), 1.98 (dd, J = 12.4, 3.5 Hz, 2H), 1.76 (d, J = 12.6 Hz, 2H). ESI MS m/z [M+H]$^+$ 427. **Step i:** To a stirred solution of this intermediate (42 mg, 0.10 mmol) in DCM (2 mL): MeOH (1 mL) was added a 50% aqueous solution of NH$_2$OH (646 µL, 10 mmol) dropwise followed by the addition of a 4 M solution of KOH in MeOH (1250 µL, 5 mmol) and the reaction was allowed to stir at 25 °C for 2 h. The reaction mixture was neutralized with a 6 N solution of HCl and the solvent was evaporated to dryness. Crude was purified by column chromatography on silica gel (DCM/MeOH/NH$_4$OH 20:1:0.1) obtaining **17** as a white solid (35 mg, yield: 83%). ^{1}H NMR (300 MHz, CD$_3$OD) δ

7.74 (d, J = 7.4 Hz, 2H), 7.47 (d, J = 7.4 Hz, 2H), 7.39 – 7.19 (m, 5H), 7.01 (d, J = 7.1 Hz, 1H), 6.90 (d, J = 7.4 Hz, 1H), 6.76 (t, J = 7.4 Hz, 1H), 3.63 (s, 2H), 3.18 (s, 2H), 2.87 (d, J = 11.8 Hz, 2H), 2.38 – 2.12 (m, 5H), 1.95 (dd, J = 17.9, 8.3 Hz, 2H), 1.69 (d, J = 13.0 Hz, 2H). ^{13}C NMR (75 MHz, CD$_3$OD) δ 166.5, 149.1, 141.2, 140.8, 139.2, 131.2, 130.2, 129.5, 128.7, 127.7, 126.8, 126.4, 125.4, 120.8, 119.0, 66.2, 62.4, 50.4, 42.0, 39.1, 35.8. ESI MS m/z [M+H]$^+$ 428.

4-((1-Benzyl-7-phenylspiro(indoline-3,4'-piperidin)-1'-yl)methyl)-N-hydroxybenzamide (18)

Step h: Starting from **43e** (35 mg, 0.10 mmol) and methyl 4-formyl benzoate (32 mg, 0.19 mmol), compound *methyl 4-((1-benzyl-7-phenylspiro(indoline-3,4'-piperidin)-1'-yl)methyl)benzoate* was obtained following the same procedure described for the synthesis of **43a** (**step e**). Crude material was purified by column chromatography on silica gel (EtOAc/petroleum ether 1:4) obtaining *methyl 4-((1-benzyl-7-phenylspiro(indoline-3,4'-piperidin)-1'-yl)methyl)benzoate* as a white solid (10 mg, yield: 20%). ^{1}H NMR (300 MHz, CDCl$_3$) δ 8.21 (d, J = 8.3 Hz, 1H), 8.13 – 7.91 (m, 3H), 7.45 (dd, J = 19.0, 7.5 Hz, 4H), 7.35 – 7.16 (m, 5H), 7.16 – 6.99 (m, 3H), 6.86 (t, J = 7.4 Hz, 1H), 3.91 (t, J = 3.9 Hz, 5H), 3.55 (s, 2H), 3.18 (s, 2H), 2.81 (s, 2H), 2.03 (s, 4H), 1.67 (d, J = 10.0 Hz, 2H). ESI MS m/z [M+H]$^+$ 503. **Step i:** To a stirred solution of this latter intermediate (10 mg, 0.02 mmol) in DCM (2 mL): MeOH (1 mL) was added a 50% aqueous solution of NH$_2$OH (132 µL, 2 mmol) dropwise followed by the addition of 4 M solution of KOH in MeOH (248 µL, 1 mmol) and the reaction was allowed to stir at 25 °C for 2 h. The reaction mixture was neutralized with a 6 N solution of HCl and the solvent was evaporated to dryness. Crude was purified by column chromatography on silica gel (DCM/MeOH/NH$_4$OH 20:1:0.1) obtaining **18** as a yellow oil (7 mg, yield: 70%). ^{1}H NMR (300 MHz, CD$_3$OD) δ 7.72 (d, J = 8.0 Hz, 2H), 7.46 (d, J = 5.5 Hz,

4H), 7.37 – 6.89 (m, 10H), 6.81 (t, J = 7.4 Hz, 1H), 3.85 (s, 2H), 3.61 (s, 2H), 3.19 (s, 2H),

2.85 (d, J = 11.5 Hz, 2H), 2.17-1.91 (m, 4H), 1.60 (d, J = 13.0 Hz, 2H). ^{13}C NMR (75 MHz,

CD$_3$OD) δ 166.5, 148.3, 140.7, 139.2, 138.6, 131.4, 130.3, 129.6, 129.5, 128.4, 128.3, 128.2,

128.0, 127.9, 127.3, 126.8, 126.5 (2C), 125.4, 121.2, 119.2, 62.5, 62.1, 55.1, 50.2, 42.2, 36.3.

ESI MS m/z [M+H]$^+$ 504.

4-((1-Benzoyl-7-phenylspiro(indoline-3,4'-piperidin)-1'-yl)methyl)-N-hydroxybenzamide (19

Starting from **43f** (35 mg, 0.10 mmol) and methyl 4-formyl benzoate (15 mg, 0.09 mmol),

compound *methyl 4-((1-benzoyl-7-phenylspiro(indoline-3,4'-piperidin)-1'-yl)methyl)benzoate*

was obtained following the same procedure described for the synthesis of **43a** (**step e**). Crude

material was purified by column chromatography on silica gel (EtOAc/petroleum ether 1:4)

obtaining *methyl 4-((1-benzoyl-7-phenylspiro(indoline-3,4'-piperidin)-1'-yl)methyl)benzoate*

as a white solid (10 mg, yield: 20%). ^{1}H NMR (300 MHz, CDCl$_3$) δ 8.00 (d, J = 8.1 Hz, 2H),

7.43 (d, J = 8.0 Hz, 2H), 7.33 – 6.68 (m, 13H), 3.91 (s, 3H), 3.59 (s, 2H), 2.90 (d, J = 6.7 Hz,

2H), 2.13 (s, 2H), 1.74 (d, J = 10.4 Hz, 2H), 1.56 – 1.47 (m, 2H), 1.43 – 1.27 (m, 2H). ESI MS

m/z [M+H]$^+$ 517. **Step i:** To a stirred solution of this latter intermediate (37 mg, 0.07 mmol) in

DCM (2 mL): MeOH (1 mL) was added a 50% aqueous solution of NH$_2$OH (467 µL, 7 mmol)

dropwise followed by the addition of 4 M solution of KOH in MeOH (889 µL, 3.5 mmol) and

reaction was allowed to stir at 25 °C for 2 h. The reaction mixture was neutralized with a 6 N

of HCl and the solvent was evaporated to dryness. Crude was purified by column

chromatography on silica gel (DCM/MeOH/NH$_4$OH 20:1:0.1) obtaining **19** as a white solid

(27 mg, yield: 75%). ^{1}H NMR (300 MHz, DMSO) δ 11.16 (s, 1H), 9.01 (s, 1H), 7.69 (d, J =

7.9 Hz, 2H), 7.52 – 6.87 (m, 15H), 4.01 (s, 2H), 3.49 (s, 2H), 2.75 (s, 2H), 1.93 (m, 4H), 1.58

(m, 4H). ^{13}C NMR (75 MHz, CDCl$_3$) δ 173.7, 169.3, 157.1, 148.3, 145.3, 144.7, 140.7, 136.7,

136.1, 134.0, 133.5, 132.8, 132.0, 131.7, 131.0, 126.8, 66.8, 66.0, 60.1, 48.9, 39.5. ESI MS m/z [M+H]$^+$ 518.

Methyl 5-formylthiophene-2-carboxylate (45)

To a solution of 4-methylmorpholine *N*-oxide (449 mg, 3.83 mmol) in MeCN (5 mL) cooled at 0 °C, in presence of molecular sieves 3Å, a solution of compound **44** in MeCN (300 mg, 1.28 mmol) was added. The reaction mixture was stirred at 25 °C for 12 h; then it was filtered and purified by column chromatography on silica gel (EtOAc/petroleum ether 1:20) to obtaining the title compound (230 mg, yield: 71%); ^{1}H NMR: (300 MHz, CDCl$_3$) δ 9.96 (s, 1H), 7.82 (d, *J* = 1.1 Hz, 1H), 7.72 (d, *J* = 2.8 Hz, 1H), 3.93 (s, 3H); ESI MS *m/z* [M+H]+ 171.

N-Hydroxy-5-((1-methylspiro(indoline-3,4'-piperidin)-1'-yl)methyl)thiophene-2-carboxamide (20)

Step b: Starting from **43a** (14 mg, 0.07 mmol) and **45** (23 mg, 0.14 mmol), compound *methyl 5-((1-methylspiro(indoline-3,4'-piperidin)-1'-yl)methyl)thiophene-2-carboxylate* (12 mg, yield: 50%) was obtained as a colorless oil following the same procedure described for the synthesis of **43a**. ^{1}H NMR (300 MHz, CDCl$_3$) δ 7.67 (d, *J* = 3.7 Hz, 1H), 7.09 (dd, *J* = 13.9, 7.2 Hz, 2H), 6.92 (d, *J* = 3.7 Hz, 1H), 6.71 (t, *J* = 7.4 Hz, 1H), 6.47 (d, *J* = 7.8 Hz, 1H), 3.87 (s, 3H), 3.76 (s, 2H), 3.18 (s, 2H), 2.90 (d, *J* = 11.7 Hz, 2H), 2.75 (s, 3H), 2.21 (td, *J* = 11.8, 2.1 Hz, 2H), 1.96 (td, *J* = 12.9, 3.9 Hz, 2H), 1.72 (d, *J* = 12.5 Hz, 2H). ESI MS *m/z* [M+H]+ 357. To a stirred solution of this latter intermediate (12 mg, 0.03 mmol) in DCM (2 mL) and MeOH (1 mL) a 50% aqueous solution of NH$_2$OH (224 µL, 3 mmol) and a 4 M solution of KOH in MeOH (420 µL, 1.5 mmol) were added. The reaction was stirred at 25 °C for 2 h. The reaction mixture was neutralized with a 6 N solution of HCl and the solvent was evaporated to dryness. Crude was purified by column chromatography on silica gel (DCM/MeOH/NH$_4$OH

20:1:0.1) obtaining **20** as a yellow oil (8 mg, yield: 67%). ^{1}H NMR (300 MHz, CD$_3$OD) δ 7.45 (s, 1H), 7.09 – 6.91 (m, 3H), 6.66 (t, J = 7.4 Hz, 1H), 6.49 (d, J = 7.7 Hz, 1H), 3.80 (s, 2H), 3.16 (s, 2H), 2.98 – 2.81 (m, 2H), 2.72 (s, 3H), 2.26 (t, J = 12.0 Hz, 2H), 2.02 – 1.85 (m, 2H), 1.68 (d, J = 13.2 Hz, 2H).^{13}C NMR (75 MHz, CD$_3$OD) δ 161.7, 152.2, 146.3, 137.5, 135.0, 127.9, 127.5, 126.9, 121.6, 118.0, 107.4, 64.8, 56.6, 50.1, 42.4, 35.3, 35.0. ESI MS *m/z* [M+H]$^+$ 358.

4-(2-(1-Benzylspiro(indoline-3,4'-piperidin)-1'-yl)-2-oxoethyl)-N-hydroxybenzamide *(21)*

Step a: To a stirred suspension of 2-(4-(methoxycarbonyl)phenyl)acetic acid (17 mg, 0.09 mmol) in dry DCM (1 mL) cooled to 0 °C DIPEA (60 µL, 0.35 mmol) EDCI (20 mg, 0.11 mmol) and 1-HOBt (17 mg, 0.13 mmol) were added. After 30 min, the reaction was cooled to 0 °C and a solution of **43b** (28 mg, 0.11 mmol) in dry DCM (1 mL) was added dropwise to the reaction mixture. The reaction was allowed to reach 25 °C and stirred for 24 h. Thereafter, a saturated solution of NH$_4$Cl (3 mL) was added and the mixture was extracted with DCM (3 x 3 mL). The combined organic layers were dried over Na$_2$SO$_4$, filtered and evaporated *in vacuo*. The crude material was purified by column chromatography using silica gel obtaining *methyl 4-(2-(1-benzylspiro(indoline-3,4'-piperidin)-1'-yl)-2-oxoethyl)benzoate* as a yellow oil (20 mg, yield: 50%). ^{1}H NMR (300 MHz, CDCl$_3$) δ 8.01 (d, J = 8.3 Hz, 2H), 7.40 – 7.22 (m, 7H), 7.10 (td, J = 7.7, 1.1 Hz, 1H), 6.98 – 6.87 (m, 1H), 6.71 (t, J = 7.1 Hz, 1H), 6.53 (d, J = 7.8 Hz, 1H), 4.56 (d, J = 13.6 Hz, 1H), 4.39 – 4.20 (m, 2H), 3.91 (s, 3H), 3.79 (d, J = 18.7 Hz, 3H), 3.23 (s, 2H), 3.16 – 2.98 (m, 1H), 2.83 – 2.64 (m, 1H), 1.89 – 1.47 (m, 4H). ESI MS m/z [M+H]$^+$ 455.

Step b: To a stirred solution of this latter intermediate (20 mg, 0.04 mmol) in DCM (2 mL) and MeOH (1 mL) a 50% aqueous solution of NH$_2$OH (293 µL, 4 mmol) and a of 4 M solution of KOH in MeOH (549 µL, 2 mmol) were added. The reaction was stirred at 25 °C for 2 h. Then the reaction was neutralized with a 6 N solution of HCl and the solvent was evaporated

to dryness. Crude was purified by column chromatography on silica gel (DCM/MeOH/NH$_4$OH 20:1:0.1) obtaining **21** as a yellow oil (11 mg, yield: 55%). ^{1}H NMR (300 MHz, DMSO) δ 11.16 (s, 1H), 9.00 (s, 1H), 7.68 (d, J = 7.9 Hz, 2H), 7.38 – 7.16 (m, 7H), 6.95 (d, J = 7.5 Hz, 2H), 6.63 – 6.41 (m, 2H), 4.30 (s, 3H), 3.96 – 3.66 (m, 3H), 3.28 (s, 2H), 3.18 – 2.98 (m, 1H), 2.77 – 2.59 (m, 1H), 1.58 (s, 4H). ^{13}C NMR (75 MHz, DMSO) δ 168.8, 164.6, 151.4, 139.9, 138.7, 137.0, 131.3, 129.5, 128.9, 128.2, 128.1, 127.4, 127.3, 122.6, 117.7, 107.4, 61.9, 55.4, 52.1, 43.2, 36.3, 35.6. ESI MS m/z [M+H]$^+$ 456; HRMS (m/z) calcd for C$_{27}$H$_{30}$N$_3$O$_2$ ([M+H]$^+$) 456.2282, found 456.2273.

1-Benzyl-N-(4-(hydroxycarbamoyl)benzyl)spiro(indoline-3,4'-piperidine)-1'-carboxamide (22)

Step c: To a solution of **43b** (20 mg, 0.07 mmol) in dry THF (1 mL) a solution of methyl 4-(isocyanatomethyl)benzoate (27 mg, 0.14 mmol) in dry THF (1 mL) and TEA (40 µL, 0.29 mmol) were added. The reaction mixture was stirred at 65 °C for 2 h. The solvent was removed *in vacuo*, and the crude was purified by column chromatography on silica gel (EtOAc/petroleum ether 1:3) obtaining *methyl 4-((1-benzylspiro(indoline-3,4'-piperidin)-1'-ylcarboxamido)methyl)benzoate* (28 mg, yield: 83%) as a yellow oil. ^{1}H NMR (300 MHz, CDCl$_3$) δ 7.99 (d, J = 8.1 Hz, 2H), 7.47 – 7.23 (m, 7H), 7.15 – 6.95 (m, 2H), 6.72 (t, J = 7.3 Hz, 1H), 6.53 (d, J = 7.8 Hz, 1H), 5.03 (s, 1H), 4.49 (d, J = 5.4 Hz, 2H), 4.30 (s, 2H), 3.92 (d, J = 10.8 Hz, 5H), 3.26 (s, 2H), 2.94 (t, J = 11.3 Hz, 2H), 1.91-1.72 (m, 4H). ESI MS m/z [M+H]$^+$ 470. **Step n:** To a stirred solution of *methyl 4-((1-benzylspiro(indoline-3,4'-piperidin)-1'-ylcarboxamido)methyl)benzoate* (28 mg, 0.06 mmol) in DCM (2 mL) and MeOH (1 mL) a 50% aqueous solution of NH$_2$OH (400 µL, 6 mmol) and a of 4 M solution of KOH in MeOH (762 µL, 3 mmol) were added. The reaction was stirred at 25 °C for 2 h then it was neutralized with a 6 N solution of HCl and the solvent was evaporated to dryness. Crude was purified by

column chromatography on silica gel (DCM/MeOH/NH$_4$OH 20:1:0.1) obtaining **22** as a brownish solid (24 mg, yield: 85%). ^{1}H NMR (300 MHz, CD$_3$OD) δ 7.71 (d, J = 8.0 Hz, 2H), 7.64 – 7.32 (m, 11H), 4.84 (s, 2H), 4.40 (s, 2H), 4.03 (d, J = 13.8 Hz, 2H), 3.83 (s, 2H), 2.92 (t, J = 12.6 Hz, 2H), 1.85 (t, J = 11.0 Hz, 2H), 1.60 (d, J = 13.4 Hz, 2H). ^{13}C NMR (75 MHz, CD$_3$OD) δ 172.3, 170.7, 162.4, 148.5, 146.0, 143.9, 134.8, 134.2, 133.6, 133.4, 133.1, 132.8, 130.9, 130.8, 128.1, 122.0, 64.3, 63.2, 48.1, 47.5, 44.8, 39.6. ESI MS m/z [M+H]$^+$ 471.

4-(Hydroxycarbamoyl)benzyl 1-benzylspiro(indoline-3,4'-piperidine)-1'-carboxylate (23)

Step d: CDI (12 mg, 0.07 mmol) was suspended in dry DCM (1 mL) and the mixture was cooled to 0 °C. Methyl 4-(hydroxymethyl)benzoate (12 mg, 0.07 mmol) dissolved in dry DCM (1 mL) was slowly added to the mixture and the reaction was stirred at 25 °C for 1 h. Compound **43b** (20 mg, 0.07 mmol) was dissolved in dry DCM (1 mL) and added to the reaction mixture, which was stirred at 25 °C for 6 h. Then, EtOAc (5 mL) was added and the mixture was extracted with EtOAC (3 x 5 mL). The combined organic layers were washed with 10% HCl (5 mL), brine (5 mL) and dried over Na$_2$SO$_4$, filtered and concentrated *in vacuo* obtaining the pure compound *4-(methoxycarbonyl)benzyl 1-benzylspiro(indoline-3,4'-piperidine)-1'-carboxylate* as a colorless oil (19 mg, yield: 58%). ^{1}H NMR (300 MHz, CDCl$_3$) δ 8.04 (d, J = 8.2 Hz, 2H), 7.42 (d, J = 8.1 Hz, 2H), 7.38 – 7.21 (m, 5H), 7.14 – 6.97 (m, 2H), 6.71 (t, J = 7.4 Hz, 1H), 6.53 (d, J = 7.8 Hz, 1H), 5.20 (s, 2H), 4.30 (s, 2H), 4.10 (s, 2H), 3.92 (s, 3H), 3.26 (s, 2H), 2.96 (s, 2H), 1.84 - 1.72 (m, 4H). ESI MS m/z [M+H]$^+$ 471. **Step b:** To a stirred solution of *4-(methoxycarbonyl)benzyl 1-benzylspiro[indoline-3,4'-piperidine]-1'-carboxylate* (19 mg, 0.04 mmol) in DCM (2 mL) and MeOH (1 mL) a 50% aqueous solution of NH$_2$OH (269 µL, 4 mmol) and a 4 M solution of KOH in MeOH (504 µL, 2 mmol) were added. The reaction was allowed to stir at 25 °C for 2 h then it was neutralized with a 6 N solution of HCl and the solvent was evaporated to dryness. Crude was purified by column chromatography on silica

gel (DCM/MeOH/NH$_4$OH 20:1:0.1) obtaining **23** as a yellow oil (14 mg, yield: 74%). ^{1}H NMR (300 MHz, CD$_3$OD) δ 7.75 (d, J = 7.8 Hz, 2H), 7.45 (d, J = 7.7 Hz, 2H), 7.40 – 7.17 (m, 5H), 7.09 – 6.92 (m, 2H), 6.64 (t, J = 7.3 Hz, 1H), 6.53 (d, J = 7.8 Hz, 1H), 5.18 (s, 2H), 4.29 (s, 2H), 4.07 (d, J = 13.2 Hz, 2H), 3.27 (s, 2H), 2.98 (s, 2H), 1.88 – 1.59 (m, 4H). ^{13}C NMR (75 MHz, CD$_3$OD) δ 166.4, 155.3, 151.2, 140.7, 138.4, 136.6, 131.7, 129.3, 128.1, 127.7, 127.5, 127.3, 127.0, 126.9, 121.8, 117.6, 107.1, 66.1, 61.6, 53.4, 52.4, 42.7, 41.0, 35.3. ESI MS m/z [M+H]$^+$ 472.

Methyl 4-((2,3-dioxoindolin-1-yl)methyl)benzoate (47)

To a solution of isatin (300 mg, 2.03 mmol) in dry DMF, cooled at 0 °C, a 60% dispersion of NaH, in mineral oil (95 mg, 2.38 mmol) was added and stirred for 5 min at 0 °C. Then, methyl 4-(bromomethyl)benzoate (2.34 g, 10.20 mmol) was added and the reaction was allowed to reach 25 °C and stirred for 12 h. Thereafter, a saturated solution of NH$_4$Cl (5 mL) was added and the mixture was extracted with EtOAc (3 x 5 mL). The combined organic layers were washed with brine, dried over Na$_2$SO$_4$ and concentrated *in vacuo*. The residue was used in the next step without further purification and affording **47** (2.00 g, yield: 99%) as a red solid. ^{1}H NMR (300 MHz, CDCl$_3$) δ 8.02 (d, 2H), 7.63 (d, J = 7.4, 1H), 7.48 (td, J = 7.8, 1.3 Hz, 1H), 7.39 (d, J = 8.4 Hz, 2H), 7.11 (t, J = 7.6, 1H), 6.71 (d, J = 8.0, 1H), 4.98 (s, 2H), 3.90 (s, 3H). ESI-MS *m/z*: [M + H]$^+$ 296.0.

Ethyl 4-((3-hydroxy-2-oxo-4-phenylquinolin-1(2H)-yl)methyl)benzoate (48a)

A solution of benzaldehyde (379 mg, 3.57 mmol) and PTSH (665 mg, 3.57 mmol) in EtOH (17 mL) was stirred at 25 °C for 2 h. After this, **47** (575 mg, 3.57 mmol) and K$_2$CO$_3$ (987 mg, 7.14 mmol) were added and the reaction was stirred at 80 °C for 12 h. The solvent was evaporated, and the crude was purified by chromatography on silica gel (20% EtOAc in

petroleum ether) giving **48a** (430 mg, yield: 64%) as a red solid. ^{1}H NMR (300 MHz, CDCl$_3$) δ 8.02 (d, J = 8.3 Hz, 2H), 7.65 – 6.99 (m, 11H), 5.74 (s, 2H), 4.49 – 4.25 (m, 2H), 1.37 (t, J = 7.1 Hz, 3H); ESI-MS m/z: [M + H]$^+$ 400.1.

Ethyl 4-((3-hydroxy-2-oxo-4-(pyridin-3-yl)quinolin-1(2H)-yl)methyl)benzoate (48b)

Starting from **47** (100 mg, 0.33 mmol) the title compound was obtained following the procedure described to get **48a**. The residue was purified by chromatography on silica gel (2% MeOH in DCM) affording **48b** (43 mg, yield: 32%) as a red solid. ^{1}H NMR (300 MHz, DMSO) δ 9.70 (s, 1H), 8.76 – 8.46 (m, 2H), 7.87 (dd, J = 26.9, 7.9 Hz, 3H), 7.55 (dt, J = 18.9, 9.4 Hz, 1H), 7.47 – 7.23 (m, 4H), 7.24 – 7.00 (m, 2H), 5.74 (s, 2H), 4.27 (q, J = 7.0 Hz, 2H), 1.25 (dd, J = 15.8, 8.9 Hz, 3H); ESI-MS m/z: [M + H]$^+$ 400.9.

N-Hydroxy-4-((3-hydroxy-2-oxo-4-phenylquinolin-1(2H)-yl)methyl)benzamide (24)

To a solution of **48a** (55 mg, 0.10 mmol) in a 2:1 mixture of DCM (4 mL): MeOH (2 mL), a 50% solution of NH$_2$OH in water (660 µL, 10.00 mmol) and a 4 M solution of KOH in methanol (1.25 mL, 5.00 mmol) were added dropwise. The reaction was stirred at 25 °C for 3 h, then it was neutralized with 6 N HCl and concentrated *in vacuo*. The residue was purified by chromatography on silica gel (0.1% NH$_4$OH, 10% MeOH in DCM) affording **24** (76 mg, yield: 79%) as a white solid. ^{1}H NMR (300 MHz, DMSO) δ 11.14 (s, 1H), 9.36 (s, 1H), 8.98 (s, 1H), 7.75 – 7.24 (m, 11H), 7.11 (d, J = 4.1 Hz, 2H), 5.69 (s, 2H); ^{13}C NMR (75 MHz, DMSO) δ 164.4, 158.9, 142.0, 140.2, 134.0, 133.9, 132.2, 130.4, 128.9, 128.2, 127.8, 127.3, 127.0, 125.7, 124.3, 123.1, 122.2, 115.6, 45.9; ESI-MS m/z: [M - H]$^+$ 385.0.

N-Hydroxy-4-((3-hydroxy-2-oxo-4-(pyridin-3-yl)quinolin-1(2H)-yl)methyl)benzamide (27)

Starting from **48b** (20 mg, 0.05 mmol) the title compound was obtained following the procedure described to get **24**. The residue was purified by chromatography on silica gel (0.1% NH$_4$OH, 10% MeOH in DCM) affording **27** (16 mg, yield: 84%). ^{1}H NMR (300 MHz, DMSO) ^{1}H NMR (300 MHz, DMSO) δ 11.15 (s, 1H), 8.99 (s, 1H), 8.65 (d, *J* = 3.5 Hz, 1H), 8.57 (s, 1H), 7.83 (d, *J* = 7.7 Hz, 1H), 7.69 (d, *J* = 8.1 Hz, 2H), 7.62 – 7.50 (m, 1H), 7.46 – 7.24 (m, 4H), 7.22 – 6.96 (m, 2H), 5.70 (s, 2H); ^{13}C NMR (75 MHz, DMSO) δ 164.3, 150.8, 149.4, 142.9, 140.1, 138.2, 133.9, 132.3, 130.0, 127.8, 127.5, 127.0, 125.3, 124.0, 123.4, 121.9, 121.0, 115.7, 46.0; ESI-MS *m/z*: [M - H]$^+$ 386.0.

Ethyl 4-((3-methoxy-2-oxo-4-phenylquinolin-1(2H)-yl)methyl)benzoate (49a)

To a solution of **48a** (100 mg, 0.25 mmol) in dry THF (3 mL) cooled at 0 °C, a 60% dispersion of NaH in mineral oil (15 mg, 0.38 mmol) was added. The mixture was stirred at 0 °C for 30 min, then MeI (78 µL, 1.25 mmol) was added. The reaction was allowed to reach 25 °C and stirred for 12 h. After this time a saturated solution of NH$_4$Cl (5 mL) was added and the mixture was extracted with EtOAc (3 x 5 mL). The combined organic layers were dried over Na$_2$SO$_4$ and concentrated in vacuo. The residue was purified by chromatography on silica gel (25% EtOAc in Petroleum ether) affording **49a** (30 mg, yield: 29%) as a colorless oil. ^{1}H NMR (300 MHz, CDCl$_3$) δ 8.11 – 7.90 (m, 2H), 7.58 – 7.44 (m, 3H), 7.44 – 7.14 (m, 7H), 7.15 – 6.99 (m, 1H), 5.69 (s, 2H), 4.34 (q, *J* = 7.1 Hz, 2H), 3.80 (s, 3H), 1.35 (t, *J* = 7.1 Hz, 3H); ESI-MS *m/z*: [M + H]$^+$ 414.0.

Ethyl 4-((3-(benzyloxy)-2-oxo-4-phenylquinolin-1(2H)-yl)methyl)benzoate (49b)

To a solution of **48a** (50 mg, 0.125 mmol) and benzyl bromide (16 µL, 0.137 mmol) in anhydrous DMF (2 mL) was added K$_2$CO$_3$ (34 mg, 0.25 mmol) followed by KI (2mg, 0.01 mmol). Reaction was refluxed for 8 h at 80 °C. Reaction mixture was then diluted with

saturated solution of NH$_4$Cl and EtOAc, and the organic layer was extracted. It was successively washed with a saturated solution of NaHCO$_3$ (5 mL) and brine (5 mL), dried over Na$_2$SO$_4$ and concentrated *in vacuo*. The residue was purified by chromatography on silica gel (25% EtOAc in petroleum ether) affording **49b** (800 mg, yield: 70%) as a pale-yellow oil. ^{1}H NMR (300 MHz, CDCl$_3$) δ 8.00 (d, *J* = 14.0 Hz, 2H), 7.57 – 7.41 (m, 3H), 7.41 – 7.13 (m, 10H), 7.14 – 6.97 (m, 3H), 5.73 (s, 2H), 5.18 (s, 2H), 4.51 – 4.19 (q, 2H), 1.46 – 1.31 (t, 3H); ESI-MS *m/z*: [M + H]$^+$ 489.9.

N-Hydroxy-4-((3-methoxy-2-oxo-4-phenylquinolin-1(2H)-yl)methyl)benzamide (25)

Starting from **49a** (30 mg, 0.07 mmol) the title compound was obtained following the procedure described to get **24**. The residue was purified by chromatography on silica gel (0.1% NH$_4$OH, 10% MeOH in DCM) affording **25** (28 mg, yield: 97%) as a white solid. ^{1}H NMR (300 MHz, CDCl$_3$) δ 7.66 (s, 2H), 7.58 – 7.41 (m, 3H), 7.41 – 6.95 (m, 8H), 5.56 (s, 2H), 3.71 (s, 3H); ^{13}C NMR (75 MHz, DMSO) δ 164.4, 158.8, 144.8, 140.3, 137.7, 136.4, 133.7, 132.2, 129.7, 129.5, 128.9, 128.6, 127.7, 127.2, 127.0, 123.0, 121.1, 115.6, 60.1, 45.6; ESI-MS *m/z*: [M + H]$^+$ 401.0.

4-((3-(Benzyloxy)-2-oxo-4-phenylquinolin-1(2H)-yl)methyl)-N-hydroxybenzamide (26)

Starting from **49b** (27 mg, 489.56 mmol) the title compound was obtained following the procedure described to get **24**. The residue was purified by chromatography on silica gel (0.1% NH$_4$OH, 10% MeOH in DCM) affording **26** (22 mg, yield: 85%) as a light brown solid. ^{1}H NMR (300 MHz, DMSO) δ 11.16 (s, 1H), 9.01 (s, 1H), 7.70 (d, *J* = 7.9 Hz, 2H), 7.59 – 6.81 (m, 16H), 5.70 (s, 2H), 5.07 (s, 2H). ^{13}C NMR (75 MHz, DMSO) δ 164.4, 159.1, 143.4, 140.3, 138.3, 137.3, 136.5, 133.6, 132.2, 129.8. 129.6, 128.8, 128.6 (2C), 128.5, 128.3, 127.7, 127.2, 127.1, 123.0, 121.2, 115.6, 73.5, 45.6; ESI-MS *m/z*: [M + H]$^+$ 476.9.

3-Hydroxy-4-phenylquinolin-2(1H)-one (50a)

A solution of benzaldehyde (100 mg, 0.94 mmol) and PTSH (175 mg, 0.94 mmol) in EtOH (5 mL) was stirred at 25 °C for 2 h. After this, isatin (138 mg, 0.94 mmol) and K_2CO_3 (260 mg, 1.88 mmol) were added and the reaction was stirred at 80 °C for 12 h. The solvent was evaporated, and the crude was purified by chromatography on silica gel (20% EtOAc in petroleum ether) giving **50a** (95 mg, yield: 42%) as a brown solid. ^{1}HNMR: 1H NMR (300 MHz, DMSO) δ 12.19 (s, 1H), 9.16 (s, $J = 0.7$ Hz, 1H), 7.57 − 7.35 (m, 3H), 7.28 (dd, $J = 8.6$, 6.0 Hz, 4H), 7.09 − 6.94 (m, 2H); ESI-MS m/z: $[M + Na]^+$ 260.1.

3-Hydroxy-4-(pyridin-3-yl)quinolin-2(1H)-one (50b)

Starting from 3-pyridinecarboxaldehyde (181 mg, 1.69 mmol) and isatin (500 mg, 1.69), the title compound was obtained following the procedure previously described for compound **50a**. The crude was purified by chromatography on silica gel (5% MeOH in DCM) giving **50b** (180 mg, yield: 45%) as a red solid. ^{1}H NMR (300 MHz, DMSO) δ 12.27 (s, 1H), 9.49 (s, 1H), 8.62 (dd, $J = 4.8$, 1.7 Hz, 1H), 8.53 (dd, $J = 2.2$, 0.8 Hz, 1H), 7.85 − 7.71 (m, 1H), 7.62 − 7.46 (m, 1H), 7.42 − 7.25 (m, 2H), 7.17 − 7.05 (m, 1H), 7.05 − 6.94 (m, 1H); ESI-MS m/z: $[M + H]^+$ 239.0.

Methyl 4-(((2-oxo-4-phenyl-1,2-dihydroquinolin-3-yl)oxy)methyl)benzoate (51a)

To a solution of **50a** (100 mg, 0.42 mmol) in dry DMF (4 mL) methyl 4-(bromomethyl)benzoate (145 mg, 0.63 mmol), KI (7 mg, 0.04 mmol) and K_2CO_3 (116 mg, 0.84 mmol) were added. The reaction mixture was stirred at 80 °C for 12 h. Thereafter the mixture was cooled down to 25 °C and a saturated solution of NH$_4$Cl (10 mL) was added. The mixture was extracted with EtOAc (10 mL) and the organic layer was washed with a saturated solution

of NaHCO$_3$ (5 mL) and brine (5 mL). Then it was dried over Na$_2$SO$_4$ and concentrated *in vacuo*. The crude was purified by chromatography on silica gel (33% EtOAc in petroleum ether) giving **51a** (61 mg, yield: 38%) as a pale brown solid. ^{1}H NMR (300 MHz, CDCl$_3$) δ 11.90 (s, 1H), 7.87 (d, *J* = 8.2 Hz, 2H), 7.45 (dt, *J* = 11.8, 4.5 Hz, 5H), 7.25 (dd, *J* = 5.9, 3.5 Hz, 3H), 7.18 – 7.07 (m, 3H), 5.23 (s, 2H), 3.90 (s, 3H); ESI-MS *m/z*: [M + H]$^+$ 386.1.

Methyl 4-(((2-oxo-4-(pyridin-3-yl)-1,2-dihydroquinolin-3-yl)oxy)methyl)benzoate (51b)

Starting from **50b** (180 mg, 0.76 mmol) the title compound was obtained following the procedure previously described for compound **51a**. The crude was purified by chromatography on silica gel (50% EtOAc in petroleum ether) giving **51b** (60 mg, yield: 20%) as a dark yellow oil. ^{1}H NMR (300 MHz, CDCl$_3$) δ 12.82 (s, 1H), 8.71 (dd, *J* = 5.0, 1.7 Hz, 1H), 8.61 – 8.47 (m, 1H), 7.98 – 7.81 (m, 2H), 7.64 – 7.32 (m, 4H), 7.24 – 7.01 (m, 4H), 5.45 – 5.15 (m, 2H), 3.89 (s, 3H); ESI-MS *m/z*: [M + H]$^+$ 387.0.

N-Hydroxy-4-(((2-oxo-4-phenyl-1,2-dihydroquinolin-3-yl)oxy)methyl)benzamide (28)

To a solution of **51a** (19 mg, 0.049 mmol) in a 2:1 mixture of DCM (2 mL): MeOH (1 mL), a 50% solution of NH$_2$OH in water (329 µL, 4.90 mmol) and a 4 M solution of KOH in methanol (616 µL, 2.45 mmol) were added dropwise. The reaction was stirred at 25 °C for 3 h, then it was neutralized with 6 N HCl and concentrated *in vacuo*. The crude was purified by chromatography on silica gel (0.1% NH$_4$OH, 10% MeOH in DCM) giving **28** (11 mg, yield: 55%) as a white solid. ^{1}H NMR (300 MHz, DMSO) δ 12.17 (s, 1H), 11.14 (s, 1H), 8.97 (s, 1H), 7.66 – 7.31 (m, 7H), 7.23 (s, 2H), 7.02 (dd, *J* = 25.8, 7.7 Hz, 4H), 5.08 (s, 2H) ^{13}C NMR (75 MHz, DMSO) δ 164.3, 159.1, 144.2, 140.6, 138.4, 136.3, 133.7, 132.5, 129.8, 129.1, 128.7, 128.5, 128.0, 127.1, 126.2, 122.5, 120.3, 115.6, 72.8; ESI-MS *m/z*: [M + H]$^+$ 387.1.

N-Hydroxy-4-(((1-methyl-2-oxo-4-phenyl-1,2-dihydroquinolin-3-yl)oxy)methyl)benzamide (29)

Step 1: To a solution of **51a** (16 mg, 0.04 mmol) in dry THF (1 mL) cooled at 0 °C, a 60% dispersion of NaH in mineral oil (15 mg, 0.06 mmol) was added. The mixture was stirred at 0 °C for 30 min then MeI (8 µL, 0.12 mmol) was added. The reaction was allowed to reach 25 °C and stirred at this temperature for 12 h. Then a saturated solution of NH_4Cl (5 mL) was added and the mixture was extracted with EtOAc (3 x 5 mL). The combined organic layers were washed with brine, dried over Na_2SO_4 and concentrated *in vacuo*. The crude was purified by chromatography on silica gel (50% EtOAc in petroleum ether) affording *methyl 4-(((1-methyl-2-oxo-4-phenyl-1,2-dihydroquinolin-3-yl)oxy)methyl)benzoate* (16 mg, yield: 99%) as a white solid. ^{1}H NMR (300 MHz, $CDCl_3$) δ 7.85 (d, J = 6.8 Hz, 2H), 7.57 – 7.32 (m, 5H), 7.32 – 7.17 (m, 3H), 7.17 – 6.95 (m, 3H), 5.13 (s, 2H), 3.95 – 3.79 (m, 6H); ESI-MS *m/z*: [M + H]+ 400.1.

Step 2: From *methyl 4-(((1-methyl-2-oxo-4-phenyl-1,2-dihydroquinolin-3-yl)oxy)methyl)benzoate* (22 mg, 0.05 mmol) the title compound was obtained following the procedure previously described for compound **28a**. The crude was purified by chromatography on silica gel (0.1% NH_4OH, 10 % MeOH in DCM) giving **29** (14 mg, yield: 64%). ^{1}H NMR (300 MHz, DMSO) δ 11.14 (s, 1H), 8.97 (s, 1H), 7.58-7.47 (m, 7H), 7.35 – 7.13 (m, 3H), 7.06 (dd, J = 8.2, 2.4 Hz, 3H), 5.04 (s, 2H), 3.76 (s, 3H) ^{13}C NMR (75 MHz, DMSO) δ 164.4, 159.1, 143.4, 140.3, 138.3, 137.3, 136.5, 133.6, 132.2, 129.8, 129.6, 128.8, 128.6 (2C), 128.5, 128.3, 127.7, 127.2, 127.1, 123.0, 121.2, 115.6, 73.5, 31.1; ESI-MS *m/z:* [M + H]+ 400.9.

N-Hydroxy-4-(((2-oxo-4-phenyl-1-(prop-2-yn-1-yl)-1,2-dihydroquinolin-3-yl)oxy)methyl)benzamide (30)

Step 1: To a solution of **51a** (50 mg, 0.13 mmol) in dry DMF cooled at 0 °C, NaH (60% in mineral oil, 7 mg, 0.194) was added. The reaction was allowed to stir for 30 mins at the same temperature, then propargyl bromide (19 μL, 0.129 mmol) was added. The reaction was allowed to reach 25 °C and stirred for 12h. After this time, a saturated solution of NH$_4$Cl (5 mL) was added and the mixture was extracted with EtOAc (3 x 5 mL). The combined organic layers were washed with brine, dried over Na$_2$SO$_4$ and concentrated *in vacuo*. The crude was purified by chromatography on silica gel (25% EtOAc in petroleum ether) affording *methyl 4-(((2-oxo-4-phenyl-1-(prop-2-yn-1-yl)-1,2-dihydroquinolin-3-yl)oxy)methyl)benzoate* (31 mg, yield: 56%) as a brown solid. ^{1}H NMR (300 MHz, CDCl$_3$) δ 7.86 (d, J = 12.6 Hz, 2H), 7.64 – 7.36 (m, 5H), 7.34 – 6.97 (m, 6H), 5.21 (d, J = 8.3 Hz, 2H), 5.13 (s, 2H), 3.88 (s, J = 3.6 Hz, 3H), 2.30 (dt, J = 15.4, 7.7 Hz, 1H); ESI-MS *m/z*: [M + H]$^+$ 424.1

Step 2: From *methyl 4-(((2-oxo-4-phenyl-1-(prop-2-yn-1-yl)-1,2-dihydroquinolin-3-yl)oxy)methyl)benzoate* (30 mg, 0.07 mmol) the title compound was obtained following the procedure previously described for compound **28**. The crude was purified by chromatography on silica gel (0.1% NH$_4$OH, 10% MeOH in DCM) giving **30** (17 mg, yield: 57%) as a brown solid. ^{1}H NMR (300 MHz, MeOD) δ 7.70 (d, J = 8.1 Hz, 1H), 7.54 (d, J = 7.5 Hz, 3H), 7.47 (s, 3H), 7.21 (s, 4H), 7.06 (d, J = 7.4 Hz, 2H), 5.27 (s, 2H), 4.97 (s, 2H), 2.76 (s, 1H) ^{13}C NMR (75 MHz, DMSO) δ 164.3, 158.0, 143.4, 140.5, 138.4, 135.9, 133.4, 132.5, 129.7, 128.8, 128.7, 128.0, 127.3, 127.1, 123.3, 121.0, 115.6, 79.3, 75.3, 73.1, 32.2; ESI-MS *m/z:* [M + H]$^+$ 425.0.

N-Hydroxy-4-(((1-methyl-2-oxo-4-(pyridin-3-yl)-1,2-dihydroquinolin-3-yl)oxy)methyl)benzamide (35)

Starting from **51b** (15 mg, 0.76 mmol) the title compound was obtained following the procedure previously described for compound **29**, **Step 1**. The crude was purified by chromatography on silica gel (33% EtOAc in petroleum ether) giving *methyl 4-(((1-methyl-2-*

oxo-4-(pyridin-3-yl)-1,2-dihydroquinolin-3-yl)oxy)methyl)benzoate (10 mg, yield: 66%) as a yellow solid. ^{1}H NMR (300 MHz, CDCl$_3$) δ 8.68 (dd, J = 4.9, 1.7 Hz, 1H), 8.48 (dd, J = 2.2, 0.9 Hz, 1H), 7.86 (d, J = 8.3 Hz, 2H), 7.62 – 7.32 (m, 4H), 7.23 – 7.03 (m, 4H), 5.31 – 5.06 (m, 2H), 3.89 (s, 3H), 3.86 (s, 3H); ESI-MS *m/z:* [M + H]$^+$ 401.1. Starting from *methyl 4-(((1-methyl-2-oxo-4-(pyridin-3-yl)-1,2-dihydroquinolin-3-yl)oxy)methyl)benzoate* (15 mg, 0.076 mmol) the title compound was obtained following the procedure previously described for compound **28**. The crude was purified by chromatography on silica gel (0.1% NH$_4$OH, 10% MeOH in DCM) giving **35** (5 mg, yield: 50%) as a white solid. ^{1}H NMR (300 MHz, MeOD) δ 8.61 (d, J = 4.8 Hz, 1H), 8.32 (s, 1H), 7.74 – 7.45 (m, 6H), 7.30 – 7.01 (m, 4H), 5.12 (d, J = 4.9 Hz, 2H), 3.88 (s, 3H); ^{13}C NMR (75 MHz, MeOD) δ 166.3, 159.2, 149.3, 148.3, 143.4, 140.2, 138.4, 137.1, 134.8, 131.8, 130.1, 129.5, 128.2, 126.6, 126.2, 123.6, 122.8, 120.2, 114.7, 72.8, 29.2; ESI-MS *m/z:* [M + Na]$^+$ 424.0.

1-Methylindoline-2,3-dione (52)

To a solution of isatin (1.0 g, 6.80 mmol) in dry DMF (4 mL), cooled at 0 °C, a 60% dispersion of NaH, in mineral oil (275 mg, 6.80 mmol) was added and stirred for 5 min at 0 °C. Then, methyl iodide (530 µL, 7.48 mmol) was added and the reaction was allowed to reach 25 °C and stirred for 12 h. Thereafter, a saturated solution of NH$_4$Cl (5 mL) was added and the mixture was extracted with EtOAc (3 x 5 mL). The combined organic layers were washed with brine, dried over Na$_2$SO$_4$ and concentrated *in vacuo*. The crude was purified by chromatography on silica gel (25% EtOAc in petroleum ether) affording **52** (1.15 g, yield: 99%) as a red solid. ^{1}H NMR (300 MHz, CDCl$_3$) δ 7.69 – 7.52 (m, 2H), 7.12 (td, J = 7.6, 0.9 Hz, 1H), 6.89 (dd, J = 8.6, 0.9 Hz, 1H), 3.25 (s, 3H).

4-Cyclohexyl-3-hydroxy-1-methylquinolin-2(1H)-one (53)

Starting from **52** (575 mg, 3.57 mmol) and cyclohexanecarboxaldehyde (431 µL, 3.57 mmol) the title compound was obtained following the procedure described to get **50a**. The residue was purified by chromatography on silica gel (20% EtOAc in petroleum ether) affording **53** (270 mg, yield: 30%) as a white solid. ^{1}H NMR (300 MHz, CDCl$_3$) δ 7.92 (d, J = 8.2 Hz, 1H), 7.54 – 7.20 (m, 4H), 3.82 (s, 3H), 3.16 (m, 1H), 2.35 – 2.12 (m, 2H), 1.99 – 1.83 (m, 2H), 1.75 (m, 4H), 1.42 (m, 2H); ESI-MS *m/z*: [M + H]$^+$ 258.1.

4-(((4-Cyclohexyl-1-methyl-2-oxo-1,2-dihydroquinolin-3-yl)oxy)methyl)-N-hydroxybenzamide (39)

Starting from **53** (270 mg, 1.05 mmol) methyl 4-(((4-cyclohexyl-1-methyl-2-oxo-1,2-dihydroquinolin-3-yl)oxy)methyl)benzoate was obtained following the procedure described to get **51a**. The residue was purified by chromatography on silica gel (33% EtOAc in petroleum ether) affording *methyl 4-(((4-cyclohexyl-1-methyl-2-oxo-1,2-dihydroquinolin-3-yl)oxy)methyl)benzoate* (317 mg, yield: 74%) as a yellow oil. ^{1}H NMR (300 MHz, CDCl$_3$) δ 8.15 – 8.01 (m, 2H), 7.96 (s, 1H), 7.61 (d, J = 7.9 Hz, 2H), 7.54 – 7.40 (m, 1H), 7.33 (dd, J = 8.6, 1.2 Hz, 1H), 7.22 (t, J = 7.6 Hz, 1H), 5.26 (s, 2H), 3.89 (s, 3H), 3.73 (s, 3H), 3.20 (d, J = 13.8 Hz, 1H), 2.16 – 1.93 (m, 2H), 1.89 – 1.52 (m, 5H), 1.48 – 1.07 (m, 3H); ESI-MS *m/z*: [M + H]$^+$ 406.1. This last intermediate (100 mg, 0.25 mmol) was converted into the final compound **39** following the procedure previously described for the synthesis of compound **28**. The residue was purified by chromatography on silica gel (0.1% NH$_4$OH, 10% MeOH in DCM) affording **39** (100 mg, yield: 98%) as a brown solid. ^{1}H NMR (300 MHz, DMSO) δ 11.21 (s, 1H), 9.01 (s, 1H), 8.04 (d, J = 8.2 Hz, 1H), 7.77 (d, J = 7.9 Hz, 2H), 7.55 (m, 4H), 7.40 – 7.16 (m, 1H), 5.16 (s, 2H), 3.68 (s, 3H), 3.25 (m, 1 H), 2.15 – 1.85 (m, 2H), 1.85 – 0.87 (m, 8H); ^{13}C NMR

(75 MHz, DMSO) δ 164.4, 158.3, 141.0, 140.5, 137.4, 132.6, 129.3, 128.3, 128.1, 127.4, 122.7, 119.8, 115.6, 72.4, 37.7, 30.4, 30.1, 27.0, 26.0; ESI-MS m/z: $[M + H]^+$ 407.1.

4-(Hydroxymethyl) pyridine (55)

To a solution of **54** (2.0 g, 18.67 mmol) in methanol (20 mL), cooled at 0 °C, NaBH$_4$ (706 mg, 18.67 mmol) was added. The reaction was stirred for 2 h and allowed to reach to 25 °C. After the complete consumption of starting material, water (20 mL) was added, solvent was evaporated, and the aqueous residue was extracted with EtOAc (3 x 15 mL). The combined organic layers were filtered over Na$_2$SO$_4$ and concentrated *in vacuo* to get **55** (1.60 g, yield: 80%) as a colorless oil. ^{1}H NMR (300 MHz, CDCl$_3$) δ 8.52 (dd, J = 4.6, 1.5 Hz, 2H), 7.40 – 7.19 (m, 2H), 4.74 (s, 2H), 3.20 (s, 1H).

4-(Bromomethyl)pyridinium bromide (56)

Compound **55** (1.810 g, 16.58 mmol) was dissolved in 48% HBr (16 mL) and stirred at reflux for 4 h. The water was removed *in vacuo* to give a thick gum which was treated with ethanol at 5 °C and then filtered. The white crystals were collected and washed with cold ethanol to get 4-(hydroxymethyl)pyridinium bromide (1.9 g). To a suspension of this salt in chloroform (25 mL) PBr$_3$ (457 μL, 4.85 mmol) was added, and the mixture was stirred at reflux for 4.5 h. After cooling down to 25 °C, the white precipitate was collected and washed with cold chloroform to give **56** (2.3 g, yield: 93%) as a white solid. ^{1}H NMR (300 MHz, CDCl$_3$) δ 8.80 (d, J = 6.4 Hz, 1H), 8.00 (d, J = 6.4 Hz, 1H), 4.61 (s, 1H).

4-(Bromomethyl)benzaldehyde (58)

To a solution of 4-(bromomethyl)benzonitrile (2.0 g, 10.20 mmol) in dry DCM (40 mL), cooled at -78 °C a 1 M solution of DIBAL-H in DCM (11.2 mL, 11.22 mmol) was slowly added. The

reaction was allowed to reach 0 °C in 1 h, then it was slowly quenched with 1 N HCl (20 mL).

The mixture was extracted with DCM (3 x 20 mL) and the combined organic layers were

washed with NaOH (2 x 20 mL), then dried over Na_2SO_4 and concentrated *in vacuo* affording

58 (2.03 g, yield: 82%) as a white solid that was used in the next step without further

purification. ^{1}H NMR (300 MHz, CDCl$_3$) δ 10.02 (s, 1H), 7.87 (d, *J* = 8.2 Hz, 2H), 7.56 (d, *J*

= 8.1 Hz, 2H), 4.52 (s, 4H).

2-(4-(Bromomethyl)phenyl)-1,3-dioxolane (59)

To a solution of **58** (2.03 g, 10.20 mmol) in toluene, ethylene glycol (1.1 mL, 20.40 mmol) and

PTSA (176 mg, 1.02 mmol) were added. The reaction was stirred at 110 °C for 12 h, then a

saturated solution of $NaHCO_3$ (20 mL) was added. The resulting mixture was extracted with

EtOAc (3 x 20 mL) and the combined organic layers were dried over Na_2SO_4 and concentrated

in vacuo. The crude was purified by chromatography on silica gel (20% EtOAc in petroleum

ether) affording **22** (1.7 g, yield: 69%) as a colorless oil. ^{1}H NMR (300 MHz, Acetone) δ 7.56

– 7.39 (m, 4H), 5.75 (s, 1H), 4.66 (s, 2H), 4.20 – 3.88 (m, 4H).

1-Benzylindoline-2,3-dione (60a)

To a solution of isatin (300 mg, 2.03 mmol) in dry DMF (2 mL), cooled at 0 °C, a 60%

dispersion of NaH, in mineral oil (95 mg, 2.38 mmol) was added and stirred for 5 min at 0 °C.

Then, benzyl bromide (266 µL, 2.34 mmol) was added and the reaction was allowed to reach

25 °C and stirred for 12 h. Thereafter, a saturated solution of NH_4Cl (5 mL) was added and the

mixture was extracted with EtOAc (3 x 5 mL). The combined organic layers were washed with

brine, dried over Na_2SO_4 and concentrated *in vacuo*. The crude was purified by

chromatography on silica gel (25% EtOAc in petroleum ether) affording **60a** (358 mg, yield:

74%) as a yellow solid. ^{1}H NMR (300 MHz, CDCl$_3$) δ 7.67 – 7.55 (m, 1H), 7.47 (td, *J* = 7.8,

1.3 Hz, 1H), 7.41 – 7.24 (m, 5H), 7.08 (t, J = 7.6 Hz, 1H), 6.77 (d, J = 8.0 Hz, 1H), 4.93 (s, 2H); ESI-MS m/z: [M + H]$^+$ 238.9.

1-(Pyridin-4-ylmethyl)indoline-2,3-dione (60b)

To a solution of **56** (860 mg, 3.39 mmol) in diethyl ether (10 mL) a 10% solution of NaHCO$_3$ (10 mL) was added. The organic layer was extracted, dried over Na$_2$SO$_4$, concentrated *in vacuo* and the residue was dissolved in dry DMF (2 mL). In another flask, a solution of isatin (500 mg, 3.39 mmol) in dry DMF (2 mL), cooled at 0 °C, was treated with a 60% dispersion of NaH, in mineral oil (163 mg, 4.07 mmol) and stirred at the same temperature for 30 min. After this time, the previously prepared solution of **56** (free base in dry DMF) was added and the reaction was allowed to reach 25 °C and stirred for 12 h. Then a saturated solution of NH$_4$Cl (5 mL) was added and the mixture was extracted with EtOAc (3 x 5 mL). The combined organic layers were washed with brine (10 mL), dried over Na$_2$SO$_4$ and concentrated *in vacuo*. The crude was purified by chromatography on silica gel (EtOAc) affording **60b** (311 mg, yield: 38%) as an orange solid; ^{1}H NMR (300 MHz, CDCl$_3$) δ 8.59 (s, 2H), 7.65 (d, J = 6.9 Hz, 1H), 7.49 (t, J = 7.2 Hz, 1H), 7.23 (s, 2H), 7.15 (d, J = 6.7 Hz, 1H), 6.68 (d, J = 7.4 Hz, 1H), 4.93 (s, 2H). ESI-MS m/z: [M + H]$^+$ 239.0.

1-Benzyl-3-hydroxy-4-phenylquinolin-2(1H)-one (61a)

Starting from benzaldehyde (67 mg, 0.62 mmol) and **60a** (150 mg, 0.62 mmol), the title compound was obtained following the procedure previously described for compound **50a**. The crude was purified by chromatography on silica gel (25% in EtOAc in petroleum ether) giving **61a** (78 mg, yield: 38%) as a brown solid. ^{1}H NMR (400 MHz, DMSO) δ 9.33 (s, 1H), 7.90 – 6.90 (m, 14H), 5.65 (s, 2H); ESI-MS m/z: 328.0.

3-Hydroxy-4-phenyl-1-(pyridin-4-ylmethyl)quinolin-2(1H)-one (61b)

Starting from benzaldehyde (53 mg, 0.62 mmol) and **60b** (120 mg, 0.50 mmol), the title compound was obtained following the procedure previously described for compound **50a**. The crude was purified by chromatography on silica gel (EtOAc) giving **61b** (64 mg, yield: 39%) as a brown solid. ^{1}H NMR (300 MHz, CDCl$_3$) δ 8.58 (d, J = 5.7 Hz, 1H), 7.65 – 7.01 (m, 6H), 5.69 (s, 1H); ESI-MS *m/z:* [M + H]$^+$ 329.

1-Benzyl-3-hydroxy-4-(pyridin-3-yl)quinolin-2(1H)-one (61c)

Starting from 3-pyridinecarboxaldehyde (67 mg, 0.62 mmol) and **60a** (150 mg, 0.62 mmol), the title compound was obtained following the procedure previously described for compound **50a**. The crude was purified by chromatography on silica gel (2% MeOH in DCM) giving **61c** (55 mg, yield: 24%) as a red solid. ^{1}H NMR (300 MHz, CDCl$_3$) δ 8.73 (s, 2H), 7.82 (dt, J = 7.8, 1.8 Hz, 1H), 7.49 (dd, J = 7.8, 4.9 Hz, 1H), 7.41 – 7.22 (m, 9H), 7.21 – 7.11 (m, 1H), 5.70 (s, 2H); ESI-MS *m/z:* [M + H]$^+$ 329.

3-Hydroxy-4-(pyridin-3-yl)-1-(pyridin-4-ylmethyl)quinolin-2(1H)-one (61d)

Starting from 3-pyridinecarboxaldehyde (54 mg, 0.503 mmol) and **60b** (120 mg, 0.503 mmol), the title compound was obtained following the procedure previously described for compound **50a**. The crude was purified by chromatography on silica gel (2% MeOH in DCM) giving **61d** (73 mg, yield: 44%) as a red solid. ^{1}H NMR (300 MHz, CDCl$_3$) δ 8.70 (s, 2H), 8.55 (s, 2H), 7.80 (d, J = 7.1 Hz, 1H), 7.47 (d, J = 4.8 Hz, 1H), 7.29 (t, J = 8.7 Hz, 2H), 7.14 (s, 4H), 5.66 (s, 2H); ESI-MS *m/z:* [M + H]$^+$ 330.

4-(((1-Benzyl-2-oxo-4-phenyl-1,2-dihydroquinolin-3-yl)oxy)methyl)-N-hydroxybenzamide (31)

Starting from **61a** (78 mg, 0.24 mmol) *methyl 4-(((1-benzyl-2-oxo-4-phenyl-1,2-dihydroquinolin-3-yl)oxy)methyl)benzoate* was obtained following the procedure previously described for compound **51a**. The crude was purified by chromatography on silica gel (50% EtOAc in petroleum ether) giving the intermediate (70 mg, yield: 62%) as a dark yellow oil. ^{1}H NMR (300 MHz, CDCl$_3$) δ 7.92 – 7.80 (m, 2H), 7.55 – 7.40 (m, 3H), 7.40 – 7.19 (m, 10H), 7.16 – 6.99 (m, 3H), 5.68 (s, 2H), 5.23 (s, *J* = 8.7 Hz, 2H), 3.90 (s, *J* = 8.5 Hz, 3H); ESI-MS *m/z:* [M + H]$^+$ 476.0. Starting from this intermediate (20 mg, 0.04 mmol) the title compound was obtained following the procedure previously described for compound **28**. The crude was purified by chromatography on silica gel (0.1% NH$_4$OH, 10% MeOH in DCM) giving **31** (9 mg, yield: 45%). ^{1}H NMR (300 MHz, DMSO) δ 11.14 (s, 1H), 8.97 (s, 1H), 7.63 – 7.19 (m, 14H), 7.11 (dd, *J* = 14.9, 7.7 Hz, 4H), 5.64 (s, 2H), 5.14 (d, *J* = 18.4 Hz, 2H); ^{13}C NMR (75 MHz, DMSO) δ 164.3, 159.0, 143.4, 140.5, 138.2, 137.1, 136.6, 133.6, 132.5, 129.8, 129.6. 129.1, 128.8, 128.6, 128.1, 127.6, 127.2, 127.1, 123.0, 121.1, 115.7, 73.0, 45.8; ESI-MS *m/z:* [M + H]$^+$ 477.0

N-Hydroxy-4-(((2-oxo-4-phenyl-1-(pyridin-4-ylmethyl)-1,2-dihydroquinolin-3-yl)oxy)methyl)benzamide (32)

Starting from **61b** (71 mg, 0.21 mmol) *methyl 4-(((2-oxo-4-phenyl-1-(pyridin-4-ylmethyl)-1,2-dihydroquinolin-3-yl)oxy)methyl)benzoate* was obtained following the procedure previously described for compound **51a**. The crude was purified by chromatography on silica gel (50% EtOAc in petroleum ether) giving the intermediate (31 mg, yield: 30%). ^{1}H NMR (300 MHz, CDCl$_3$) δ 8.56 (d, *J* = 5.2 Hz, 2H), 7.85 (d, *J* = 8.2 Hz, 2H), 7.52 – 7.41 (m, 3H), 7.31 (m, *J* = 11.3, 9.9, 5.3 Hz, 5H), 7.19 – 7.00 (m, 6H), 5.65 (s, 2H), 5.17 (s, 2H), 3.89 (s, *J* = 6.1 Hz, 3H). ESI-MS *m/z:* [M + H]$^+$ 477.0. Starting from this intermediate (10 mg, 0.02 mmol) the title compound was obtained following the procedure previously described for compound **28**. The

crude was purified by chromatography on silica gel (0.1% NH_4OH, 10% MeOH in DCM) giving **32** (8 mg, yield: 90%). ^{1}H NMR (300 MHz, MeOD) δ 8.48 (d, J = 5.2 Hz, 2H), 7.63 – 7.23 (m, 12H), 7.21 – 7.01 (m, 3H), 5.73 (s, J = 27.5 Hz, 2H), 5.07 (s, 2H); ^{13}C NMR (75 MHz, MeOD) δ 168.6, 159.8, 148.9, 147.4, 142.9, 140.6, 139.9, 136.2, 133.1, 131.6, 129.4, 129.3, 129.1, 128.1, 128.0, 127.7, 127.3, 126.5, 122.8, 121.3, 114.7, 73.0, 45.0. ESI-MS *m/z:* [M + H][+] 478.0

4-(((1-Benzyl-2-oxo-4-(pyridin-3-yl)-1,2-dihydroquinolin-3-yl)oxy)methyl)-N-hydroxybenzamide (36)

Starting from **61c** (56 mg, 0.17 mmol) *methyl 4-(((1-benzyl-2-oxo-4-(pyridin-3-yl)-1,2-dihydroquinolin-3-yl)oxy)methyl)benzoate* was obtained following the procedure previously described for compound **51a**. The crude was purified by chromatography on silica gel (2% MeOH in DCM) giving the intermediate (53 mg, yield: 65%). ^{1}H NMR (300 MHz, CDCl3) δ 8.69 (s, 1H), 8.51 (s, 1H), 7.86 (d, J = 8.2 Hz, 2H), 7.53 (t, J = 10.4 Hz, 1H), 7.46 – 7.20 (m, 8H), 7.20 – 7.01 (m, 4H), 5.67 (s, 2H), 5.37 – 5.12 (m, 2H), 3.89 (s, 3H); ESI-MS *m/z:* [M + H][+] 477.0.Starting from this intermediate (53 mg, 0.11 mmol) the title compound was obtained following the procedure previously described for compound **28**. The crude was purified by chromatography on silica gel (0.1% NH_4OH, 10% MeOH in DCM) giving **36** (33 mg, yield: 62%). ^{1}H NMR (300 MHz, DMSO) δ 11.15 (s, 1H), 8.98 (s, 1H), 8.67 (d, J = 3.6 Hz, 1H), 8.49 (s, 1H), 7.79 – 7.65 (m, 1H), 7.59 (d, J = 8.2 Hz, 2H), 7.54 – 7.38 (m, 3H), 7.38 – 7.20 (m, 5H), 7.20 – 6.96 (m, 4H), 5.66 (s, 2H), 5.18 (s, 2H) ^{13}C NMR (75 MHz, DMSO) δ 164.3, 158.8, 150.1, 149.7, 143.9, 140.2, 137.7, 137.0, 136.6, 134.8, 132.7, 129.8, 129.6, 129.2, 128.2, 127.6, 127.2, 127.1, 126.9, 123.9, 123.2, 120.7, 115.9, 73.0, 45.8; ESI-MS *m/z:* [M + H][+] 477.0

N-Hydroxy-4-(((2-oxo-4-(pyridin-3-yl)-1-(pyridin-4-ylmethyl)-1,2-dihydroquinolin-3-yl)oxy)methyl) benzamide (37)

Starting from **61d** (67 mg, 0.20 mmol) *methyl 4-(((2-oxo-4-(pyridin-3-yl)-1-(pyridin-4-ylmethyl)-1,2-dihydroquinolin-3-yl)oxy)methyl)benzoate* was obtained following the procedure previously described for compound **51a**. The crude was purified by chromatography on silica gel (2% MeOH in DCM) giving the intermediate (31 mg, yield: 32%). ^{1}H NMR (300 MHz, CDCl$_3$) δ 8.70 (dt, *J* = 8.3, 4.1 Hz, 1H), 8.63 – 8.42 (m, 2H), 8.11 – 7.94 (m, 1H), 7.85 (d, *J* = 8.2 Hz, 2H), 7.61 – 7.45 (m, 2H), 7.46 – 7.29 (m, 1H), 7.29 – 6.97 (m, 7H), 5.65 (s, 2H), 5.35 – 5.08 (m, 2H), 3.89 (s, 3H). ESI-MS *m/z:* [M + H]$^+$ 478.0. Starting from this intermediate (30 mg, 0.06 mmol) the title compound was obtained following the procedure previously described for compound **28**. The crude was purified by chromatography on silica gel (0.1% NH$_4$OH, 10% MeOH in DCM) giving **37** (18 mg, yield: 60%). ^{1}H NMR (300 MHz, MeOD) δ 8.63 (d, *J* = 4.1 Hz, 1H), 8.49 (d, *J* = 5.5 Hz, 2H), 8.38 (s, 1H), 7.72 (d, *J* = 7.8 Hz, 1H), 7.62 – 7.34 (m, 5H), 7.30 (d, *J* = 5.6 Hz, 2H), 7.19 (dd, *J* = 8.4, 5.4 Hz, 2H), 7.10 (d, *J* = 8.1 Hz, 2H), 5.78 (s, 2H), 5.25 – 5.03 (m, 2H); ^{13}C NMR (75 MHz, MeOD) δ 166.3, 159.3, 149.3, 149.0, 148.5, 147.1, 143.3, 140.2, 138.4, 136.2, 135.5, 131.9, 129.6, 128.3, 126.7, 123.7, 123.1, 122.0, 120.6, 115.0, 72.9, 45.0; ESI-MS *m/z:* [M + H]$^+$ 479.0

1-Benzylpiperidin-4-one (63)

To a solution of 4-piperidone monohydrate hydrochloride (1.0 g, 5.83 mmol) in dry DMF (10 mL) K$_2$CO$_3$ (2.42 g, 17.49 mmol) and benzyl bromide (830 µL, 6.99 mmol) were added. The reaction was stirred at 80 °C for 12 h, then a saturated solution of NH$_4$Cl (20 mL) and EtOAc (20 mL) were added and the organic layer was extracted. It was successively washed with a saturated solution of NaHCO$_3$ (10 mL) and brine (10 mL), dried over Na$_2$SO$_4$ and concentrated *in vacuo*. The residue was purified by chromatography on silica gel (15% EtOAc in petroleum

ether) affording **63** (800 mg, yield: 70%) as a yellow oil. ^{1}H NMR (300 MHz, CDCl$_3$) δ 7.50 – 7.20 (m, 5H), 3.62 (s, 2H), 2.84 – 2.65 (m, 4H), 2.56 – 2.36 (m, 4H); ESI-MS *m/z*: [M + Na]$^+$ 222.1.

1-Benzyl-N-phenylpiperidin-4-amine (64)

To a solution of aniline (303 µL, 3.35 mmol) in DCM (10 mL) **63** (800 mg, 4.02 mmol) and AcOH (19 µL, 0.34 mmol) were added. The mixture was stirred at 20 °C for 4 h, then NaBH(OAc)$_3$ (1.07 g, 5.03 mmol) was added and the reaction stirred at 25 °C for 12 h. After this time a saturated solution of NaHCO$_3$ (10 mL) was added and the mixture was extracted with DCM (3 x 10 mL). The combined organic layers were dried over Na$_2$SO$_4$ and concentrated in vacuo. The residue was purified by chromatography on silica gel (10% EtOAc in petroleum ether) affording **64** (950 mg, yield: 89%) as a white solid. ^{1}H NMR (300 MHz, CDCl$_3$) δ 7.58 – 7.30 (m, 5H), 7.30 – 7.15 (m, 2H), 6.84 – 6.71 (m, 1H), 6.71 – 6.58 (m, 2H), 3.60 (s, 2H), 3.36 (m, 1H), 2.92 (m, 2H), 2.36 – 1.99 (m, 4H), 1.68 – 1.42 (m, 2H); ESI-MS *m/z*: [M + H]$^+$ 267.1.

1-(1-Benzylpiperidin-4-yl)indoline-2,3-dione (65)

To a solution of oxalyl chloride (316 µL, 7.14 mmol) in dry DCM (6 mL) cooled at 0 °C, a solution of **64** (950 mg, 3.57 mmol) in DCM (4 mL) was slowly added. The reaction was allowed to reach 25 °C and stirred for 2 h, then the solvent was evaporated. The residue was dissolved in DCM (5 mL), cooled at 0 °C and AlCl$_3$ (952 mg, 7.14 mmol) was added. The new mixture was stirred at 40 °C for 2 h, then poured on ice and neutralized with a saturated solution of NaHCO$_3$ (15 mL). The mixture was filtered through paper and extracted with DCM (3 x 10 mL). The combined organic layers were dried over Na$_2$SO$_4$ and concentrated in vacuo. The residue was purified by chromatography on silica gel (3% MeOH in DCM) affording **65** (600

mg, yield: 52%) as a red solid. ^{1}H NMR (300 MHz, CDCl$_3$) δ 7.72 – 7.48 (m, 2H), 7.46 – 7.15 (m, 6H), 7.09 (m, 1H), 4.34 – 4.05 (m, 1H), 3.57 (s, 2H), 3.04 (d, J = 11.3 Hz, 2H), 2.58 – 2.27 (m, 2H), 2.27 – 2.00 (m, 2H), 1.75 (d, J = 12.3 Hz, 2H); ESI-MS m/z: [M + H]$^+$ 321.1.

4-(((1-(1-Benzylpiperidin-4-yl)-2-oxo-4-phenyl-1,2-dihydroquinolin-3-yl)oxy)methyl)-N-hydroxybenzamide (33)

Compound **65** (200 mg, 0.62 mmol) was submitted to the ring expansion reaction with benzaldehyde (63 μL, 0.62 mmol) following the same condition described for the synthesis of compound **50a**. The purification of the crude by chromatography on silica gel (5% MeOH in DCM) afforded 1-(1-benzylpiperidin-4-yl)-3-hydroxy-4-phenylquinolin-2(1H)-one (140 mg, yield: 55%) as a red solid. ^{1}H NMR (300 MHz, CDCl$_3$) δ 7.81 (s, 1H), 7.62 – 7.21 (m, 12H), 7.21 – 7.01 (m, 2H), 3.77 – 3.46 (m, 3H), 3.26 – 2.82 (m, 4H), 2.41 – 2.19 (m, 2H), 1.89 – 1.69 (m, 2H).; ESI-MS m/z: [M + H]$^+$ 411.1. This intermediate (140 mg, 0.59 mmol) was subjected to the alkylation procedure with methyl 4-(bromomethyl)benzoate (263 mg, 0.88 mmol) previously described for compound **51a**. Purification of the crude by chromatography on silica gel (3% MeOH in DCM) afforded methyl 4-(((1-(1-benzylpiperidin-4-yl)-2-oxo-4-phenyl-1,2-dihydroquinolin-3-yl)oxy)methyl)benzoate (50 mg, yield: 15%) as a pale red solid. ^{1}H NMR (300 MHz, CDCl$_3$) δ 7.84 (d, J = 8.3 Hz, 3H), 7.57 – 7.16 (m, 12H), 7.16 – 6.99 (m, 3H), 5.10 (s, 2H), 3.88 (s, 3H), 3.65 (s, 2H), 3.13 (s, 5H), 2.31 (s, 2H), 1.81 (d, J = 12.3 Hz, 2H); ESI-MS m/z: [M + H]$^+$ 559.2. This latter intermediate (16 mg, 0.03 mmol) was submitted to the reaction with a 50% solution of NH$_2$OH in water (190 μL, 2.87 mmol) previously described for compound **28**. Purification of the crude by chromatography on silica gel (0.1% NH$_4$OH, 10% MeOH in DCM) affording **33** (10 mg, yield: 62%) as a brown solid. ^{1}H NMR (300 MHz, MeOD) δ 7.89 (s, 1H), 7.69 – 7.26 (m, 11H), 7.26 – 6.91 (m, 6H), 4.97 (s, 2H), 3.72 (s, 2H), 3.17 (d, J = 12.1 Hz, 5H), 2.43 (s, 2H), 1.77 (d, J = 11.7 Hz, 2H); ^{13}C NMR (75 MHz, MeOD)

δ 166.4, 160.2, 143.2, 140.7, 138.9, 136.3, 133.3, 131.5, 129.5, 129.4, 128.7, 128.1, 128.0 (2C), 127.4, 126.5, 122.2, 121.7, 72.8, 62.0, 53.0, 29.3, 26.8; ESI-MS *m/z*: $[M + H]^+$ 560.1.

1-(4-(1,3-Dioxolan-2-yl)benzyl)indoline-2,3-dione (66)

Starting from isatin (500 mg, 3.40 mmol) and **59** (1.24 g, 5.10 mmol) the title compound was synthetized following the same procedure to obtain compound **60a**. The residue was used in the next step without further purifications and affording **66** (1.36 g, yield: 99%) as a red solid. ^{1}H NMR (300 MHz, CDCl₃) δ 7.68 – 7.56 (m, 1H), 7.56 – 7.30 (m, 5H), 7.09 (td, *J* = 7.5, 0.8 Hz, 1H), 6.80 – 6.66 (m, 1H), 5.78 (s, 1H), 4.94 (s, 2H), 4.22 – 3.91 (m, 4H).

1-(4-(1,3-Dioxolan-2-yl)benzyl)-3-hydroxy-4-phenylquinolin-2(1H)-one (67a)

Starting from **66** (500 mg, 1.62 mmol) the title compound was obtained following the procedure described to get **50a**. The residue was purified by chromatography on silica gel (33% EtOAc in petroleum ether) affording **67a** (310 mg, yield: 48%) as a brown solid. ^{1}H NMR (300 MHz, CDCl₃) δ 7.70 – 7.46 (m, 6H), 7.46 – 7.26 (m, 5H), 7.26 – 7.02 (m, 2H), 5.81 (s, 1H), 5.72 (s, 2H), 4.25 – 3.94 (m, 4H); ESI-MS *m/z*: $[M + H]^+$ 400.0.

1-(4-(1,3-Dioxolan-2-yl)benzyl)-3-hydroxy-4-(pyridin-3-yl)quinolin-2(1H)-one (67b)

Starting from **66** (500 mg, 1.62 mmol) the title compound was obtained following the procedure described to get **50b**. The residue was purified by chromatography on silica gel (3% MeOH in DCM) affording **67b** (310 mg, yield: 48%) as a brown solid. ^{1}H NMR (300 MHz, CDCl₃) δ 8.75 (d, *J* = 2.0 Hz, 2H), 8.10 (s, 1H), 7.84 (d, *J* = 7.8 Hz, 1H), 7.60 – 7.42 (m, 3H), 7.40 – 7.25 (m, 5H), 7.25 – 7.06 (m, 1H), 5.80 (s, 1H), 5.72 (s, 2H), 4.23 – 3.92 (m, 4H); ESI-MS *m/z*: $[M + H]^+$ 401.0.

Methyl 4-(((1-(4-(1,3-dioxolan-2-yl)benzyl)-2-oxo-4-phenyl-1,2-dihydroquinolin-3-yl)oxy)methyl)ben-zoate (68a)

Starting from **67a** (310 mg, 0.78 mmol) the title compound was obtained following the procedure described to get **51a**. The residue was purified by chromatography on silica gel (50% EtOAc in petroleum ether) affording **68a** (340 mg, yield: 80%) as a yellow oil. ^{1}H NMR (300 MHz, CDCl$_3$) δ 7.85 (d, *J* = 8.3 Hz, 2H), 7.55 – 7.38 (m, 5H), 7.38 – 7.17 (m, 7H), 7.17 – 6.94 (m, 3H), 5.77 (s, 1H), 5.67 (s, 2H), 5.19 (s, 2H), 4.20 – 3.92 (m, 4H), 3.87 (s, 3H); ESI-MS *m/z*: [M + H]$^+$ 548.0.

Methyl 4-(((1-(4-(1,3-dioxolan-2-yl)benzyl)-2-oxo-4-(pyridin-3-yl)-1,2-dihydroquinolin-3-yl)oxy)methyl-)benzoate (68b)

Starting from **67b** (310 mg, 0.77 mmol) the title compound was obtained following the procedure described to get **51a**. The residue was purified by chromatography on silica gel (33% Petroleum ether in EtOAc) affording **68b** (231 mg, yield: 55%) as a red oil. ^{1}H NMR (300 MHz, CDCl$_3$) δ 8.68 (dd, *J* = 5.0, 1.7 Hz, 1H), 8.49 (d, *J* = 2.1 Hz, 1H), 7.85 (d, *J* = 8.3 Hz, 2H), 7.63 – 7.20 (m, 8H), 7.20 – 6.91 (m, 4H), 5.76 (s, 1H), 5.66 (s, 2H), 5.37 – 5.08 (m, 2H), 4.19 – 3.93 (m, 4H), 3.86 (s, 3H); ESI-MS *m/z*: [M + H]$^+$ 549.0.

4-(((1-(4-((Diethylamino)methyl)benzyl)-2-oxo-4-phenyl-1,2-dihydroquinolin-3-yl)oxy)methyl)-N-hydroxybenzamide (34)

To a solution of **68a** (230 mg, 0.62 mmol) in THF (5 mL) a 1 N solution of HCl in water (5 mL) was added. The reaction was stirred at 25 °C for 1 h, then a saturated solution of NaHCO$_3$ (10 mL) was added and the mixture was extracted with EtOAc (3 x 10 mL). The combined organic layers were dried over Na$_2$SO$_4$ and concentrated in vacuo. The residue was used in the next step without further purifications. *Methyl 4-(((1-(4-formylbenzyl)-2-oxo-4-phenyl-1,2-*

dihydroquinolin-3-yl)oxy)methyl)benzoate (310 mg, yield: 99%) was obtained as a yellow oil. ^{1}H NMR (300 MHz, CDCl$_3$) δ 9.99 (s, 1H), 7.98 – 7.72 (m, 4H), 7.60 – 6.91 (m, 13H), 5.74 (s, 2H), 5.19 (s, 2H), 3.90 (s, 3H). This intermediated was dissolved in DCM (5 mL) and dimethylamine (96 µL, 0.93 mmol) and AcOH (4 µL, 0.06 mmol) were added. This mixture was stirred at 25 °C for 2 h then a NaBH(OAc)$_3$ (197 mg, 0.93 mmol) was added and the reaction was stirred at 25 °C for 12 h. After this time, a saturated solution of NaHCO$_3$ (5 mL) was added and the mixture was extracted with DCM (3 x 5 mL). The combined organic layers were dried over Na$_2$SO$_4$ and concentrated in vacuo. The residue was purified by chromatography on silica gel (5% MeOH in DCM) affording *methyl 4-(((1-(4-((diethylamino)methyl)benzyl)-2-oxo-4-phenyl-1,2-dihydroquinolin-3-yl)oxy)methyl)-benzoate* (204 mg, yield: 59%) as a colorless oil. ^{1}H NMR (300 MHz, CDCl$_3$) δ 7.86 (d, J = 8.3 Hz, 2H), 7.57 – 7.42 (m, 3H), 7.42 – 7.18 (m, 9H), 7.18 – 6.95 (m, 3H), 5.84 – 5.48 (m, 2H), 5.21 (s, 2H), 3.88 (s, 3H), 3.56 (s, 2H), 2.53 (q, J = 7.1 Hz, 4H), 1.04 (t, J = 7.1 Hz, 6H); ESI-MS *m/z*: [M + H]$^+$ 561.2. Starting from this intermediate (100 mg, 0.18 mmol) the title compound was obtained following the procedure described to get **28**. The residue was purified by chromatography on silica gel (0.1% NH$_4$OH, 10% MeOH in DCM) affording **34** (75 mg, yield: 74%) as a white solid. ^{1}H NMR (300 MHz, MeOD) δ 7.65 – 7.48 (m, 5H), 7.48 – 7.35 (m, 4H), 7.34 – 7.20 (m, 5H), 7.19 – 6.97 (m, 3H), 5.74 (s, 2H), 5.08 (s, 2H), 3.86 (s, 2H), 2.78 (q, J = 7.2 Hz, 4H), 1.16 (t, J = 7.2 Hz, 6H); ^{13}C NMR (75 MHz, DMSO) δ 164.2, 159.0, 143.5, 140.5, 139.4, 138.2, 136.6, 135.3, 133.6, 132.5, 129.8, 129.6, 129.2, 128.8, 128.6, 128.1, 127.2, 127.1, 126.9, 122.9, 121.1, 115.7, 73.0, 57.0, 46.5, 45.6, 12.0; ESI-MS *m/z*: [M + H]$^+$ 562.2.

4-(((1-(4-((Diethylamino)methyl)benzyl)-2-oxo-4-(pyridin-3-yl)-1,2-dihydroquinolin-3-yl)oxy)methyl)-N-hydroxybenzamide (38)

Starting from **68b** (230 mg, 0.42 mmol) *methyl 4-(((1-(4-((diethylamino)methyl)benzyl)-2-oxo-4-(pyridin-3-yl)-1,2-dihydroquinolin-3-yl)oxy)-methyl)benzoate* was obtained following the procedure described for **34**. The residue was purified by chromatography on silica gel (10% MeOH in DCM) affording *methyl 4-(((1-(4-((diethylamino)methyl)benzyl)-2-oxo-4-(pyridin-3-yl)-1,2-dihydroquinolin-3-yl)oxy)-methyl)benzoate* (110 mg, yield: 47% (over two steps)) as a brown oil. ^{1}H NMR (300 MHz, CDCl$_3$) δ 8.69 (dd, J = 4.7, 1.7 Hz, 1H), 8.50 (s, 1H), 7.96 – 7.75 (m, 2H), 7.62 – 7.45 (m, 1H), 7.45 – 6.95 (m, 11H), 5.64 (s, 2H), 5.25 (q, J = 11.7 Hz, 2H), 3.87 (s, 3H), 3.55 (s, 2H), 2.63 – 2.35 (m, 4H), 1.15 – 0.86 (m, 6H); ESI-MS *m/z*: [M + H]$^+$ 562.2. Starting from this intermediate (55 mg, 0.10 mmol) the title compound was obtained following the procedure described to get **28**. The residue was purified by chromatography on silica gel (0.1% NH$_4$OH, 10% MeOH in DCM) affording **38** (45 mg, yield: 80%) as a white solid. ^{1}H NMR (300 MHz, MeOD) δ 8.63 (dd, J = 4.9, 1.7 Hz, 1H), 8.36 (dd, J = 2.2, 0.9 Hz, 1H), 7.71 (m, 1H), 7.65 – 7.41 (m, 5H), 7.34 (d, J = 8.1 Hz, 2H), 7.25 (d, J = 8.1 Hz, 2H), 7.21 – 7.00 (m, 4H), 5.90 – 5.59 (m, 2H), 5.19 (d, J = 4.2 Hz, 2H), 3.64 (s, 2H), 2.58 (q, J = 7.1 Hz, 4H), 1.08 (t, J = 7.2 Hz, 6H); ^{13}C NMR: (75 MHz, DMSO) δ 164.3, 158.8, 150.0, 149.7, 143.9, 140.2, 139.0, 137.7, 136.6, 135.3, 134.8, 132.6, 129.8, 129.5, 129.4, 128.2, 127.2, 127.0, 123.9, 123.2, 120.6, 115.9, 73.0, 56.8, 46.4, 45.7, 11.8 ; ESI-MS *m/z*: [M + H]$^+$ 563.2.

In vitro testing of HDAC1, HDAC6 and HDAC8

OptiPlate-96 black microplates (PerkineElmer) were employed with an assay volume of 60 µL. Human recombinant HDAC1 (BPS Bioscience, Catalog #: 50051) or human recombinant HDAC6 (BPS Bioscience, Catalog #: 50006) were diluted in incubation buffer (50 mM Tris-HCl, pH 8.0, 137 mM NaCl, 2.7 mM KCl, 1 mM MgCl$_2$ and 1 mg/mL BSA). A total of 52 µL of this dilution were incubated with 3 µL of different concentrations of inhibitors in DMSO and 5 µL of the fluorogenic substrate ZMAL (Z-(Ac)Lys-AMC)[20,21] (126 µM) at 37 °C. After

90 min incubation time, 60 µL of the stock solution (33 µM Trichostatin A and 6 mg/mL trypsin in trypsin buffer [Tris-HCl 50 mM, pH 8.0, NaCl 100 mM]), were added. After a following incubation at 37 °C for 30 min, the fluorescence was measured on a BMG LABTECH POLARstar OPTIMA plate reader (BMG Labtechnologies, Germany) with an excitation wavelength of 390 nm and an emission wavelength of 460 nm.[21,22]

Recombinant human HDAC8 was purchased as part of the Fluor de Lys HDAC8 fluorometric drug discovery kit (Enzo Life Sciences, No. BMLAK518). Inhibition assays were performed as previously described (Marek et al, 2018) with minor modifications.[23,24] DMSO concentration was kept constant to 0.5%, the enzyme incubated with DMSO only was used as control. To keep safe from the possibility of a slow-binding inhibition, enzyme was preincubated with the selected compounds 15 min before substrate addition to the mixture. The Fluor de Lys substrate was added at the final concentration of 50 µM whereas the enzyme was at concentration of 0.45U/reaction; the reaction was allowed to proceed for 1 h at 30 °C. 2 µM TSA within 50 µL of 1× Developer II was added to quench the reaction and the mixture was further incubated for 1 h at 30 °C. Fluorescence was measured in a plate reader (Varioskan Lux, Thermofisher Scientifica) with excitation wavelength at $\lambda = 370$ nm and emission wavelength at $\lambda = 450$ nm. IC_{50} was estimated by nonlinear regression curve fit performed by means of GNU/Octave, according to a generalized form of a dose−response curve equation, as reported by Copeland.[25]

In vitro testing for cytotoxicity assay

KYSE-520

KYSE-520 esophageal squamous cell carcinoma cell line (DSMZ cell bank, Germany) was cultured in RPMI 1640 medium supplemented with 10% fetal bovine serum (FBS) (Gibco), 2 mM L-glutamine (Gibco), and 100 units/ml penicillin-streptomycin (Gibco). Cells were cultured at 37°C, in a humidified atmosphere, containing 5% CO_2.

Cytotoxicity assay:

For the IC_{50} determination, cells were seeded in a 96-well plate at the density of 5 x 10^3 cells/well. After adhesion, cells were treated with a range of concentrations of the tested molecules and 0.01% of DMSO as the vehicle for 48 h in triplicate. Afterwards, 10% (v/v) Alamar Blue reagent (Invitrogen) was added to each well and the plates were incubated for 3 h in 37°C in the dark. Fluorescence levels were read on a SPECTRAMAX Gemini Microplate Spectrofluorometer (Molecular Devices) with excitation at 544 nm, and emission at 590 nm. The IC_{50} values were determined as means of three separate experiments.

Flow cytometric analysis of apoptosis levels

The analysis of apoptosis in KYSE-520 cells after 48 h treatment was performed using the Annexin V/Propidium Iodide (PI) staining. In this assay, early apoptotic cells stain positive for Annexin V, as they express phosphatidylserine on the outer surface of their intact plasma membrane. Later stages of apoptosis are associated with the loss of the integrity of the plasma membrane, allowing the PI to permeate the membrane. Thus, late apoptotic cells stain positive for both Annexin V and PI. For this analysis, KYSE-520 cells were seeded at the density of 1.5 x 10^5 cells/ml and treated with 30 μM and 100 μM of the tested molecules or 0.01% DMSO (v/v) as the vehicle control for 48 h. Cells were then harvested and stained with Annexin V-FITC (IQ Products) and PI (Invitrogen) and analyzed by flow cytometry using BD Accuri™ C6 (BD Biosciences) software.

Ca9.22 and TR-146

Cell lines:

Ca9.22 gingival squamous cell carcinoma cells (Health Science Research Resources Bank, Osaka, Japan) were cultured in minimum essential media (MEM) with 10% (v/v) foetal bovine serum (FBS), Penicillin/Streptomycin (100U/mL penicillin, 0.1mg/mL streptomycin) and L-Glutamine (2mM). Cells were cultured at 37°C, in a humidified atmosphere, containing 5%

CO_2. TR-146 keratinizing squamous cell carcinoma of buccal mucosal origin cells (HPA Cultures, UK) were cultured in high glucose Dulbecco Modified Eagle's Medium (DMEM) with 10% (v/v) FBS and Penicillin/Streptomycin (100U/mL penicillin, 0.1mg/mL streptomycin)

Cytotoxicity assay:

For the IC_{50} determination, cells were seeded in a 96-well plate at the density of 30 x 10^4 cells/well. After adhesion, cells were treated with a range of concentrations of the tested molecules and 1% EtOH as the vehicle for 48 h in triplicate. Afterwards, 10% (v/v) Alamar Blue reagent (Invitrogen) was added to each well and the plates were incubated for 3 h in 37^oC in the dark. Fluorescence levels were read on a SPECTRAMAX Gemini Microplate Spectrofluorometer (Molecular Devices) with excitation at 544 nm, and emission at 590 nm. The IC_{50} values were determined as means of three separate experiments.

Cytotoxicity assessment of compounds the growth on Ca9.22 gingival squamous carcinoma (p53 mutated) and TR-146 keratinizing squamous cell carcinoma of buccal mucosal origin.

IC_{50} values determined in Ca9.22 gingival squamous carcinoma cells and TR-146 keratinizing squamous cell carcinoma of buccal mucosal origin ; cells were treated with increasing concentrations of each compound for 48 h. Data represent the mean of three independent experiments. Data represent the mean of three independent experiments. Data represent the mean of three independent experiments.

(A) Ca9.22 cells were seeded at a density of 30 X 10^4 cells/mL and were left untreated (control) or treated with either vehicle (1% EtOH (v/v)) or 500 nM of compound for 48 h. (B) TR-146 cells were seeded at a density of 30 X 10^4 cells/mL and were treated with either vehicle control (1% EtOH (v/v)) or or 500 nM of compound for 48 h. After incubation cells were harvested and stained with Annexin V/Propidium Iodide (PI) and were analyzed by flow cytometry using

BD FACs Accuri software. 10,000 cells were gated on vehicle treated cells. Values represent the mean ± S.E.M of three independent experiments (n=3).

Statistical analysis was performed using a T-test. **p = 0.001".

OE33

To determine the clinical potential for these HDAC6 inhibitors in an esophageal adenocarcinoma setting, a preliminary screening was carried out on the OE33 cell line. Cell viability was assessed by MTT assay (3-(4,5-dimethylthiazol-2-yl)-2,5-diphenyltetrazolium bromide). Cells were seeded at 2000 cells/well in a 96-well plate and were treated in six replicates with vehicle (0.1% (v/v) DMSO) or with the indicated compounds for 72 h. Cell viability was measured following 72 h of drug treatment by incubating the cells with 10% (v/v) MTT. Culture media was removed, and the reduced form of MTT to formazan was dissolved in 70μL of DMSO. The formazan reduction was measured at absorbance 568:568 nm using a Synergy II microplate reader (Biotek) using the Gen5 software. Dose-response curves were generated using Prism 5.0 software (GraphPad Software Inc.) IC_{50} values were the mean of a minimum of three separate determinations.

Biological Assays on U937 and NB4

Cell culture

U937 and NB4 cells (DSMZ) were cultured in RPMI 1640 medium (Euroclone, Italy) supplemented with 10% heat-inactivated FBS (Sigma-Aldrich, Italy), 1% glutamine (Euroclone) and 1% penicillin/streptomycin (Euroclone) at 37°C and 5% CO_2.

Cells were stimulated with the indicated drugs for 24 and 48 h at 1, 5 and 10 μM. Control cells were treated with DMSO (Sigma-Aldrich, Italy).

Western blot and total protein extraction.

Cells were harvested, washed with PBS (Euroclone), and lysed for 15 min at 4 °C in lysis RIPA buffer supplemented with protease and phosphatase inhibitors cocktail (Roche): 50 mM Tris-HCl pH 7.5, 150 mM NaCl, 1% NP40, 1% Triton X-100, 1mM EDTA pH 8.0, 0.5 mM EGTA. Cells were then centrifuged at 13200 rpm for 30 min at 4^0 C and supernatant was used to determine the protein concentration by colorimetric assay (Biorad, Italy). Cell extracts were diluted 1:1 in 2X Laemmli sample buffer (100mM Tris-HCl pH 6.8, 2% SDS, 20% glycerol, 0.026% Bromophenol blue, 4% beta-mercaptoethanol), and then boiled for 5 min. Equal amounts of total protein extracts (20 µg) were analysed by SDS-PAGE gel (acrylamide gel) and immunoblotted with the indicated antibodies. Primary antibodies: acetyl-tubulin (Sigma) and Cleaved PARP1 antibody [E51] (ab32064) (Abcam). Actin (Santa Cruz Biotechnology) was used as loading control.

Quantification of band intensities was performed by ImageJ software and normalized to loading control.

Cell cycle and PI analysis

Cells (2.0×10^5) were collected, washed with phosphate-buffered saline (PBS) once, and resuspended in hypotonic buffer (0.1% NP-40, 0.1% sodium citrate, 50 µg/µL PI, RNAse A). Cells were then incubated in the dark for at least 30 min and measured by BD Accuri C6 flow cytometer (BD Biosciences). For PI analysis, cells were collected, washed with PBS twice, resuspended in PI buffer (0.2 µg/µL PI, PBS 1%) and measured BD Accuri C6 flow cytometer (BD Biosciences). Flow cytometric data were analyzed using BD Accuri C6 software. Experiments were performed in duplicate.

Statistical analysis was performed by two-tailed unpaired t-test. $P < 0.05$ was considered significant.

STAT3 phosphorylation in MEC-1

MEC-1 cells were resuspended at 1 x10^6 cells/ml in DMEM medium supplemented with 10 % bovine calf serum and treated with either vehicle (DMSO 1% V/V) or compound **14** and **23** (5 µM or 10 µM) for 30 h at 37 °C. Cells were lysed in lysis buffer (1% Triton X-100 in 20 mM Tris-HCl (pH 8), 150 mM NaCl) containing protease inhibitors Cocktail set III (Calbiochem). Post nuclear supernatants were resolved by SDS-PAGE and transferred to nitrocellulose. Immunoblot analysis was performed using as primary antibody anti-pSTAT3 (Tyr 705) (Cell Signalling) or anti-actin (Millipore) and peroxidase-labeled secondary antibodies (GE Healthcare). Blots were visualized with the chemiluminescence detection kit (Bio-rad Laboratories Inc., Milan, Italy) and densitometry analysis was performed on scanned filter using ImageJ software.

Solubility and chemical stability studies

HPLC analysis of compounds 25 and 32, 38

For the HPLC analysis a Chromolith HPLC column RP-18 was employed. The runs were performed by a gradient elution starting from a mixture 20% MeCN (0.1% TFA as phase modifier) in H$_2$O (0.1% TFA as phase modifier) to 90% MeCN (0.1% TFA) in H$_2$O (0.1% TFA) in 15 min. The flow speed was settled at 1.0 mL/min and the temperature was maintained at 25 °C. The volume of injection of the sample was of 10 mL and the wavelength selected for the detection was 254 nM. The retention times obtained following this protocol for compounds **25** and **32, 38** were 7.3 min, 5.6 min and 3.7 min, respectively.

Solubility assay and chemical stability at 25 °C

A stock solution for each tested compound was prepared dissolving the sample in DMSO to a final concentration of 10 mM. From the stock solution, three samples were prepared: one was used as the standard solution and the other two as the test solutions at pH 3.0 and pH 7.4. The samples' concentration of these solutions was 250 µM with a DMSO content of 2.5% (v/v). The standard solution was prepared by dilution of the stock solution in PBS-buffer solution

(MeCN/water, 60:40); the dilution of the stock solution in 50 mM acetic acid afforded the samples' solution at pH 3.0; and the dilution of the stock solution in 50 mM aqueous PBS-buffer afforded the samples' solution at pH 7.4. These suspension/solutions were sealed and left for 24 h at 25 °C under orbital shaking to achieve "pseudothermodynamic equilibrium". After that time the solutions were filtered using PTFE filters and successively diluted 1:2 with the buffer solution used for the preparation of the samples. Then they were analyzed by HPLC/UV/ DAD, using UV detection at 254 nm for quantitation. Solubility was calculated by comparing areas of the sample and of the standard:

$$S = \frac{A_{smp} \; x \; FD \; x \; C_{st}}{A_{st}}$$

S = solubility of the compound (μM); A_{smp} = UV area of the sample solution; FD = dilution factor (2); C_{st} = standard concentration (250 μM); A_{st} = UV area of the standard solution.

For each sample the analysis was performed in triplicate and the solubility result reported was obtained from the average of the three values. The same sample solutions were prepared to evaluate the chemical stability of the compounds after 24 h at 25 °C and analyzed by HPLC/UV/DAD, using UV detection at 254 nm for quantitation. Stability was calculated by comparing the area of the peak at T_0 and the area of the peak of the same solution after 24 h. A stability percentage value was calculated by this method at pH 3.0 and pH 7.4 for each compound by applying the following formula:

$$\%_{remaining} = \frac{AC_{24}}{AC_{T0}} \; X \; 100$$

Ac_{24} = area of the sample after 24 h at 25 °C; Ac_{T0} = area of the sample at T_0. For each sample the analysis was performed in triplicate and the stability result reported was obtained from the average of the three values.

In vitro testing of HDAC1 and HDAC6

OptiPlate-96 black microplates (PerkineElmer) were employed with an assay volume of 60 mL. Human recombinant HDAC1 (BPS Bioscience, Catalog #: 50051) or human recombinant HDAC6 (BPS Bioscience, Catalog #: 50006) were diluted in incubation buffer (50 mM Tris-HCl, pH 8.0, 137 mM NaCl, 2.7 mM KCl, 1 mM $MgCl_2$ and 1 mg/mL BSA). A total of 52 µL of this dilution were incubated with 3 µL of different concentrations of inhibitors in DMSO and 5 µL of the fluorogenic substrate ZMAL (Z-(Ac)Lys-AMC) [30,31] (126 µM) at 37 °C. After 90 min incubation time, 60 µL of the stop solution (33 µM Trichostatin A and 6 mg/mL trypsin in trypsin buffer [Tris-HCl 50 mM, pH 8.0, NaCl 100 mM]), were added. After a following incubation at 37 °C for 30 min, the fluorescence was measured on a BMG LABTECH POLARstar OPTIMA plate reader (BMG Labtechnologies, Germany) with an excitation wavelength of 390 nm and an emission wavelength of 460 nm [31,32].

In vitro testing of HDAC8

Recombinant human HDAC8 was purchased as part of the Fluor-de-Lys HDAC8 fluorimetric drug discovery kit (Enzo Life Sciences, No. BMLAK518). Dose-response curves were built for each inhibitor in order to estimate the respective IC_{50}. DMSO concentration was kept constant to 0.5% and, for each compound, a control curve (enzymes incubated with DMSO only) was added. The Fluor-de-Lys substrate was used at 50 µM. A preincubation period of 15 min was chosen to keep safe from the possibility of a slow-binding inhibition. Hence, the

compounds, substrate, and enzyme (266 nM) were incubated, and the reaction was allowed to proceed for 1 h at 30 °C; 2 μM TSA within 50 μL of 1× Enzo Developer II was added to quench the reaction and the mixture was further incubated for 1 h at 30 °C. Fluorescence was measured in a plate reader (Varioskan Lux, Thermo Fisher Scientific) with excitation wave length at 370 nm and emission at 450 nm. Data were analyzed by nonlinear regression fit using a generalized form of a dose-response curve:[33]

$$y_{res} = y_{min} + \frac{y_{max} - y_{min}}{\left(1 + \frac{[I]}{IC_{50}}\right)}$$

y_{res}= is the residual activity of the enzyme in the presence of inhibitor at concentration [I]; y_{max} = the maximum observed value for the enzyme at zero inhibitor concentration; y_{min} = the minimum observed value for the enzyme at the highest inhibitor concentration. The model did fit three parameters, namely: IC_{50}, y_{max}, and y_{min}.

In addition, since the total enzyme concentration used in the assay (266 nM) was in the same order of magnitude to the obtained IC_{50}s for two out of three inhibitors (namely, **37** and **38**), a more accurate model was chosen to fit the experimental data, ultimately to account for the possibility of a tight-binding interaction. The fit model was in the form of the Morrison equation as implemented in Copeland as reported below:[33]

$$\frac{v_i}{v_0} = 1 - \frac{\sqrt{\left([E] - [I] - K_i^{app}\right)^2 - 4[E][I]}}{2[E]}$$

v_0 and v_i = were the rate observed in the absence or in the presence of the inhibitor at concentration [I], and [E] was kept fixed at 266 nM. It was assumed that the ratio v_i/v_0 was

proportional to the signal (arbitrary fluorescence unit) as obtained by using Fluor-de-Lys kit. This model yields apparent inhibitor constant which should be regarded as a better estimate of interaction with respect to IC_{50}.

Mutagenicity assay: Ames test

The TA100 and TA98 strains of *Salmonella Typhimurium* and S9 fraction were utilized for mutagenicity assay. Approximately 107 bacteria were exposed to 6 concentrations of each test compound, as well as a positive and a negative control, for 90 min in medium containing sufficient histidine to support approximately two cell divisions. After 90 min, the exposure cultures were diluted in pH indicator medium lacking histidine, and aliquoted into 48 wells of a 384-well plate. Within two days, cells which had undergone the reversion to His grew into colonies. Metabolism by the bacterial colonies reduced the pH of the medium, changing the color of that well. This color change can be detected visually or by microplate reader. The number of wells containing revertant colonies were counted for each dose and compared to a zero-dose control. Each dose was tested in six replicates. The test was performed both with and without S9 fraction.

Abbreviations list

5-mC = 5-methyl cytosine

ADP = adenosine diphosphate

AKT = protein Kinase B

APC = antigen presenting cells

ATP = adenosine triphosphate

Bax = Bcl-2-associated X protein

BCL3 = B-cell lymphoma 3

BDNF = brain-derived neurotrophic factor

Ca9-22 = gingival squamous cell carcinoma

CDI = 1,1'-carbonyldiimidazole

ChIP-seq = chromatin immunoprecipitation and next-generation sequencing

CYLD = cylindromatosis gene

DCM = dichloromethane

DIBAL = diisobutylaluminium hydride

DIPEA = N,N-diisopropylethylamine

DMF = dimethyl formamide

DMSO = dimethyl sulfoxide

DNA = deoxyribonucleic acid

DNMT = DNA methyltransferase

EDCI = 1-ethyl-3-(3-dimethylaminopropyl)carbodiimide

EGFR = epidermal growth factor receptor

ERK = extracellular receptor kinase

FK-228 = romidepsin

FLIP = FADD-like IL-1 β-converting enzyme

HAT = histone acetyltransferase

HCA = homocysteic acid

HDAC = histone deacetylase

HDAH = histone deacetylase-like amidohydrolase

HDLP = histone deacetylase-like protein

HMT = histone methyltransferase

HOBT = 1-hydroxybenzotriazole hydrate

HSF1 = heat shock transcription factor 1

HSP90 = heat shock protein 90

IBC = inflammatory breast cancer

IgF2 = insulin-growth factor 2

JAK = janus kinase

JIP1 = JNK-interacting protein

KDM = lysine demethylase

KYSE520 = esophageal squamous cell carcinoma

LBH-589 = panobinostat

LC-MS = liquid chromatography mass spectroscopy

lncRNA = long ncRNA

MAPK = mitogen-activated protein kinase

MCF7 = breast cancer cell line

MEC1 = human chronic lymphocytic leukemia

MHC = major histocompatibility complex

MMP = matrix metalloproteases

mRNA = messenger RNA

mRNA = microRNA

MT = microtubule

NAD^+ = nicotinamide adenine dinucleotide

NaHMDS = sodium bis(trimethylsilyl)amide

NB4 = acute promyelocytic leukemia

ncRNA = non-coding RNA

NES = nuclear export signal

NF-κB = nuclear factor kappa-light-chain-enhancer of activated B cells

NIH3T3 = mouse fibroblast

NMO = 4-methylmorpholine *N*-oxide

NMR = nuclear magnetic resonance

OE33 = esophageal adenocarcinoma

OEC = oral and esophageal cancer

PARP = poly (ADP-ribose) polymerase

PI = propidium iodide

PI3K = phosphoinositide-3-kinase

piRNA = piwi-interacting RNA

PLAP = phospholipase A2 inactivating protein

PRC1 = polycomb repressive complex 1

PRMT = protein arginine methyltransferase

PTM = post-translational modifications

PTSA = *p*-toluene sulfonic acid

PTSH = *p*-toluenesulfonyl hydrazide

PXD-101 = belinostat

RNA = ribonucleic acid

ROS = reactive oxygen species

SAHA = suberanilohydroxamic acid

SAR = structure-activity relationships

Ser-Glu-containing tetradecapeptide = SE14

siRNA = small interfering RNA

SIRT = sirtuins

SKBR3 = breast carcinoma cell line

SKOV3 = ovarian cancer cell line

snRNA = small nucleolar RNA

STAT3 = signal transducer and activator of transcription 3

TA98 and TA100 = *Salmonella typhimurium strains*

TEA = triethylamine

TET = Ten-eleven translocation methylcytosine dioxygenase

TF = transcription factor

THF = tetrahydrofuran

TR-146 = buccal mucosa squamous cell carcinoma

tRNA = transfer RNA

TSA = trichostatin A

TSS = transcription suppression sites

U937 = monocytic leukemia

UBP = ubiquitin-specific proteases

VCP = valosin containing protein

ZBG = zinc-binding group

Bibliography

1.   Watson, J. D.; Crick, F. H. Molecular structure of nucleic acids. *Nature* **1953,** 171, 737-738.

2.   Crick, F. Central dogma of molecular biology. *Nature* **1970,** 227, 561-563.

3.   Ehrlich, M.; Gama-Sosa, M. A.; Huang, L.-H.; Midgett, R. M.; Kuo, K. C.; McCune, R. A.; Gehrke, C. Amount and distribution of 5-methylcytosine in human DNA from different types of tissues or cells. *Nucleic Acids Res* **1982,** 10, 2709-2721.

4.   Wu, H.; Zhang, Y. Reversing DNA methylation: mechanisms, genomics, and biological functions. *Cell* **2014,** 156, 45-68.

5.   Holliday, R.; Pugh, J. E. DNA modification mechanisms and gene activity during development. *Science* **1975,** 187, 226-232.

6.   Riggs, A. D. X inactivation, differentiation, and DNA methylation. *Cytogenet Genome Res* **1975,** 14, 9-25.

7.   Lin, J. C.; Jeong, S.; Liang, G.; Takai, D.; Fatemi, M.; Tsai, Y. C.; Egger, G.; Gal-Yam, E. N.; Jones, P. A. Role of nucleosomal occupancy in the epigenetic silencing of the MLH1 CpG island. *Cancer Cell* **2007,** 12, 432-444.

8.   Wade, P. A.; Wolffe, A. P. ReCoGnizing methylated DNA. *Nat Struct Biol* **2001,** 8, 575-577.

9.   Wolf, S. F.; Jolly, D. J.; Lunnen, K. D.; Friedmann, T.; Migeon, B. R. Methylation of the hypoxanthine phosphoribosyltransferase locus on the human X chromosome: implications for X-chromosome inactivation. *Proc Nat Acad Sci USA* **1984,** 81, 2806-2810.

10.   Fatemi, M.; Hermann, A.; Pradhan, S.; Jeltsch, A. The activity of the murine DNA methyltransferase Dnmt1 is controlled by interaction of the catalytic domain with the N-terminal part of the enzyme leading to an allosteric activation of the enzyme after binding to methylated DNA. *J Mol Biol* **2001,** 309, 1189-1199.

11.   Hermann, A.; Goyal, R.; Jeltsch, A. The Dnmt1 DNA-(cytosine-C5)-methyltransferase methylates DNA processively with high preference for hemimethylated target sites. *J Biol Chem* **2004,** 279, 48350-48359.

12.   Okano, M.; Bell, D. W.; Haber, D. A.; Li, E. DNA methyltransferases Dnmt3a and Dnmt3b are essential for de novo methylation and mammalian development. *Cell* **1999,** 99, 247-257.

13.   Christman, J. K. 5-Azacytidine and 5-aza-2′-deoxycytidine as inhibitors of DNA methylation: mechanistic studies and their implications for cancer therapy. *Oncogene* **2002,** 21, 5483-5495.

14.   Garcia-Manero, G.; Kantarjian, H. M.; Sanchez-Gonzalez, B.; Yang, H.; Rosner, G.; Verstovsek, S.; Rytting, M.; Wierda, W. G.; Ravandi, F.; Koller, C. Phase 1/2 study of the combination of 5-aza-2′-deoxycytidine with valproic acid in patients with leukemia. *Blood* **2006,** 108, 3271-3279.

15.   Momparler, R. L.; Rivard, G. E.; Gyger, M. Clinical trial on 5-aza-2′-deoxycytidine in patients with acute leukemia. *Pharmacol Therap* **1985,** 30, 277-286.

16.   Ito, S.; Shen, L.; Dai, Q.; Wu, S. C.; Collins, L. B.; Swenberg, J. A.; He, C.; Zhang, Y. Tet proteins can convert 5-methylcytosine to 5-formylcytosine and 5-carboxylcytosine. *Science* **2011,** 333, 1300-1303.

17.   Rivera, C. M.; Ren, B. Mapping human epigenomes. *Cell* **2013,** 155, 39-55.

18.   Workman, J.; Kingston, R. Alteration of nucleosome structure as a mechanism of transcriptional regulation. In Annual Reviews 4139 El Camino Way, PO Box 10139, Palo Alto, CA 94303-0139, USA: 1998.

19.   Bannister, A. J.; Kouzarides, T. Regulation of chromatin by histone modifications. *Cell Res* **2011,** 21, 381-395.

20.   Pasini, D.; Hansen, K. H.; Christensen, J.; Agger, K.; Cloos, P. A.; Helin, K. Coordinated regulation of transcriptional repression by the RBP2 H3K4 demethylase and Polycomb-Repressive Complex 2. *Genes Dev* **2008,** 22, 1345-1355.

21.   Djebali, S.; Davis, C. A.; Merkel, A.; Dobin, A.; Lassmann, T.; Mortazavi, A.; Tanzer, A.; Lagarde, J.; Lin, W.; Schlesinger, F. Landscape of transcription in human cells. *Nature* **2012,** 489, 101-108.

22.   Uchida, S.; Dimmeler, S. Long noncoding RNAs in cardiovascular diseases. *Circ Res* **2015,** 116, 737-750.

23.   Wang, K. C.; Chang, H. Y. Molecular mechanisms of long noncoding RNAs. *Mol Cell* **2011,** 43, 904-914.

24.   Sadoul, K.; Boyault, C.; Pabion, M.; Khochbin, S. Regulation of protein turnover by acetyltransferases and deacetylases. *Biochimie* **2008,** 90, 306-312.

25.   Roche, J.; Bertrand, P. Inside HDACs with more selective HDAC inhibitors. *Eur J Med Chem* **2016,** 121, 451-483.

26.   Joshi, P.; Greco, T. M.; Guise, A. J.; Luo, Y.; Yu, F.; Nesvizhskii, A. I.; Cristea, I. M. The functional interactome landscape of the human histone deacetylase family. *Mol Syst Biol* **2013,** 9.

27.   Bolden, J. E.; Peart, M. J.; Johnstone, R. W. Anticancer activities of histone deacetylase inhibitors. *Nat Rev Drug Discov* **2006,** 5, 769-784.

28.   Shakespear, M. R.; Halili, M. A.; Irvine, K. M.; Fairlie, D. P.; Sweet, M. J. Histone deacetylases as regulators of inflammation and immunity. *Trends Immunol* **2011,** 32, 335-343.

29.   Chuang, D.-M.; Leng, Y.; Marinova, Z.; Kim, H.-J.; Chiu, C.-T. Multiple roles of HDAC inhibition in neurodegenerative conditions. *Trends Neurosci* **2009,** 32, 591-601.

30.   Sangwan, R.; Rajan, R.; Mandal, P. K. HDAC as onco target: Reviewing the synthetic approaches with SAR study of their inhibitors. *Eur J Med Chem* **2018,** 158, 620-706.

31.   New, M.; Olzscha, H.; La Thangue, N. B. HDAC inhibitor-based therapies: can we interpret the code? *Mol Oncol* **2012,** 6, 637-656.

32.   Barneda-Zahonero, B.; Parra, M. Histone deacetylases and cancer. *Mol Oncol* **2012,** 6, 579-589.

33.   Finnin, M. S.; Donigian, J. R.; Cohen, A.; Richon, V. M.; Rifkind, R. A.; Marks, P. A.; Breslow, R.; Pavletich, N. P. Structures of a histone deacetylase homologue bound to the TSA and SAHA inhibitors. *Nature* **1999,** 401, 188-193.

34.   Vanommeslaeghe, K.; De Proft, F.; Loverix, S.; Tourwe, D.; Geerlings, P. Theoretical study revealing the functioning of a novel combination of catalytic motifs in histone deacetylase. *Biorg Med Chem* **2005,** 13, 3987-3992.

35.   Corminboeuf, C.; Hu, P.; Tuckerman, M. E.; Zhang, Y. Unexpected deacetylation mechanism suggested by a density functional theory QM/MM study of histone-deacetylase-like protein. *J Am Chem Soc* **2006,** 128, 4530-4531.

36.   Bottomley, M. J.; Surdo, P. L.; Di Giovine, P.; Cirillo, A.; Scarpelli, R.; Ferrigno, F.; Jones, P.; Neddermann, P.; De Francesco, R.; Steinkühler, C. Structural and functional analysis of the human HDAC4 catalytic domain reveals a regulatory structural zinc-binding domain. *J Biol Chem* **2008,** 283, 26694-26704.

37.   Hildmann, C.; Ninkovic, M.; Dietrich, R.; Wegener, D.; Riester, D.; Zimmermann, T.; Birch, O. M.; Bernegger, C.; Loidl, P.; Schwienhorst, A. A new amidohydrolase from Bordetella or Alcaligenes strain FB188 with similarities to histone deacetylases. *J Bacteriol* **2004,** 186, 2328-2339.

38.   Schuetz, A.; Min, J.; Allali-Hassani, A.; Schapira, M.; Shuen, M.; Loppnau, P.; Mazitschek, R.; Kwiatkowski, N. P.; Lewis, T. A.; Maglathin, R. L. Human HDAC7 harbors a class IIa histone deacetylase-specific zinc binding motif and cryptic deacetylase activity. *J Biol Chem* **2008,** 283, 11355-11363.

39.   Estiu, G.; Greenberg, E.; Harrison, C. B.; Kwiatkowski, N. P.; Mazitschek, R.; Bradner, J. E.; Wiest, O. Structural origin of selectivity in class II-selective histone deacetylase inhibitors. *J Med Chem* **2008,** 51, 2898-2906.

40.   Grozinger, C. M.; Hassig, C. A.; Schreiber, S. L. Three proteins define a class of human histone deacetylases related to yeast Hda1p. *Proc Nat Acad Sci USA* **1999,** 96, 4868-4873.

41.   Zhang, Y.; Gilquin, B.; Khochbin, S.; Matthias, P. Two catalytic domains are required for protein deacetylation. *J Biol Chem* **2006,** 281, 2401-2404.

42.   Verdel, A.; Curtet, S.; Brocard, M.-P.; Rousseaux, S.; Lemercier, C.; Yoshida, M.; Khochbin, S. Active maintenance of mHDA2/mHDAC6 histone-deacetylase in the cytoplasm. *Curr Biol* **2000,** 10, 747-749.

43.   Yang, X.-J.; Grégoire, S. Class II histone deacetylases: from sequence to function, regulation, and clinical implication. *Mol Cell Biol* **2005,** 25, 2873-2884.

44.   Zhang, Y.; Li, N.; Caron, C.; Matthias, G.; Hess, D.; Khochbin, S.; Matthias, P. HDAC-6 interacts with and deacetylates tubulin and microtubules in vivo. *EMBO J* **2003,** 22, 1168-1179.

45.   Haggarty, S. J.; Koeller, K. M.; Wong, J. C.; Grozinger, C. M.; Schreiber, S. L. Domain-selective small-molecule inhibitor of histone deacetylase 6 (HDAC6)-mediated tubulin deacetylation. *Proc Nat Acad Sci USA* **2003,** 100, 4389-4394.

46.   Zou, H.; Wu, Y.; Navre, M.; Sang, B.-C. Characterization of the two catalytic domains in histone deacetylase 6. *Biochem Biophys Res Commun* **2006,** 341, 45-50.

47.   Bertos, N. R.; Gilquin, B.; Chan, G. K.; Yen, T. J.; Khochbin, S.; Yang, X.-J. Role of the tetradecapeptide repeat domain of human histone deacetylase 6 in cytoplasmic retention. *J Biol Chem* **2004,** 279, 48246-48254.

48.   Bertos, N. R.; Wang, A. H.; Yang, X.-J. Class II histone deacetylases: structure, function, and regulation. *Biochem Cell Biol* **2001,** 79, 243-252.

49.   Seigneurin-Berny, D.; Verdel, A.; Curtet, S.; Lemercier, C.; Garin, J.; Rousseaux, S.; Khochbin, S. Identification of components of the murine histone deacetylase 6 complex: link between acetylation and ubiquitination signaling pathways. *Mol Cell Biol* **2001,** 21, 8035-8044.

50.   Boyault, C.; Gilquin, B.; Zhang, Y.; Rybin, V.; Garman, E.; Meyer-Klaucke, W.; Matthias, P.; Müller, C. W.; Khochbin, S. HDAC6–p97/VCP controlled polyubiquitin chain turnover. *EMBO J* **2006,** 25, 3357-3366.

51.   Hook, S. S.; Orian, A.; Cowley, S. M.; Eisenman, R. N. Histone deacetylase 6 binds polyubiquitin through its zinc finger (PAZ domain) and copurifies with deubiquitinating enzymes. *Proc Nat Acad Sci USA* **2002,** 99, 13425-13430.

52.   Kawaguchi, Y.; Kovacs, J. J.; McLaurin, A.; Vance, J. M.; Ito, A.; Yao, T.-P. The deacetylase HDAC6 regulates aggresome formation and cell viability in response to misfolded protein stress. *Cell* **2003,** 115, 727-738.

53. Luxton, G. G.; Gundersen, G. G. HDAC6-pack: cortactin acetylation joins the brew. *Dev Cell* **2007,** 13, 161-162.

54. Valenzuela-Fernandez, A.; Cabrero, J. R.; Serrador, J. M.; Sánchez-Madrid, F. HDAC6: a key regulator of cytoskeleton, cell migration and cell–cell interactions. *Trends Cell Biol* **2008,** 18, 291-297.

55. Hubbert, C.; Guardiola, A.; Shao, R.; Kawaguchi, Y.; Ito, A.; Nixon, A.; Yoshida, M.; Wang, X.-F.; Yao, T.-P. HDAC6 is a microtubule-associated deacetylase. *Nature* **2002,** 417, 455-458.

56. Westermann, S.; Weber, K. Post-translational modifications regulate microtubule function. *Nat Rev Mol Cell Biol* **2003,** 4, 938-948.

57. Verhey, K. J.; Gaertig, J. The tubulin code. *Cell Cycle* **2007,** 6, 2152-2160.

58. Bulinski, J. C. Microtubule modification: acetylation speeds anterograde traffic flow. *Curr Biol* **2007,** 17, R18-R20.

59. Reed, N. A.; Cai, D.; Blasius, T. L.; Jih, G. T.; Meyhofer, E.; Gaertig, J.; Verhey, K. J. Microtubule acetylation promotes kinesin-1 binding and transport. *Curr Biol* **2006,** 16, 2166-2172.

60. Dompierre, J. P.; Godin, J. D.; Charrin, B. C.; Cordelieres, F. P.; King, S. J.; Humbert, S.; Saudou, F. Histone deacetylase 6 inhibition compensates for the transport deficit in Huntington's disease by increasing tubulin acetylation. *J Neurosci* **2007,** 27, 3571-3583.

61. Zhang, X.; Yuan, Z.; Zhang, Y.; Yong, S.; Salas-Burgos, A.; Koomen, J.; Olashaw, N.; Parsons, J. T.; Yang, X.-J.; Dent, S. R. HDAC6 modulates cell motility by altering the acetylation level of cortactin. *Mol Cell* **2007,** 27, 197-213.

62. Ridley, A. J. Rho GTPases and actin dynamics in membrane protrusions and vesicle trafficking. *Trends Cell Biol* **2006,** 16, 522-529.

63.	Destaing, O.; Saltel, F.; Gilquin, B.; Chabadel, A.; Khochbin, S.; Ory, S.; Jurdic, P. A novel Rho-mDia2-HDAC6 pathway controls podosome patterning through microtubule acetylation in osteoclasts. *J Cell Sci* **2005,** 118, 2901-2911.

64.	Kovacs, J. J.; Murphy, P. J.; Gaillard, S.; Zhao, X.; Wu, J.-T.; Nicchitta, C. V.; Yoshida, M.; Toft, D. O.; Pratt, W. B.; Yao, T.-P. HDAC6 regulates Hsp90 acetylation and chaperone-dependent activation of glucocorticoid receptor. *Mol Cell* **2005,** 18, 601-607.

65.	Boyault, C.; Zhang, Y.; Fritah, S.; Caron, C.; Gilquin, B.; Kwon, S. H.; Garrido, C.; Yao, T.-P.; Vourc'h, C.; Matthias, P. HDAC6 controls major cell response pathways to cytotoxic accumulation of protein aggregates. *Genes Dev* **2007,** 21, 2172-2181.

66.	Kopito, R. R. Aggresomes, inclusion bodies and protein aggregation. *Trends Cell Biol* **2000,** 10, 524-530.

67.	Garcia-Mata, R.; Gao, Y. S.; Sztul, E. Hassles with taking out the garbage: aggravating aggresomes. *Traffic* **2002,** 3, 388-396.

68.	Hicke, L.; Schubert, H. L.; Hill, C. P. Ubiquitin-binding domains. *Nat Rev Mol Cell Biol* **2005,** 6, 610-621.

69.	Lee, Y.-S.; Lim, K.-H.; Guo, X.; Kawaguchi, Y.; Gao, Y.; Barrientos, T.; Ordentlich, P.; Wang, X.-F.; Counter, C. M.; Yao, T.-P. The cytoplasmic deacetylase HDAC6 is required for efficient oncogenic tumorigenesis. *Cancer Res* **2008,** 68, 7561-7569.

70.	Putcha, P.; Yu, J.; Rodriguez-Barrueco, R.; Saucedo-Cuevas, L.; Villagrasa, P.; Murga-Penas, E.; Quayle, S. N.; Yang, M.; Castro, V.; Llobet-Navas, D. HDAC6 activity is a non-oncogene addiction hub for inflammatory breast cancers. *Breast Cancer Res* **2015,** 17, 149.

71.	Witt, O.; Deubzer, H. E.; Milde, T.; Oehme, I. HDAC family: What are the cancer relevant targets? *Cancer Lett* **2009,** 277, 8-21.

72.	Saji, S.; Kawakami, M.; Hayashi, S.-i.; Yoshida, N.; Hirose, M.; Horiguchi, S.-i.; Itoh, A.; Funata, N.; Schreiber, S. L.; Yoshida, M. Significance of HDAC6 regulation via estrogen

signaling for cell motility and prognosis in estrogen receptor-positive breast cancer. *Oncogene* **2005,** 24, 4531-4539.

73.   Dai, Y.; Chen, S.; Wang, L.; Pei, X. Y.; Kramer, L. B.; Dent, P.; Grant, S. Bortezomib interacts synergistically with belinostat in human acute myeloid leukaemia and acute lymphoblastic leukaemia cells in association with perturbations in NF-κB and Bim. *Br J Haematol* **2011,** 153, 222-235.

74.   Zhang, L.; Liu, N.; Xie, S.; He, X.; Tala; Zhou, J.; Liu, M.; Li, D. HDAC6 regulates neuroblastoma cell migration and may play a role in the invasion process. *Cancer Biol Ther* **2014,** 15, 1561-1570.

75.   Wickström, S. A.; Masoumi, K. C.; Khochbin, S.; Fässler, R.; Massoumi, R. CYLD negatively regulates cell-cycle progression by inactivating HDAC6 and increasing the levels of acetylated tubulin. *EMBO J* **2010,** 29, 131-144.

76.   Ishikawa, Y.; Tsunoda, K.; Shibazaki, M.; Takahashi, K.; Akasaka, T.; Masuda, T.; Maesawa, C. Downregulation of cylindromatosis gene, CYLD, confers a growth advantage on malignant melanoma cells while negatively regulating their migration activity. *Int J Oncol* **2012,** 41, 53-60.

77.   Ikeda, F.; Dikic, I. CYLD in ubiquitin signaling and tumor pathogenesis. *Cell* **2006,** 125, 643-645.

78.   Massoumi, R.; Chmielarska, K.; Hennecke, K.; Pfeifer, A.; Fässler, R. Cyld inhibits tumor cell proliferation by blocking Bcl-3-dependent NF-κB signaling. *Cell* **2006,** 125, 665-677.

79.   Balliu, M.; Guandalini, L.; Romanelli, M. N.; D'Amico, M.; Paoletti, F. HDAC-inhibitor (S)-8 disrupts HDAC 6-PP 1 complex prompting A375 melanoma cell growth arrest and apoptosis. *J Cell Mol Med* **2015,** 19, 143-154.

80.   Sunshine, J. C.; Nguyen, P. L.; Kaunitz, G. J.; Cottrell, T. R.; Berry, S.; Esandrio, J.; Xu, H.; Ogurtsova, A.; Bleich, K. B.; Cornish, T. C. PD-L1 expression in melanoma: a quantitative immunohistochemical antibody comparison. *Clin Cancer Res* **2017,** 23, 4938-4944.

81.   Selenica, M.-L.; Benner, L.; Housley, S. B.; Manchec, B.; Lee, D. C.; Nash, K. R.; Kalin, J.; Bergman, J. A.; Kozikowski, A.; Gordon, M. N. Histone deacetylase 6 inhibition improves memory and reduces total tau levels in a mouse model of tau deposition. *Alzheimers Res Ther* **2014,** 6, 12.

82.   Zhang, L.; Sheng, S.; Qin, C. The role of HDAC6 in Alzheimer's disease. *J Alzheimers Dis* **2013,** 33, 283-295.

83.   Gao, Y.-s.; Hubbert, C. C.; Yao, T.-P. The microtubule-associated histone deacetylase 6 (HDAC6) regulates epidermal growth factor receptor (EGFR) endocytic trafficking and degradation. *J Biol Chem* **2010,** 285, 11219-11226.

84.   Gu, Y.-z.; Xue, Q.; Chen, Y.-j.; Yu, G.-H.; Shen, Y.; Wang, M.-y.; Shi, Q.; Zhang, X.-G. Different roles of PD-L1 and FasL in immunomodulation mediated by human placenta-derived mesenchymal stem cells. *Hum Immunol* **2013,** 74, 267-276.

85.   Liu, W.; Fan, L. X.; Zhou, X.; Sweeney Jr, W. E.; Avner, E. D.; Li, X. HDAC6 regulates epidermal growth factor receptor (EGFR) endocytic trafficking and degradation in renal epithelial cells. *PloS One* **2012,** 7.

86.   Wen, J.; Fu, J.; Ling, Y.; Zhang, W. MIIP accelerates epidermal growth factor receptor protein turnover and attenuates proliferation in non-small cell lung cancer. *Oncotarget* **2016,** 7, 9118.

87.   Foss, F.; Advani, R.; Duvic, M.; Hymes, K. B.; Intragumtornchai, T.; Lekhakula, A.; Shpilberg, O.; Lerner, A.; Belt, R. J.; Jacobsen, E. D. A Phase II trial of Belinostat (PXD 101)

in patients with relapsed or refractory peripheral or cutaneous T-cell lymphoma. *Br J Haematol* **2015,** 168, 811-819.

88.   Aoyagi, S.; Archer, T. K. Modulating molecular chaperone Hsp90 functions through reversible acetylation. *Trends Cell Biol* **2005,** 15, 565-567.

89.   Tsutsumi, S.; Beebe, K.; Neckers, L. Impact of heat-shock protein 90 on cancer metastasis. *Future Oncol* **2009,** 5, 679-688.

90.   Dallavalle, S.; Pisano, C.; Zunino, F. Development and therapeutic impact of HDAC6-selective inhibitors. *Biochem Pharmacol* **2012,** 84, 756-765.

91.   Subramanian, C.; Jarzembowski, J. A.; Opipari Jr, A. W.; Castle, V. P.; Kwok, R. P. HDAC6 deacetylates Ku70 and regulates Ku70-Bax binding in neuroblastoma. *Neoplasia (New York, NY)* **2011,** 13, 726.

92.   Kerr, E.; Holohan, C.; McLaughlin, K.; Majkut, J.; Dolan, S.; Redmond, K.; Riley, J.; McLaughlin, K.; Stasik, I.; Crudden, M. Identification of an acetylation-dependant Ku70/FLIP complex that regulates FLIP expression and HDAC inhibitor-induced apoptosis. *Cell Death Differ* **2012,** 19, 1317-1327.

93.   Chen, C.-S.; Weng, S.-C.; Tseng, P.-H.; Lin, H.-P.; Chen, C.-S. Histone acetylation-independent effect of histone deacetylase inhibitors on Akt through the reshuffling of protein phosphatase 1 complexes. *J Biol Chem* **2005,** 280, 38879-38887.

94.   Kim, I. A.; No, M.; Lee, J. M.; Shin, J. H.; Oh, J. S.; Choi, E. J.; Kim, I. H.; Atadja, P.; Bernhard, E. J. Epigenetic modulation of radiation response in human cancer cells with activated EGFR or HER-2 signaling: potential role of histone deacetylase 6. *Radiother Oncol* **2009,** 92, 125-132.

95.   Tien, S.; Chang, Z. Oncogenic Shp2 disturbs microtubule regulation to cause HDAC6-dependent ERK hyperactivation. *Oncogene* **2014,** 33, 2938-2946.

96.   Tumeh, P. C.; Harview, C. L.; Yearley, J. H.; Shintaku, I. P.; Taylor, E. J.; Robert, L.; Chmielowski, B.; Spasic, M.; Henry, G.; Ciobanu, V. PD-1 blockade induces responses by inhibiting adaptive immune resistance. *Nature* **2014,** 515, 568-571.

97.   Shimizu, T.; Seto, T.; Hirai, F.; Takenoyama, M.; Nosaki, K.; Tsurutani, J.; Kaneda, H.; Iwasa, T.; Kawakami, H.; Noguchi, K. Phase 1 study of pembrolizumab (MK-3475; anti-PD-1 monoclonal antibody) in Japanese patients with advanced solid tumors. *Invest New Drug* **2016,** 34, 347-354.

98.   Hao, M.; Zhao, G.; Du, X.; Yang, Y.; Yang, J. Clinical characteristics and prognostic indicators for metastatic melanoma: data from 446 patients in north China. *Tumor Biol* **2016,** 37, 10339-10348.

99.   Woan, K.; Lienlaf, M.; Perez-Villaroel, P.; Lee, C.; Cheng, F.; Knox, T.; Woods, D.; Barrios, K.; Powers, J.; Sahakian, E. Targeting histone deacetylase 6 mediates a dual anti-melanoma effect: Enhanced antitumor immunity and impaired cell proliferation. *Mol Oncol* **2015,** 9, 1447-1457.

100.   Cheng, F.; Lienlaf, M.; Perez-Villarroel, P.; Wang, H.-W.; Lee, C.; Woan, K.; Woods, D.; Knox, T.; Bergman, J.; Pinilla-Ibarz, J. Divergent roles of histone deacetylase 6 (HDAC6) and histone deacetylase 11 (HDAC11) on the transcriptional regulation of IL10 in antigen presenting cells. *Mol Immunol* **2014,** 60, 44-53.

101.   Yu, H.; Pardoll, D.; Jove, R. STATs in cancer inflammation and immunity: a leading role for STAT3. *Nat Rev Cancer* **2009,** 9, 798-809.

102.   Abdelhamed, S.; Ogura, K.; Yokoyama, S.; Saiki, I.; Hayakawa, Y. AKT-STAT3 pathway as a downstream target of EGFR signaling to regulate PD-L1 expression on NSCLC cells. *J Cancer* **2016,** 7, 1579.

103.   Lienlaf, M.; Perez-Villarroel, P.; Knox, T.; Pabon, M.; Sahakian, E.; Powers, J.; Woan, K.; Lee, C.; Cheng, F.; Deng, S. Essential role of HDAC6 in the regulation of PD-L1 in melanoma. *Mol Oncol* **2016,** 10, 735-750.

104.   Yu, H.; Lee, H.; Herrmann, A.; Buettner, R.; Jove, R. Revisiting STAT3 signalling in cancer: new and unexpected biological functions. *Nat Rev Cancer* **2014,** 14, 736-746.

105.   Cheng, F.; Lienlaf, M.; Wang, H.-W.; Perez-Villarroel, P.; Lee, C.; Woan, K.; Rock-Klotz, J.; Sahakian, E.; Woods, D.; Pinilla-Ibarz, J. A novel role for histone deacetylase 6 in the regulation of the tolerogenic STAT3/IL-10 pathway in APCs. *J Immunol* **2014,** 193, 2850-2862.

106.   Ray, A.; Das, D. S.; Song, Y.; Hideshima, T.; Tai, Y.-T.; Chauhan, D.; Anderson, K. C. Combination of a novel HDAC6 inhibitor ACY-241 and anti-PD-L1 antibody enhances anti-tumor immunity and cytotoxicity in multiple myeloma. *Leukemia* **2018,** 32, 843-846.

107.   Kalin, J. H.; Butler, K. V.; Kozikowski, A. P. Creating zinc monkey wrenches in the treatment of epigenetic disorders. *Curr Opin Chem Biol* **2009,** 13, 263-271.

108.   Kozikowski, A. P.; Butler, K. V. Chemical origins of isoform selectivity in histone deacetylase inhibitors. *Curr Pharm Des* **2008,** 14, 505-528.

109.   Juliandi, B.; Abematsu, M.; Sanosaka, T.; Tsujimura, K.; Smith, A.; Nakashima, K. Induction of superficial cortical layer neurons from mouse embryonic stem cells by valproic acid. *Neurosci Res* **2012,** 72, 23-31.

110.   Zhan, P.; Itoh, Y.; Suzuki, T.; Liu, X. Strategies for the discovery of target-specific or isoform-selective modulators. *J Med Chem* **2015,** 58, 7611-7633.

111.   Micelli, C.; Rastelli, G. Histone deacetylases: structural determinants of inhibitor selectivity. *Drug Discov Today* **2015,** 20, 718-735.

112.   Wagner, F. F.; Weïwer, M.; Lewis, M. C.; Holson, E. B. Small molecule inhibitors of zinc-dependent histone deacetylases. *Neurotherapeutics* **2013,** 10, 589-604.

113.   Cappellacci, L.; Perinelli, D. R.; Maggi, F.; Grifantini, M.; Petrelli, R. Recent progress in histone deacetylase inhibitors as anticancer agents. *Curr Med Chem* **2019**.

114.   Eckschlager, T.; Plch, J.; Stiborova, M.; Hrabeta, J. Histone deacetylase inhibitors as anticancer drugs. *Int J Mol Sci* **2017,** 18, 1414.

115.   Yang, Z.; Wang, T.; Wang, F.; Niu, T.; Liu, Z.; Chen, X.; Long, C.; Tang, M.; Cao, D.; Wang, X. Discovery of selective histone deacetylase 6 inhibitors using the quinazoline as the cap for the treatment of cancer. *J Med Chem* **2016,** 59, 1455-1470.

116.   Gryder, B. E.; Sodji, Q. H.; Oyelere, A. K. Targeted cancer therapy: giving histone deacetylase inhibitors all they need to succeed. *Future Med Chem* **2012,** 4, 505-524.

117.   Reid, T.; Valone, F.; Lipera, W.; Irwin, D.; Paroly, W.; Natale, R.; Sreedharan, S.; Keer, H.; Lum, B.; Scappaticci, F. Phase II trial of the histone deacetylase inhibitor pivaloyloxymethyl butyrate (Pivanex, AN-9) in advanced non-small cell lung cancer. *Lung Cancer* **2004,** 45, 381-386.

118.   Ma, N.; Luo, Y.; Wang, Y.; Liao, C.; Ye, W.-C.; Jiang, S. Selective histone deacetylase inhibitors with anticancer activity. *Curr Top Med Chem* **2016,** 16, 415-426.

119.   Seidel, C.; Schnekenburger, M.; Dicato, M.; Diederich, M. Histone deacetylase 6 in health and disease. *Epigenomics* **2015,** 7, 103-118.

120.   Govindarajan, N.; Rao, P.; Burkhardt, S.; Sananbenesi, F.; Schlüter, O. M.; Bradke, F.; Lu, J.; Fischer, A. Reducing HDAC6 ameliorates cognitive deficits in a mouse model for Alzheimer's disease. *EMBO Mol Med* **2013,** 5, 52-63.

121.   Brindisi, M.; Saraswati, A. P.; Brogi, S.; Gemma, S.; Butini, S.; Campiani, G. Old but Gold: Tracking the New Guise of Histone Deacetylase 6 (HDAC6) Enzyme as a Biomarker and Therapeutic Target in Rare Diseases. *J Med Chem* **2020,** 63, 23-39.

122.   Shen, S.; Kozikowski, A. P. A patent review of histone deacetylase 6 inhibitors in neurodegenerative diseases (2014-2019). *Expert Opin Ther Pat* **2020,** 30, 121-136.

123. Wang, X.-X.; Wan, R.-Z.; Liu, Z.-P. Recent advances in the discovery of potent and selective HDAC6 inhibitors. *Eur J Med Chem* **2018,** 143, 1406-1418.

124. Hai, Y.; Christianson, D. W. Histone deacetylase 6 structure and molecular basis of catalysis and inhibition. *Nature Chem Biol* **2016,** 12, 741.

125. Butler, K. V.; Kalin, J.; Brochier, C.; Vistoli, G.; Langley, B.; Kozikowski, A. P. Rational Design and Simple Chemistry Yield a Superior, Neuroprotective HDAC6 Inhibitor, Tubastatin A. *J Am Chem Soc* **2010,** 132, 10842-10846.

126. Haggarty, S. J.; Koeller, K. M.; Wong, J. C.; Butcher, R. A.; Schreiber, S. L. Multidimensional chemical genetic analysis of diversity-oriented synthesis-derived deacetylase inhibitors using cell-based assays. *Chem Biol* **2003,** 10, 383-396.

127. Bali, P.; Pranpat, M.; Bradner, J.; Balasis, M.; Fiskus, W.; Guo, F.; Rocha, K.; Kumaraswamy, S.; Boyapalle, S.; Atadja, P. Inhibition of histone deacetylase 6 acetylates and disrupts the chaperone function of heat shock protein 90 a novel basis for antileukemia activity of histone deacetylase inhibitors. *J Biol Chem* **2005,** 280, 26729-26734.

128. Mai, A.; Massa, S.; Pezzi, R.; Simeoni, S.; Rotili, D.; Nebbioso, A.; Scognamiglio, A.; Altucci, L.; Loidl, P.; Brosch, G. Class II (IIa)-selective histone deacetylase inhibitors. 1. Synthesis and biological evaluation of novel (aryloxopropenyl) pyrrolyl hydroxyamides. *J Med Chem* **2005,** 48, 3344-3353.

129. Hideshima, T.; Bradner, J. E.; Wong, J.; Chauhan, D.; Richardson, P.; Schreiber, S. L.; Anderson, K. C. Small-molecule inhibition of proteasome and aggresome function induces synergistic antitumor activity in multiple myeloma. *Proc Nat Acad Sci USA* **2005,** 102, 8567-8572.

130. Bieliauskas, A. V.; Pflum, M. K. H. Isoform-selective histone deacetylase inhibitors. *Chem Soc Rev* **2008,** 37, 1402-1413.

131. Anandan, S.-K.; Ward, J. S.; Brokx, R. D.; Bray, M. R.; Patel, D. V.; Xiao, X.-X. Mercaptoamide-based non-hydroxamic acid type histone deacetylase inhibitors. *Bioorg Med Chem Lett* **2005,** 15, 1969-1972.

132. Chen, B.; Petukhov, P. A.; Jung, M.; Velena, A.; Eliseeva, E.; Dritschilo, A.; Kozikowski, A. P. Chemistry and biology of mercaptoacetamides as novel histone deacetylase inhibitors. *Bioorg Med Chem Lett* **2005,** 15, 1389-1392.

133. Suzuki, T.; Matsuura, A.; Kouketsu, A.; Nakagawa, H.; Miyata, N. Identification of a potent non-hydroxamate histone deacetylase inhibitor by mechanism-based drug design. *Bioorg Med Chem Lett* **2005,** 15, 331-335.

134. Kozikowski, A. P.; Chen, Y.; Gaysin, A.; Chen, B.; D'Annibale, M. A.; Suto, C. M.; Langley, B. C. Functional differences in epigenetic modulators superiority of mercaptoacetamide-based histone deacetylase inhibitors relative to hydroxamates in cortical neuron neuroprotection studies. *J Med Chem* **2007,** 50, 3054-3061.

135. Itoh, Y.; Suzuki, T.; Kouketsu, A.; Suzuki, N.; Maeda, S.; Yoshida, M.; Nakagawa, H.; Miyata, N. Design, synthesis, structure− selectivity relationship, and effect on human cancer cells of a novel series of histone deacetylase 6-selective inhibitors. *J Med Chem* **2007,** 50, 5425-5438.

136. Suzuki, T. Explorative study on isoform-selective histone deacetylase inhibitors. *Chem Pharm Bull* **2009,** 57, 897-906.

137. Heltweg, B.; Dequiedt, F.; Marshall, B. L.; Brauch, C.; Yoshida, M.; Nishino, N.; Verdin, E.; Jung, M. Subtype selective substrates for histone deacetylases. *J Med Chem* **2004,** 47, 5235-5243.

138. Day, J. A.; Cohen, S. M. Investigating the Selectivity of Metalloenzyme Inhibitors. *J Med Chem* **2013,** 56, 7997-8007.

139. Shen, S.; Kozikowski, A. P. Why Hydroxamates May Not Be the Best Histone Deacetylase Inhibitors—What Some May Have Forgotten or Would Rather Forget? *ChemMedChem* **2016,** 11, 15-21.

140. Groutas, W.; Giri, P.; Crowley, J.; Castrisos, J.; Brubaker, M. The lossen rearrangement in biological systems. inactivation of leukocyte elastase and alpha-chymotrypsin by (DL)-3-benzyl-N-(methanesulfonyloxy) succinimide. *Biochem Biophys Res Commun* **1986,** 141, 741-748.

141. Lee, M.-S.; Isobe, M. metabolic activation of the potent mutagen, 2-naphthohydroxamic acid, in salmonella typhimurium TA98. *Cancer Res* **1990,** 50, 4300-4307.

142. Cross, J. B.; Duca, J. S.; Kaminski, J. J.; Madison, V. S. The Active Site of a Zinc-Dependent Metalloproteinase Influences the Computed p K a of Ligands Coordinated to the Catalytic Zinc Ion. *J Am Chem Soc* **2002,** 124, 11004-11007.

143. Rambaldi, A.; Dellacasa, C. M.; Finazzi, G.; Carobbio, A.; Ferrari, M. L.; Guglielmelli, P.; Gattoni, E.; Salmoiraghi, S.; Finazzi, M. C.; Di Tollo, S. A pilot study of the Histone-Deacetylase inhibitor Givinostat in patients with JAK2V617F positive chronic myeloproliferative neoplasms. *Br J Haematol* **2010,** 150, 446-455.

144. Sholler, G. S.; Currier, E. A.; Dutta, A.; Slavik, M. A.; Illenye, S. A.; Mendonca, M. C. F.; Dragon, J.; Roberts, S. S.; Bond, J. P. PCI-24781 (abexinostat), a novel histone deacetylase inhibitor, induces reactive oxygen species-dependent apoptosis and is synergistic with bortezomib in neuroblastoma. *J Cancer Ther Res* **2013,** 2, 21.

145. Brindisi, M.; Senger, J.; Cavella, C.; Grillo, A.; Chemi, G.; Gemma, S.; Cucinella, D. M.; Lamponi, S.; Sarno, F.; Iside, C.; Nebbioso, A.; Novellino, E.; Shaik, T. B.; Romier, C.; Herp, D.; Jung, M.; Butini, S.; Campiani, G.; Altucci, L.; Brogi, S. Novel spiroindoline HDAC inhibitors: Synthesis, molecular modelling and biological studies. *Eur J Med Chem* **2018,** 157, 127-138.

146. Hai, Y.; Christianson, D. W. Histone deacetylase 6 structure and molecular basis of catalysis and inhibition. *Nature Chem Biol* **2016,** 12, 741-747.

147. Ghosh, A. K.; Veitschegger, A. M.; Nie, S.; Relitti, N.; MacRae, A. J.; Jurica, M. S. Enantioselective Synthesis of Thailanstatin A Methyl Ester and Evaluation of in Vitro Splicing Inhibition. *J Org Chem* **2018,** 83, 5187-5198.

148. Kraus, J. M.; Tatipaka, H. B.; McGuffin, S. A.; Chennamaneni, N. K.; Karimi, M.; Arif, J.; Verlinde, C. L. M. J.; Buckner, F. S.; Gelb, M. H. Second Generation Analogues of the Cancer Drug Clinical Candidate Tipifarnib for Anti-Chagas Disease Drug Discovery. *J Med Chem* **2010,** 53, 3887-3898.

149. Balasubramanian, G.; Kilambi, N.; Rathinasamy, S.; Rajendran, P.; Narayanan, S.; Rajagopal, S. Quinolone-based HDAC inhibitors. *J Enzyme Inhib Med Chem* **2014,** 29, 555-562.

150. Hawtin, R. E.; Stockett, D. E.; Byl, J. A. W.; McDowell, R. S.; Tan, N.; Arkin, M. R.; Conroy, A.; Yang, W.; Osheroff, N.; Fox, J. A. Voreloxin is an anticancer quinolone derivative that intercalates DNA and poisons topoisomerase II. *PLoS One* **2010,** 5.

151. Wang, X.; Jiang, X.; Sun, S.; Liu, Y. Synthesis and biological evaluation of novel quinolone derivatives dual targeting histone deacetylase and tubulin polymerization as antiproliferative agents. *RSC Adv* **2018,** 8, 16494-16502.

152. Brindisi, M.; Senger, J.; Cavella, C.; Grillo, A.; Chemi, G.; Gemma, S.; Cucinella, D. M.; Lamponi, S.; Sarno, F.; Iside, C. Novel spiroindoline HDAC inhibitors: Synthesis, molecular modelling and biological studies. *Eur J Med Chem* **2018,** 157, 127-138.

153. Brindisi, M.; Cavella, C.; Brogi, S.; Nebbioso, A.; Senger, J.; Maramai, S.; Ciotta, A.; Iside, C.; Butini, S.; Lamponi, S. Phenylpyrrole-based HDAC inhibitors: synthesis, molecular modeling and biological studies. *Future Med Chem* **2016,** 8, 1573-1587.

154.   Tangella, Y.; Manasa, K. L.; Krishna, N. H.; Sridhar, B.; Kamal, A.; Nagendra Babu, B. Regioselective Ring Expansion of Isatins with In Situ Generated α-Aryldiazomethanes: Direct Access to Viridicatin Alkaloids. *Org Lett* **2018,** 20, 3639-3642.

155.   Liu, K. G.; Robichaud, A. J.; Lo, J. R.; Mattes, J. F.; Cai, Y. Rearrangement of 3,3-Disubstituted Indolenines and Synthesis of 2,3-Substituted Indoles. *Org Lett* **2006,** 8, 5769-5771.

156.   Campiani, G.; Fiorini, I.; De Filippis, M. P.; Ciani, S. M.; Garofalo, A.; Nacci, V.; Giorgi, G.; Sega, A.; Botta, M.; Chiarini, A.; Budriesi, R.; Bruni, G.; Romeo, M. R.; Manzoni, C.; Mennini, T. Cardiovascular Characterization of Pyrrolo[2,1-d][1,5]benzothiazepine Derivatives Binding Selectively to the Peripheral-Type Benzodiazepine Receptor (PBR): From Dual PBR Affinity and Calcium Antagonist Activity to Novel and Selective Calcium Entry Blockers. *J Med Chem* **1996,** 39, 2922-2938.

157.   Mackwitz, M. K.; Hamacher, A.; Osko, J. D.; Held, J.; Schöler, A.; Christianson, D. W.; Kassack, M. U.; Hansen, F. K. Multicomponent synthesis and binding mode of imidazo [1, 2-a] pyridine-capped selective HDAC6 inhibitors. *Org Lett* **2018,** 20, 3255-3258.

158.   Osko, J. D.; Porter, N. J.; Reddy, P. A. N.; Xiao, Y.-C.; Rokka, J.; Jung, M.; Hooker, J. M.; Salvino, J. M.; Christianson, D. W. Exploring Structural Determinants of Inhibitor Affinity and Selectivity in Complexes with Histone Deacetylase 6. *J Med Chem* **2019**.

159.   Porter, N. J.; Osko, J. D.; Diedrich, D.; Kurz, T.; Hooker, J. M.; Hansen, F. K.; Christianson, D. W. Histone deacetylase 6-selective inhibitors and the influence of capping groups on hydroxamate-zinc denticity. *J Med Chem* **2018,** 61, 8054-8060.

160.   Bhatia, S.; Krieger, V.; Groll, M.; Osko, J. D.; Reßing, N.; Ahlert, H.; Borkhardt, A.; Kurz, T.; Christianson, D. W.; Hauer, J. Discovery of the first-in-class dual histone deacetylase–proteasome Inhibitor. *J Med Chem* **2018,** 61, 10299-10309.

161.   Frank, D. A. STAT3 as a central mediator of neoplastic cellular transformation. *Cancer Lett* **2007,** 251, 199-210.

162.   Keremu, A.; Aimaiti, A.; Liang, Z.; Zou, X. Role of the HDAC6/STAT3 pathway in regulating PD-L1 expression in osteosarcoma cell lines. *Cancer Chemoth Pharm* **2019,** 83, 255-264.

163.   Hazan-Halevy, I.; Harris, D.; Liu, Z.; Liu, J.; Li, P.; Chen, X.; Shanker, S.; Ferrajoli, A.; Keating, M. J.; Estrov, Z. STAT3 is constitutively phosphorylated on serine 727 residues, binds DNA, and activates transcription in CLL cells. *Blood* **2010,** 115, 2852-2863.

164.   Stacchini, A.; Aragno, M.; Vallario, A.; Alfarano, A.; Circosta, P.; Gottardi, D.; Faldella, A.; Rege-Cambrin, G.; Thunberg, U.; Nilsson, K. MEC1 and MEC2: two new cell lines derived from B-chronic lymphocytic leukaemia in prolymphocytoid transformation. *Leukemia Res* **1999,** 23, 127-136.

165.   Napier, K. J.; Scheerer, M.; Misra, S. Esophageal cancer: A Review of epidemiology, pathogenesis, staging workup and treatment modalities. *World J Gastrointest Oncol* **2014,** 6, 112.

166.   Moore, K.; Ford, P.; Farah, C. Support needs and quality of life in oral cancer: a systematic review. *Int J Dent Hyg* **2014,** 12, 36-47.

167.   Lernoux, M.; Schnekenburger, M.; Dicato, M.; Diederich, M. Anti-cancer effects of naturally derived compounds targeting histone deacetylase 6-related pathways. *Pharmacol Res* **2018,** 129, 337-356.

168.   Bradbury, C.; Khanim, F.; Hayden, R.; Bunce, C.; White, D.; Drayson, M.; Craddock, C.; Turner, B. Histone deacetylases in acute myeloid leukaemia show a distinctive pattern of expression that changes selectively in response to deacetylase inhibitors. *Leukemia* **2005,** 19, 1751-1759.

169.   Bazzaro, M.; Lin, Z.; Santillan, A.; Lee, M. K.; Wang, M.-C.; Chan, K. C.; Bristow, R. E.; Mazitschek, R.; Bradner, J.; Roden, R. B. Ubiquitin proteasome system stress underlies synergistic killing of ovarian cancer cells by bortezomib and a novel HDAC6 inhibitor. *Clin Cancer Res* **2008,** 14, 7340-7347.

170.   Kanno, K.; Kanno, S.; Nitta, H.; Uesugi, N.; Sugai, T.; Masuda, T.; Wakabayashi, G.; Maesawa, C. Overexpression of histone deacetylase 6 contributes to accelerated migration and invasion activity of hepatocellular carcinoma cells. *Oncol Rep* **2012,** 28, 867-873.

171.   Sakuma, T.; Uzawa, K.; Onda, T.; Shiiba, M.; Yokoe, H.; Shibahara, T.; Tanzawa, H. Aberrant expression of histone deacetylase 6 in oral squamous cell carcinoma. *Int J Oncol* **2006,** 29, 117-124.

172.   Cao, J.; Lv, W.; Wang, L.; Xu, J.; Yuan, P.; Huang, S.; He, Z.; Hu, J. Ricolinostat (ACY-1215) suppresses proliferation and promotes apoptosis in esophageal squamous cell carcinoma via miR-30d/PI3K/AKT/mTOR and ERK pathways. *Cell Death Dis* **2018,** 9, 1-11.

173.   Skipper, P. L.; Tannenbaum, S. R.; Thilly, W. G.; Furth, E. E.; Bishop, W. W. Mutagenicity of hydroxamic acids and the probable involvement of carbamoylation. *Cancer Res* **1980,** 40, 4704-4708.

174.   Brodská, B.; Holoubek, A. Generation of reactive oxygen species during apoptosis induced by DNA-damaging agents and/or histone deacetylase inhibitors. *Oxid Med Cellular Longev* **2011,** 2011.

175.   Miles, M. A.; Harris, M. A.; Hawkins, C. J. Proteasome inhibitors trigger mutations via activation of caspases and CAD, but mutagenesis provoked by the HDAC inhibitors vorinostat and romidepsin is caspase/CAD-independent. *Apoptosis* **2019,** 24, 404-413.

Publications

1.   Saraswati, A. P.; Relitti, N.; Brindisi, M.; Gemma, S.; Zisterer, D.; Butini, S.; Campiani, G. *Drug Discovery Today* 2019, 24, 1370-1388.

2.   Brindisi, M.; Saraswati, A. P.; Brogi, S.; Gemma, S.; Butini, S.; Campiani, G. *Journal of Medicinal Chemistry* 2020, 63, 23-39.

3.   Saccoccia, F.; Brindisi, M.; Gimmelli, R.; Relitti, N.; Guidi, A.; Saraswati, A. P.; Cavella, C.; Brogi, S.; Chemi, G.; Butini, S.; Papoff, G.; Senger, J.; Herp, D.; Jung, M.; Campiani, G.; Gemma, S.; Ruberti, G. *ACS Infectious Diseases* 2020, 6, 100-113.

4.   Nicola, R.; Saraswati, A. P.; Stefano, F.; Tuhina, K.; Margherita, B.; Daniela, Z.; Simone, B.; Sandra, G.; Stefania, B.; Giuseppe, C. *Current Topics in Medicinal Chemistry* 2020, 20, 433-457.